Gene editing to prevent ventricular arrhythmias associated with cardiomyocyte cell therapy

Gene editing to prevent ventricular arrhythmias associated with cardiomyocyte cell therapy

Authors: Silvia Marchiano[1,2,3], Kenta Nakamura[1,2,4], Hans Reinecke[1,2,3], Lauren Neidig[1,2,5], Michael Lai[6], Shin Kadota[1,2,3,4,7], Filippo Perbellini[6], Xiulan Yang[1,2,3], Jordan M. Klaiman[1,2,3], Leslie P. Blakley[1,2,3], Elaheh Karbassi[1,2,3], Paul A. Fields[1,2,3,8], Aidan M. Fenix[1,2,3], Kevin M. Beussman[1,2,9], Anu Jayabalu[1,2,3,6], Faith A. Kalucki[1,2,3,6], Akiko Futakuchi-Tsuchida[1,2,3,6], Gerhard J. Weber[1,2,4], Sarah Dupras[1,2,3,6], Hiroshi Tsuchida[1,2,3,6], Lil Pabon[1,2,3,6], Lili Wang[10], Björn C. Knollmann[10], Steven Kattman[1,2,3,6], R. Scott Thies[1,2,3,6], Nathan Sniadecki[1,2,3,9,11], W. Robb MacLellan[1,2,4], Alessandro Bertero[1,2,3,#,†], and Charles E. Murry[1,2,3,4,6,11,†,*].

Affiliations:
[1]Institute for Stem Cell and Regenerative Medicine, University of Washington, 850 Republican Street, Brotman Building Room 453, Seattle, WA 98109, USA.
[2]Center for Cardiovascular Biology, University of Washington, Seattle, WA 98109, USA
[3]Department of Laboratory Medicine & Pathology, University of Washington, Seattle, WA 98195, USA
[4]Division of Cardiology, Department of Medicine, University of Washington, Seattle, WA 98195, USA
[5]Department of Comparative Medicine, University of Washington, Seattle, WA 98195, USA
[6]Sana Biotechnology, Seattle, WA 98102, USA
[7]Department of Regenerative Science and Medicine, Shinshu University, Matsumoto 390-8621, Japan
[8]Adaptive Biotechnologies, Seattle, WA 98102, USA
[9]Department of Mechanical Engineering, University of Washington, 3720 15th Avenue NE, Seattle, WA 98105, USA
[10]Division of Clinical Pharmacology, Vanderbilt University School of Medicine, Nashville, TN 37232, USA
[11]Department of Bioengineering, University of Washington, Seattle, WA 98195, USA
[#]Current affiliation: Molecular Biotechnology Center “Guido Tarone”, Department of Molecular Biotechnology and Health Sciences, University of Torino, Torino, 10126, Italy.
[†]Equal contributions
*Corresponding author: murry@uw.edu

Summary:
Human pluripotent stem cell-derived cardiomyocytes (hPSC-CMs) offer a promising cell-based therapy for myocardial infarction. However, the presence of transitory ventricular arrhythmias, termed engraftment arrhythmias (EAs), hampers clinical applications. We hypothesized that EA results from pacemaker-like activity of hPSC-CMs associated with their developmental immaturity. We characterized ion channel expression patterns during maturation of transplanted hPSC-CMs, and used pharmacology and genome editing to identify those responsible for automaticity *in vitro.* Multiple engineered cell lines then were transplanted *in vivo* into uninjured porcine hearts. Abolishing depolarization-associated genes *HCN4, CACNA1H,* and *SLC8A1*, along with overexpressing hyperpolarization-associated *KCNJ2*, creates hPSC-CMs that lack automaticity but contract when externally stimulated. When transplanted *in vivo*, these cells engrafted and coupled electromechanically with host cardiomyocytes without causing sustained EA. This study supports the hypothesis that the immature electrophysiological prolife of hPSC-CM mechanistically underlies EA. Thus, targeting automaticity should improve the safety profile of hPSC-CMs for cardiac remuscularization.

Keywords:
Human Pluripotent Stem Cell-derived Cardiomyocytes, cell therapy, heart regeneration, myocardial infarction, cardiac remuscularization, arrhythmia, engraftment arrhythmia, automaticity, pacemaker, hPSC-CM maturation.

Introduction

The human heart loses its regenerative potential soon after birth[1,2]. After a myocardial infarction (MI), ~1 billon adult cardiomyocytes are replaced by non-contractile scar tissue; this impairs heart function and often progresses to chronic heart failure[3-6]. Ischemic heart disease affects over 120 million individuals per year, and it is the leading cause of death and hospitalization worldwide[5,6]. The discovery of pluripotent stem cells (PSCs) opened a new horizon in the treatment of MI and the prevention of heart failure[7]. Human PSCs, indeed, can be differentiated rapidly and at large scale into highly pure cardiomyocytes (hPSC-CMs). Intra-myocardial transplant of hPSC-CMs leads to long-lasting grafts of new myocardium in infarcted hearts[8,9]. These grafts form a functional syncytium with the host and are able to follow pacing from the sinoatrial node[8,9]. Moreover, in mouse[10], rat[11], guinea pig[12], and non-human primate (NHP)[13,14] models of subacute MI, transplantation of hPSC-CMs improves heart contractile function. For all these reasons, hPSC-CMs are being studied intensively as preclinical candidates for *bona fide* human heart regeneration[9,15].

Compared to adult ventricular CMs (vCMs), however, hPSC-CMs exhibit automaticity, described as the ability to spontaneously and rhythmically depolarize and elicit action potentials (APs)[16-18]. Automaticity is a feature of all early-stage cardiomyocytes that, during normal development, becomes restricted to specialized cells in the pacemaking/conduction system. Upon transplantation of hPSC-CMs into large animal models (e.g., NHPs and pigs), whose heart rates compares to that of humans (~70 beats per minute, bpm), we and others observed transitory but severe arrhythmias, hampering the translation of this technology into the clinic[13,14,19-21]. We named this phenomenon “engraftment arrhythmia” (EA, see the Method section for our detailed clinical characterization of EA)[20]. EA typically presents as polymorphic sustained ventricular tachycardia (VT) arising after graft-host electrical coupling (~1 week after transplantation) and lasting on average 1 month[13,14,19,20,22]. In severe cases, the heart rate of pigs and NHPs can reach ~300 bpm[13,14,19,20]. Although EA is well tolerated in NHPs and gradually wanes as the grafts mature[13,14], it can be lethal for arrhythmia-sensitive animals such as pigs[19,20,22]. Likewise, humans may not tolerate rapid EA, and it is imperative to identify strategies to prevent or at least control EA until electrical maturation of the graft[20].

Electrical mapping studies in NHPs and pigs indicated that EA originates locally from the sites of cell transplant, suggesting that an abnormal impulse generation from the graft, rather than conduction defects (i.e., re-entry pathways), represents the major source of EA[14,23]. Indeed, overdrive pacing and cardioversion, which typically restore sinus rhythm if re-entry pathways are responsible, could not terminate EA[14,23]. We thus proposed that spontaneous impulse generation by the graft is a critical aspect in the etiology of EA. Compared to mature adult vCMs, hPSC-CMs have a more depolarized membrane potential and shorter AP duration[18,24]. This corresponds to a fetal-like gene expression profile for most ion channels[24-27]. We therefore hypothesized that the arrhythmogenic currents causing EA result from the presence of depolarizing fetal channels that are normally absent in adult vCMs and/or from the absence of hyperpolarizing channels that are normally present in the adult state.

In this work, we determined the expression dynamics of all ion channel genes after hPSC-CM transplantation to establish a list of candidate EA mediators. Using CRISPR/Cas9 technology, we systematically knocked out and/or overexpressed ion channel genes – singly and in combination – with the goal of generating cardiomyocytes that, like adult vCMs, have reduced automaticity but beat in response to electrical stimulation. We characterized their electrophysiological behavior *in vitro* and quantified the burden of EA after cell transplantation in uninjured Yucatán minipigs[20]. After screening over ten different cell lines, we found that simultaneous modification of four genes (knockout of *HCN4* *CACNA1H*, and *SLC8A1*, coupled with knock-in of *KCNJ2* under the transcriptional control of the *HCN4* promoter) eliminated automaticity *in vitro* without affecting the ability of the cell to fire action potentials when stimulated. Importantly, compared to WT controls and the other cell lines, transplantation of this quadruple-gene edited CMs did not result in sustained EA. These modifications prevented the otherwise high morbidity and mortality and acute heart failure associated with hPSC-CM transplantation

in pigs[19,20,22]. These results identify multiple redundant mechanisms that control automaticity in hPSC-CMs and provide evidence that pacemaker-like activity of the immature graft is the primary source of EA. Interventions that reduce graft automaticity therefore should minimize arrhythmic complications of hPSC-CM transplantation.

Results

Maturation of hPSC-CMs in vivo remodels the expression of ion channels involved in automaticity.

As shown in Fig. 1A, the AP in immature hPSC-CMs has several differences from an adult vCM. It exhibits a spontaneous diastolic depolarization (or phase 4, generally absent in adult vCMs[16,17,25]), a slower phase 0, the absence of a notch in phase 1, and shorter repolarization phases 2 and 3; this leads to an overall shorter AP duration compared to adult cells[18,24]. Maturation of hPSC-CMs strongly affects AP morphology, and this correlates with changes in ion channel expression[24,25]. While some degree of hPSC-CM maturation can be achieved through *in vitro* long-term culture, electromechanical, and/or hormonal stimulation, the gene expression profile following prolonged culture never reaches a *bona fide* adult stage[16,17]. In contrast, we have previously shown that hPSC-CMs transplanted into the infarcted rat heart mature to have adult-like myofibril isoform expression and organization[28]. Most importantly, this model more closely mimics the maturation milieu that would be experienced by hPSC-CMs in human subjects, and is thus more clinically relevant. To characterize the genome-wide expression dynamics of hPSC-CMs during *in vivo* maturation, we performed laser-capture microdissection (LCM) followed by bulk RNA-seq time-course of human induced pluripotent stem cell-derived cardiomyocytes (hiPSC-CMs) from 1 day to 12 weeks after transplantation in infarcted rat hearts (Fig. 1B). As a comparison, we analyzed hiPSC-CMs cultured long-term *in vitro* for up to 1 year. To identify and extract *in vivo*-transplanted hiPSC-CMs from the host rat heart, we transduced them with GCaMP3 prior to injection[28], and isolated the GCaMP3+ (i.e., green fluorescent) grafts from tissue sections using LCM (Fig. 1C). To distinguish rat host signal from human graft signal, human-specific RNA-seq reads were then analyzed separately from those mapping ambiguously or clearly rat-specific, which were both discarded (Supplementary Fig. 1A). Dimensionality reduction of the data through Principal Component Analysis (PCA, Fig. 1D) revealed that the hiPSC-CM transcriptome was strongly altered rapidly upon early stages of engraftment (PC1), possibly a response to the associated stress. A similar magnitude of gene expression variability was explained by PC2, which separated samples by both time in culture and time *in vivo*. We interpreted PC2 as a maturation index. In agreement with protein expression studies previously reported by our group[28], gene expression profiles showed stronger and faster maturation *in vivo* compared to *in vitro* culture, which lagged behind even after 1 year in culture (Fig. 1E, Supplementary Fig. 1B and Supplementary Table 1). For instance, fetal to adult isoform switching of myofibril-related genes (*TNNI1* to *TNNI3*, *MYH*6 to *MYH7*, and *MYL7* to *MYL2*) as well as upregulation of genes involved in oxidative metabolism were more strongly induced by *in vivo* transplantation (Fig. 1E).

We then analyzed changes in gene expression specifically of ion channels involved in hPSC-CM APs (Fig. 1F). At early time points, corresponding to the onset of EA in large animals, we saw strong expression of *HCN4* and *CACNA1H* (whose protein products mediate I_f and I_{CaT}, responsible for Na^+/K^+ and Ca^{2+} currents, respectively, and are involved in phase 4), while we detected barely any *KCNJ2* transcript (which encodes for Kir2.1, responsible for the inward rectifying K^+ current, I_{K1}, one of the major repolarizing potassium currents). By 3 months, well after EA would be resolved and corresponding to a more mature hiPSC-CM state, this relationship was inverted, with *KCNJ2* expression being strongly upregulated (~1,000% more compared to early time points), while *HCN4* and *CACNA1H* decreased by ~50% and >90%, respectively. We also evaluated the expression kinetics of the other subunits that potentially contribute to I_f (*HCN1*, *HCN2* and *HCN3*), as well as I_{CaT} (*CACNA1G* and *CACNA1I*). As shown in Supplementary Figures 1C, D, the expression of these subunits in hiPSC-CMs is substantially lower compared to *HCN4* and *CACNA1H*, suggesting that in hiPSC-CMs, *HCN4* and *CACNA1H* are the major contributors for I_f and I_{CaT}, respectively. Overall, the expression patterns

of *HCN4*, *CACNA1H*, and *KCNJ2* correlate with the absence of phase 4 spontaneous depolarization in more mature hPSC-CMs and vCMs[16].

SCN5A (mediating the I_{Na} current)*, CACNA1C* (mediating the I_{CaL} current), and *SLC8A1* (mediating the I_{NCX} current) regulate the amount of depolarizing current after the initiation of the AP in vCMs. In hiPSC-CMs, I_{Na} and I_{CaL} were significantly lower than in adult vCMs[24-27], and, as shown in Fig. 1F (Phase 0, 2), *SCN5A* and *CACNA1C* expression levels were almost 4 times lower than *SLC8A1.* This is consistent with studies indicating a predominant role of I_{NCX} in the control of calcium handling in hPSC-CMs[27,29,30]. We also analyzed the expression of potassium channels responsible for the repolarization phase of the AP, including *KCND3* (I_{to}), *KCNQ1* (I_{Ks}) and *KCNH2* (I_{Kr}). Electrophysiological studies previously reported that maturation of hPSC-CMs coincides with increased repolarizing currents as well as the presence of the characteristic notch in the AP trace, mediated by the upregulation of *KCND3*/I_{to}[16,24]. As shown in Fig. 1F (Phase 1, 3), as hiPSC-CMs matured *in vivo* the expression of *KCND3*, *KCNQ1* and *KCNH2* increased with time. All together, these results indicate that *in vivo* transplantation progressively affects ion channels expression towards a more mature, adult-like phenotype. This suggests that inducing a more adult-like ion channel gene expression profile in hPSC-CMs could reduce automaticity and, potentially, the burden of EA after transplantation.

Pharmacologic studies link hPSC-CMs automaticity to calcium trafficking.

The role of ion channels in automaticity has been largely studied in the context of the adult mouse sinoatrial node[31-36]. Whether the same mechanisms also apply to hPSC-CMs remains controversial[29]. Moreover, the electrophysiological properties of hPSC-CMs may differ based on the specific differentiation protocol and/or the homogeneity of the population[24,26,29,37]. We thus set out to understand the drivers of automaticity in human embryonic stem cell-derived cardiomyocytes (hESC-CMs) differentiated by modulating the WNT pathway with small molecules.

We began by testing a variety of pharmacological compounds using multielectrode array system (MEA). First, we studied the role of HCN4 (I_f), a key mediator of spontaneous phase 4 depolarization[38]. Inhibition of I_f with Ivabradine potently reduced hESC-CM beating frequency[39,40]. Nevertheless, Ivabradine did not prevent spontaneous AP firing, even at high doses (Supplementary Fig. 2A). Zacopride, a reported agonist for the Kir2.1 channel (*KCNJ2*/I_{K1})[41], did not show measurable effects on the beat rate of hESC-CMs, likely due to the very low expression of the target ion channel in immature hPSC-CMs (Supplementary Fig. 2B). We attempted to inhibit I_{CaT} using both ML-218 and Mibefradil (Supplementary Figs. 2C, D), reported to inhibit I_{CaT} with moderate selectivity[42,43]. Mibefradil caused a dose-dependent reduction in beating rate and, at higher concentrations, reduced spike amplitude. ML-218 reduced hESC-CMs beating rate only at concentrations associated with undetectable spike amplitudes (Supplementary Fig. 2C, right panel). Since both inhibitors can block I_{CaL}[42,43] at high concentrations, we consider this evidence for I_{CaT} in automaticity, but not definitive proof.

Arguing for an important role of I_{CaL} for AP generation, we treated hESC-CMs with Verapamil, a class IV antiarrhythmic that blocks L-type calcium channels[44]. Verapamil, indeed, is indicated for the treatment of supraventricular arrhythmias, where it decreases the firing rate of nodal cells by reducing the rate of phase 4 depolarization[45]. In hESC-CMs, Verapamil caused a strong and progressive decrease in both the beat rate and the spike amplitude (Supplementary Fig. 2E), suggesting that the same mechanisms controlling AP firing in nodal cells might apply to hESC-CMs as well. A strong dose-response reduction in frequency and spike amplitude was observed also after the inhibition of the sodium-calcium exchanger NCX1 with the inhibitors SEA0400 and KB-R3702 (Supplementary Fig. 2F)[46,47]. NCX1 could also participate in AP generations because it mediates the uptake of three Na^+ ions for every Ca^{2+} ion extruded, independent from voltage membrane. This creates an influx of positive charge per cycle that could increase the spontaneous activity of hPSC-CMs in case of Ca^{2+} intracellular accumulation[33,48]. All together, these results highlight the importance of Ca^{2+} trafficking in hESC-CMs automaticity.

Gene editing to suppress automaticity

Pharmacologic studies are inherently limited by the specificity of drugs. To assess definitively the role of specific ion currents, we genetically manipulated candidate genes encoding for those ion channels likely to play an important role in hESC-CMs automaticity, based on our transcriptomic and pharmacological evidence. Specifically, we sought to obtain hESC-CMs that are quiescent-yet-excitable, like mature vCMs. This required the targeting of *HCN4* (HCN4), *CACNA1H* (Cav3.2), *SLC8A1* (NCX1) and *KCNJ2* (Kir2.1). Gene edits were performed individually and combinatorically to identify the minimum set of perturbations needed to abrogate automaticity and/or EA (Fig. 2A and Supplementary Fig. 3A).

We began with knockout (KO) perturbations. First, we abrogated the expression of *HCN4*, either alone and/or in combination with *CACNA1H* (Supplementary Figs. 3A, B). Western blot analyses confirmed the absence of HCN4 protein (Supplementary Fig. 3C) and, most importantly, patch clamp measurements demonstrated functional ablation of I_f (Fig. 2B) and a significant reduction in I_{CaT} (Fig. 2C), in agreement with the absence of compensatory upregulation on the other lowly expressed genes potentially contributing to these currents (Supplementary Figs. 3D, E). Confirming pharmacological observations, KO of *HCN4* alone did not eliminate hESC-CM automaticity *in vitro*, but rather, it reduced their beating frequency by nearly half (Fig. 2D). Interestingly, we also observed a moderate increase in the spike amplitude, that was significant for only one of the two clones studied (Fig. 2E). KO of *CACNA1H* did not alter hESC-CMs beat rate (Fig. 2F) or spike amplitude (Supplementary Fig. 3F). The combination of *HCN4*/*CACNA1H* 2KO showed a slightly more suppressed beat rate than *HCN4* KO alone, but automaticity was not completely abrogated (Fig. 2F).

To test the impact of gene edits on EA, we developed an *in vivo* model where 150 million hESC-CMs are transplanted into the uninjured hearts of immunosuppressed Yucatán minipigs (Supplementary Video 1 and Supplementary Table 2). We monitored heart rate and rhythm by telemetric continuous electrocardiogram (ECG) system. The number of animals treated with gene edited cells was, of necessity, limited since we wished to screen multiple genomic edits and were seeking dramatic impacts on EA. Indeed, moderate improvement of EA burden can be achieved already with pharmacologic therapy[20]. Moreover, although we did not utilize infarcted pigs in this work, the complication rate due to unstable EA (including sudden cardiac death and heart failure), as well as the general burden of EA, was comparable with our previous study where 500 million hESC-CMs were transplanted into infarcted pig hearts (Supplementary Figs. 3G, H)[20]. In all, we reasoned that gene editing would be clinically relevant only if it led to much greater safety profiles in a model where EA has the same clinical severity. Seven pigs received WT cells and served as controls. In WT-receiving hearts, EA commenced by day 4 and progressed to occupy more than ~50% of the day, especially in the first two weeks after engraftment (Fig. 2G, left panel). As described previously[20], EA began as premature ventricular contractions (PVCs), progressed into non-sustained ventricular tachycardia (NSVT) and then to sustained VT. The VT was often polymorphic, with both wide- and narrow-QRS complexes. As grafts mature, EA slows down, associated with increasing duration of normal sinus rhythm. Three control subjects exited the study prematurely based on prespecified EA severity endpoints described in the Methods section: one animal was euthanized due to unstable VT and cardiogenic shock at day 6, and two required acute pharmacological intervention with anti-arrhythmic therapy at day 4 and day 14, therefore these animals were excluded from further analysis (Fig. 2G, red points). The remaining four controls survived until planned endpoints of 14 (n=2), 35 (n=1), or 49 (n=1) days (See Methods for explanation of time points).

We began analysis of gene-edited hESC-CM using *HCN4* KO cells (n=2). Both animals receiving *HCN4* KO CMs developed EA: although there was a trend toward a reduced arrhythmia burden (% of the day in VT) and both subjects survived to the planned endpoint of 4 weeks, the removal of *HCN4* did not

significantly reduce the rapid rise in heart rate (Fig. 2G, right panel). We concluded that additional reductions in EA severity were needed to increase safety.

Next, we turned to the possibility of overexpressing hyperpolarizing currents (Supplementary Fig. 3A). Since the I_{K1} current is virtually absent in hESC-CMs[16,49] and is known to set the resting membrane potential at a more hyperpolarized, less excitable level in adult cardiomyocytes[50-52], we decided to overexpress *KCNJ2* (Kir2.1/I_{K1})[49]. We initially attempted to constitutively overexpress this channel through knock-in into the *AAVS1* genomic safe harbor with a constitutively active promoter[53]. However, despite numerous attempts and the fact that a control *EGFP* knock-in was consistently successful, we could not isolate any correctly targeted *KCNJ2*-overexpressing hESCs (data not shown). This unexpected finding strongly suggested that *KCNJ2* overexpression is not compatible with maintenance of pluripotency. To overcome this issue, we knocked in *KCNJ2* into the *HCN4* locus (Fig. 3A and Supplementary Fig. 4A). This strategy allowed us to both overexpress *KCNJ2* and knockout *HCN4* in a single gene-editing step and drive *KCNJ2* expression only after cardiac specification (Figs. 3A, B). Indeed, *KCNJ2* expression during hESC-CMs differentiation paralleled the normal pattern of *HCN4*, rising after the transition from progenitor to definitive cardiomyocyte (Fig. 3B). Given our earlier observation that during *in vivo* maturation of hiPSC-CMs *HCN4* levels decrease as endogenous *KCNJ2* is activated, this knock-in/knockout strategy provided the added potential benefit of providing temporally controlled *KCNJ2* upregulation, bridging its expression from immature to mature cardiomyocytes. We then compared *HCN4* KO/*KCNJ2* KI hESC-CMs with control cells that have *EGFP* knocked-in to the *HCN4* locus. Interestingly, even though the dual perturbation did not affect cardiac differentiation efficiency (Supplementary Fig. 4B), it significantly delayed the onset of spontaneous beating (Fig. 3C). Moreover, these dual edited hESC-CMs exhibited rapid and irregular bursts of electrical activity interposed with long quiescent pauses (Fig. 3D). This suggests that automaticity relies on the simultaneous activity of more than one or two ion channels[31-34].

Intrigued and puzzled by these results, we decided to test *HCN4* KO/*KCNJ2* KI hESC-CMs *in vivo.* Both animals receiving the dual edited cells showed a delay in the onset of EA by ~3 days (Fig. 3E). Once EA commenced, however, it rapidly degenerated into unstable VT in both animals, reaching euthanasia criteria on days 10 and 11. Collectively, these data indicate a complex role of *KCNJ2* in the regulation of both automaticity and EA, possibly through the interplay with other ion channels[31-34].

Triple gene editing: deletion of CACNA1H reduces pacemaker activity but does not prevent EA.
Work from others has shown that, in a simplified *in silico* model and in a non-excitable cell, the balanced alternation of hyperpolarization-potentiated depolarizing I_f and depolarization-activated repolarizing I_{K1} is sufficient to create rhythmic oscillations in the membrane potential, thus setting the stage for AP formation[40,50]. However, these antagonizing currents lead to moderate oscillations in the voltage membrane that alone cannot reach the threshold for phase 0 depolarization, and an additional depolarizing current is required for triggering the AP[40]. In agreement with other results suggesting the existence of multiple mechanisms regulating automaticity for nodal cells[29,32], our results indicate that a more complex circuit regulates hESC-CM automaticity as well. Indeed, the perturbation of *HCN4* and *KCNJ2* resulted in a slower and/or irregular beat rate, suggesting that the oscillation created by I_f and I_{K1} might principally set the depolarizing rhythm, whereas a second mechanism is required to maintain and stabilize automaticity. We thus focused on both the T-type calcium channel (*CACNA1H*) and NCX1 (*SLC8A1*). I_{CaT} is activated at a more hyperpolarized voltage compared to I_{CaL} or I_{Na}[32,35,40], whereas I_{NCX} is mainly regulated by the concentration of Na^+/Ca^{2+} across the sarcolemma, rather than membrane voltage[29,31,32,35]. We hypothesized that I_{CaT} and/or I_{NCX} might participate in cooperative mechanisms of automaticity, as suggested by *in silico* and *in vitro* results[33,40].

We decided first to generate hESCs lacking both depolarizing I_f and I_{CaT} currents with *KCNJ2* overexpression (Supplementary Figs. 3A and 4C). Triple edited hESCs maintained a normal karyotype and cardiac differentiation potential (Supplementary Figs. 4D, E). Since knockout of a gene may lead

to compensatory upregulation of genes sharing sequence similarity[54], we evaluated the expression of other ion channels mediating I_f and I_{CaT}. As shown in Fig. 4A, knockout of *HCN4* and *CACNA1H* did not affect the expression of gene family members. Triple edited *HCN4*/*CACNA1H* 2KO/*KCNJ2* KI hESC-CMs displayed delayed and inconsistent beating during differentiation (Fig. 4B), and MEA analysis indicated either complete absence of depolarization or irregular burst activity (Fig. 4C; Supplementary Fig. 4F). Nevertheless, when transplanted *in vivo* triple edited hESC-CMs still elicited EA at day 6 post engraftment (Fig. 4D). Once initiated, heart rate progressively accelerated and reached euthanasia criteria by day 8 (Fig. 4D). Collectively, adding *CACNA1H* KO appeared to further reduce automaticity *in vitro* compared to the parental *HCN4* KO/*KCNJ2* KI cells, but these hESC-CMs still caused severe EA *in vivo*. This indicated that another mechanism maintains some degree of automaticity in hPSC-CMs. We hypothesized that this mechanism might be mediated by NCX1, as described in the next section.

An SLC8A1-dependent mechanism critically contributes to pacemaker activity and EA burden.
As mentioned above, the opening of NCX1, mediated by the concentration of Na^+/Ca^{2+} across the sarcolemma, might contribute to the generation of AP as a cooperative mechanism for hPSC-CM automaticity. Indeed, the existence of both a "voltage-clock", mostly mediated by $I_f/I_{CaT}/I_{K1}$, and a "calcium-clock", where the main player is NCX1, has been described not only for nodal cells but also proposed for immature hPSC-CMs[29,30]. Although NCX1 is expressed in adult vCMs, we consider that its role might be ancillary in calcium handling in adulthood, compared to immature cardiomyocytes[55,56]. The calcium-induced calcium release (CICR) during excitation-contraction coupling in adult CMs is mainly regulated by L-type calcium channels, ryanodine receptors, and the Sarco-Endoplasmic Reticulum Calcium ATPase, (SERCA2A), pump[55]. In immature CMs, such as hPSC-CMs, CICR has not developed yet[16,48]; hence, NCX1 might play a predominant role in calcium cycling in immature CMs. This notion is supported by the pharmacological suppression of automaticity by NCX1 inhibition (Supplementary Fig. 2F).

All considered, we decided to knockout the gene encoding NCX1 (*SLC8A1*) either alone or in combination with the dual targeting of *HCN4*/*KCNJ2* (Supplementary Figs. 3A and 4G, H). Western blot confirmed the absence of NCX1 protein in both single and triple-edited clones (Fig. 4E). *SLC8A1* KO hESC-CMs showed no differences in the onset of beating during differentiation but exhibited intermittent periods of quiescence (Fig. 4F). Quiescence was accentuated in the triply edited *SLC8A1*/*HCN4* 2KO/*KCNJ2* KI (Fig. 4F). Indeed, from both observation during differentiation and MEA analysis, the triply edited hESC-CMs remained mostly quiescent, with only very sporadic beating episodes (Fig. 4G).

These results encouraged us to proceed with the *in vivo* transplantation of *SLC8A1*/*HCN4* 2KO/*KCNJ2* KI cardiomyocytes. Two out of three pigs, over the 4-weeks observation period, showed minimal EA with only episodes of PVCs (see the Method section for detailed definition of EA presentation). The third one developed unstable VT requiring euthanasia on day 9 post-transplant (Fig. 4H). Although graft size varied among animals, all pigs had readily detectable grafts (Fig. 4H, right panel; Supplementary Table 2). Notably, we had not seen the absence of EA in any animal to this point in the study. In combination with the *in vitro* data, we concluded that deactivation of both the calcium and voltage clocks significantly reduces automaticity *in vitro* and potentially reduced EA burden *in vivo*. This suggested that a state of total quiescence might be necessary to completely abrogate EA.

MEDUSA: a quadruple gene-edit that induces hESC-CM quiescence but maintains excitability.
Since the triply edited *SLC8A1/HCN4* 2KO/*KCNJ2* KI CMs can still exhibit some automaticity and caused EA, we hypothesized that removal of *CACNA1H* might deactivate what redundant depolarization mechanisms remain. We therefore generated a clone of *HCN4/CACNA1H/SLC8A1* 3KO/*KCNJ2* KI hESCs. Despite undergoing four sequential rounds of genome editing (Supplementary Fig. 3A), this cell line retained a normal karyotype and homogeneous expression of pluripotency

markers (Supplementary Figs. 5A, B). Henceforth, we will refer to this quadruple edited cell line with the shorter acronym MEDUSA (Modification of Electrophysiological DNA to Understand and Suppress Arrhythmias). MEDUSA hESCs were still able to differentiate into cardiomyocytes (Supplementary Figs. 5C, D) that, as expected, lack expression of *HCN4*, *CACNA1H* and showed increased expression of *KCNJ2* (Fig. 5A and Supplementary Figs. 5E, F). *SLC8A1* mRNA did not undergo nonsense-mediated decay, yet the gene edit prevented NCX1 translation as expected (Fig. 5A, insert and Supplementary Fig. 5E). As before, also in this quadruple gene edited cell line we did not observe compensatory upregulation of the other ion channel isoforms (Supplementary Fig. 5F). MEDUSA hESC-CMs remained quiescent with sporadic beating seen only when the cells were undergoing stress (e.g., lactate selection or heat-shock, Fig. 5B). Similarly, on the MEA system (Fig. 5C), we observed minimal spontaneous activity (less than 5 beats/hour), even after 2 weeks of observation, indicating that these cells are more quiescent compared to both the WT and the other cell lines tested so far.

To gain further insight on the excitability of MEDUSA CMs, we performed patch clamp experiments in the perforated-patch configuration on individual CMs. Similar to what was observed in MEA experiments, we found that MEDUSA hESC-CMs were essentially quiescent, as only 1/12 CMs (8%) exhibited automaticity after engaging the patch electrode (in contrast with 70% of WT hESC-CMs; Fig. 5D). Consistent with our expectations for CMs that overexpress *KCNJ2*, we found that the resting membrane potentials of quiescent MEDUSA hESC-CMs were significantly more hyperpolarized compared to spontaneously beating WT hESC-CMs, both in terms of resting membrane potential (RMP) and maximum diastolic potential (MDP; Figs. 5E, F). Moreover, the action potential duration at 90% repolarization was not different between MEDUSA and WT-CMs (Supplementary Fig. 5G). The capacitance of MEDUSA hESC-CMs did not differ from WT hESC-CMs (Supplementary Fig. 5G), indicating that membrane surface area was comparable.

Before proceeding with *in vivo* transplantation, we tested whether quiescent MEDUSA hESC-CMs were still excitable. Both patch clamp analyses (Fig. 5G) and calcium transient measurements (Fig. 5H and Supplementary Fig. 5H) confirmed that MEDUSA hESC-CMs can follow electrical pacing, generate APs and Ca^{2+} transients, and visibly contract up to 3 Hz stimulation (Fig. 5G). Calcium transients showed a delayed decay in MEDUSA CMs, potentially due to lack of NCX1 (Fig. 5H and Supplementary Fig. 5H). We wondered whether MEDUSA cardiomyocytes might compensate for lack of NCX1 by down-regulating systolic calcium entry. Interestingly, MEDUSA hESC-CMs showed reduced I_{CaL} currents, compared to WT control (Supplementary Fig. 5I), despite no significant changes in *CACNA1C* transcript levels ($p = 0.82$ with unpaired t-test). This suggest that, like the mouse cardiac NCX1 knockout [56], MEDUSA cardiomyocytes might reduce influx of Ca^{2+} via L-type Ca^{2+} channels to prevent calcium overload. Together, these data indicate that MEDUSA gene edits result in cardiomyocytes that are quiescent under baseline conditions but are still able to fire action potentials upon stimulation.

MEDUSA gene edits attenuate EA in vivo.

To test the efficacy of MEDUSA hESC-CMs in preventing EA, we proceeded with their transplantation into pig hearts. Remarkably, all three animals receiving 150M MEDUSA hESC-CMs showed no sustained VT for the entire period of observation (Figs. 6A, B) and reached the planned endpoints of 4 or 7 weeks (2 animals and 1 animal, respectively), without any adverse events. Pigs spent >95% of the time post-transplantation in stable sinus rhythm (Fig. 6B), with only sporadic PVCs and rare NSVT (Fig. 6A, right panel, see the Methods for detailed definitions). No sustained VT occurred at any point of the study (Fig. 6B). Indeed, MEDUSA hESC-CMs showed ~95% reduction in combined EA burden (VT, PVC, NSVT) for the first 2 weeks after transplant, compared to WT hESC-CMs ($p < 0.001$; Fig. 6C and Supplementary Fig. 6A). Importantly, the MEDUSA graft size was consistent with others examined at comparable endpoints (Fig. 6D and Supplementary Table 2).

As cardiomyocytes mature, they undergo isoform switching of several myofibril proteins such as MLC2a to MLC2v and ssTnI to cTnI, providing developmental benchmarks[16,17,28]. Immunofluorescence imaging

revealed that MEDUSA hESC-CM grafts undergo progressive maturation *in vivo*. Indeed, we observed signs of increased maturation of sarcomere as indicated by the isoforms switching from MLC2a→MLC2v and ssTnI→ cTnI (Fig. 6E). This indicates ongoing but not yet complete maturation at 7 weeks, consistent with what we previously observed with WT CMs engrafted in rat hosts.

Encouraged by the results of these studies, we proceeded with a dose-escalation study, transplanting 500 million the MEDUSA CMs (n=2) to more rigorously study safety at a clinically-relevant dose. Our recent data in this model demonstrated that this dose leads to 100% EA penetrance, persisting for multiple weeks, and resulting 67% mortality when WT hESC-CMs are employed[20]. Upon high-dose engraftment of MEDUSA hESC-CMs we observed brief, self-terminating episodes of VT shortly after transplantation lasting less than 24 hours, followed by return to normal sinus rhythm until endpoint at 3 months (Figs. 7A, B and Supplementary Fig. 6B). This brief and abruptly self-terminating presentation of VT was never observed in animals receiving WT hESC-CMs at the same dose, which exhibited a gradual onset of ectopy developing into sustained VT and lasting uninterrupted for weeks until electrical maturation at 4-6 weeks after transplantation. The MEDUSA grafts were large and viable out to 3 months post-transplantation and comparable in size with the ones previously seen in the infarcted heart (Supplementary Figs. 6C, D and Supplementary Table 2), ruling out reduced durability from the multiple edits.

Histological analyses showed that MEDUSA CMs formed gap junctions with the host, demonstrating a structural basis for electrical coupling (Fig. 7C). To assess the electrical integration of MEDUSA grafts in the porcine heart, we performed calcium imaging in live cardiac slices. Through field stimulation, we first assessed that MEDUSA grafts at 3 months after transplant were still viable and able follow electrical pacing (Supplementary Video 2). Importantly, we found that MEDUSA grafts fired APs in response to electrical point stimulation of the host myocardium up to 2 Hz (the fasted rate tested, Fig. 7D). Conversely, pacing the MEDUSA grafts resulted in the synchronous depolarization of the host myocardium (Supplementary Fig. 6E). This indicates that depolarizing impulses can flow bidirectionally between graft and host. Thus, MEDUSA hESC-CM grafts show electrical coupling with host myocardium that appears identical to what we have previously reported for WT hESC-CMs[12,57]. Moreover, we observed increased sign of maturation at 3 months after injection; indeed, the transition from MLC2a to MLC2v that was largely complete, as well as the switch from ssTnI to cTnI (Fig. 7E).

Taken together these results demonstrate that a nearly complete suppression of spontaneous electrical activity of quadruple gene edited MEDUSA hESC-CMs *in vitro* is associated with potent mitigation of EA *in vivo*. This supports the hypothesis that a series of electrical currents underlying automaticity are a primary cause of EA. The fact that multiple ion channel manipulations are required to abrogate automaticity and EA indicates complex and partially redundant roles among the resulting currents.

Discussion

Clinical translation of hPSC-CM cell therapy for heart regeneration has been complicated by transient arrhythmias following engraftment[13,14,19,20]. Engraftment arrhythmias (EA) were not observed in small animal models[10-12], likely being masked by theirs high heart rates at baseline, but are readily observed in large animal models, where heart rates approach that of humans[58]. Although NHPs tolerate EA, it can be lethal in pigs[19,20]. In general terms, arrhythmias arise from either a defect in conduction that leads to re-entry or from the presence of abnormal depolarization (pacemaker-like activity or after-depolarization)[59]. Invasive electrophysiology studies in monkeys and pigs demonstrate that EA has a focal source, cannot be extinguished by overdrive pacing or direct-current (DC) cardioversion, and cannot be induced by programmed electrical stimulation[14,23]; these findings favor local impulse generation rather than reentry. This led us to hypothesize that currents that normally underlie automaticity in immature hPSC-CMs are culprits in generating EA. Automaticity in hPSC-CMs is incompletely understood, and the mechanisms proposed are largely based on sinoatrial node models, with additional insights drawn from computational modeling and limited *in vitro* experiments[29,33,36].

Multiple mechanisms have been proposed depending on the differentiation protocol and/or the maturation state of the hPSC-CMs[29,49,50]; these models involve either the voltage clock, the calcium clock, or both[32-34].

To address this hypothesis experimentally, we first analyzed ion channel mRNA expression dynamics in hPSC-CMs as they matured after engraftment (Fig. 1), arguably the most powerful and physiologically relevant model of hPSC-CM maturation available to date. We used this information to identify key ion channels in hPSC-CMs, with a goal of engineering their electrophysiology towards an adult-like phenotype. Interestingly, single, double, and triple edits could reduce the beating rate and destabilize the rhythm, but they were insufficient to eliminate automaticity *in vitro* or EA *in vivo*. We eventually discovered that a quadruple edit (KO of *HCN4, CACNA1H,* and *SLC8A1*, along with overexpression of *KCNJ2*, which we termed MEDUSA) generated hESC-CMs that were quiescent-yet-excitable. When transplanted into the uninjured pig hearts, MEDUSA cardiomyocytes engrafted stably for 3 months, beat synchronously with the host myocardium, and markedly attenuated ventricular arrhythmias.

These findings support the hypothesis that sarcolemmal currents involved in automaticity underlie the pathogenesis of EA. Achieving electrically quiescent cardiomyocytes required manipulation of Na^+, Ca^{2+}, and K^+ channels and transporters, resulting in hyperpolarized cells that lacked diastolic depolarization currents. This indicates considerable redundancy in the circuitry underlying automaticity (perhaps not surprisingly, considering its importance to life). For example, KO of *HCN4* or its pharmacologic inhibition by ivabradine reduced *in vitro* beating rates by ~50% but eliminated neither automaticity nor EA (Fig. 2 and Supplementary Fig. 2). Layering onto the *HCN4* KO the overexpression of *KCNJ2* to hyperpolarize cells induced periods of electrical quiescence (Fig. 3), interrupted by irregular bursts of beating activity. These cells also caused EA after transplantation. Further layering onto these edits the KO of depolarizing genes *CACNA1H* or *SLC8A1* similarly failed to induce full quiescence or to prevent EA (Fig. 4). Only when we combined the KO of *CACNA1H* and *SLC8A1* with *HCN4* KO and *KCNJ2* overexpression we were successful in generating quiescent-yet-excitable cells with markedly reduction in arrhythmogenicity post-transplantation (Figs. 5-7 and Supplementary Figs. 6A, B). These findings support a model whereby trans-sarcolemmal movement of Na^+ and Ca^{2+} *via* the HCN4 channel, the T-Type Ca^{2+} channel, and the sodium-calcium exchanger triggers action potentials within the hESC-CM grafts, a process that is antagonized by hyperpolarization via the I_{K1} current encoded by *KCNJ2*. Why these pacemaking-like activities accelerate after transplantation remains unknown.

While our manuscript was in revision, a relevant paper from Selvakumar *et al.* appeared in preprint form[22]. These scientists studied EA after transplanting 750M hPSC-CMs into infarcted pig hearts. They confirmed our earlier findings[20] that amiodarone plus ivabradine partially suppresses EA, and they showed that ablating grafts with radiofrequency catheters could reduce EA burden (although with time EA recurred, driven from other foci). They also showed that cell preparations with a higher percentage of atrial or pacemaker-like cells, and faster *in vitro* beating, caused more severe EA. These observations further link the phenotype of graft cell automaticity to EA burden.

Our path to generate the MEDUSA line was non-linear, in that it involved multiple iterations of exploratory research to arrive at the final combination of gene edits (Supplementary Fig. 3A). We performed one at a time, and clonal lines were derived, qualified, and tested electrophysiologically prior to adding the next edit. Now that this combination is known, new lines can be generated much more quickly, e.g., through multiplexed editing. For example, one could perform simultaneous KO of *SLC8A1* and *CACNA1H* and then, using the bulk-edited cells, perform a second round of editing to knock *KCNJ2* into the *HCN4* locus, followed by cell cloning to derive the final lines. Alternatively, the knock-out and knock-in edits could be done simultaneously in bulk, followed by clone selection. Strategies like these should markedly reduce the time from initiation of editing to final line qualification.

It is interesting to speculate how MEDUSA cardiomyocytes would compare functionally to host cardiomyocytes after maturation *in situ*. After transplantation, MEDUSA cells retained their ability to engraft long term, to undergo myofibril developmental maturation, and to form gap junctions and beat synchronously with host myocardium. The KO of *HCN4* and *CACNA1H* should not affect function, since these genes are downregulated in mature cardiomyocytes[16,17]. Similarly, our strategy to overexpress *KCNJ2* should not affect mature cell function, since the transgene locus (inside *HCN4*) should naturally be downregulated with maturation, simultaneously with activation of the endogenous *KCNJ2* loci[25,26]. The impact of deleting *SLC8A1* is less clear, because the NCX1 channel is the adult cardiomyocyte's principal route of Ca^{2+} extrusion. Although the global deletion of *Slc8a1* is embryonically lethal in mice[60], mice with cardiac-specific deletion of *Slc8a1* are viable, grow to adulthood, and are fertile[56]. These animals exhibit modestly reduced systolic function but appear to have adapted to the absence of NCX1 by reducing the amount of Ca^{2+} entering the cell during the AP. This suggests that adult cardiomyocytes may be less dependent on NCX1 for function[48,55], and that hPSC-CMs lacking NCX1 may still be efficacious and healthy. Indeed, MEDUSA CMs are still responsive to pacing and exhibit calcium transients even after long-term engraftment (Supplementary Videos 2 and 3), suggesting the absence of calcium overload. Further studies are needed to test whether MEDUSA hESC-CMs are efficacious after transplantation into infarcted hearts.

It should be noted that MEDUSA cells are not perfectly quiescent. We occasionally observed spontaneous beating when the cells were stressed, e.g., during lactate selection or heat shock. While we do not know the source of the depolarizing current in these situations, one could imagine that stresses related to transplantation such as ischemia or inflammation could induce similar beating activity *in vivo*. This could underlie the brief, self-limited episodes of EA we observed when we implanted high doses of MEDUSA cells (Figs. 7A, B). Although this does not exclude other mechanisms of automaticity or arrhythmogenicity (i.e., macro-re-entry), MEDUSA cardiomyocytes have a substantially improved safety profile compared to their WT counterpart. Combining less arrhythmogenic cardiomyocytes with anti-arrhythmic pharmacology, such as amiodarone/ivabradine, may offer additive safety benefit for clinical trials.

In conclusion, these results provide new insights into the mechanisms behind automaticity of hESC-CMs and strongly support the hypothesis that EA results from pacemaker-like activity in the graft that wanes as ion channels mature toward an adult state. Although additional studies are needed to determine whether MEDUSA cardiomyocytes have retained the ability to restore systolic function, these cells represent an advance toward safely remuscularizing the injured heart.

Limitations of the study

The principal aim of this study was to understand the mechanism of engraftment arrhythmia by identifying the culprit ion channels involved in its pathogenesis. Because there is currently no *in vitro* or small animal model for EA, we used an *in vivo* pig model, transplanting cells into the normal heart to test the efficacy of our gene edits. This was an expensive and labor-intensive approach (typically with n=2 pigs/group), which limited the screen's statistical robustness to identifying only large treatment effects. As such, the negative predictive power for arrhythmia is less than its positive predictive power in this screen. Once the MEDUSA hit was identified, we increased our animal numbers and cell doses to have greater statistical confidence in the findings. Moreover, assessing the efficacy of MEDUSA hPSC-CMs for functional remuscularization will require properly controlled and adequately powered experiments in infarcted hearts with clinically relevant cell doses.

Acknowledgments

We thank the UW Department of Comparative Medicine for their exceptional veterinary care and consultation for the animal experiments. We also thank Dr. Naoto Muraoka, Ms. Elisabeth Mahen and Ms. Cathy Sanford for their help and experimental support. This research was assisted by the University

of Washington Cell Analysis Facility (Department of Immunology), the Lynn and Mike Garvey Cell Imaging Core and the Tom and Sue Ellison Stem Cell Core from the Institute for Stem Cell and Regenerative Medicine) and Specialty VETPATH for histology services. These studies were supported by the UW Medicine Heart Regeneration Program, the Washington Research Foundation, a gift from Mike and Lynn Garvey, and a sponsored research agreement from Sana Biotechnology (all Seattle, WA). This work also was supported in part by NIH grants R01HL128368, R01HL146868, and R01HL148081 (to C.E.M.), a grant from the Fondation Leducq Transatlantic Network of Excellence (Boston, MA; to C.E.M.), and the Bruce-Laughlin Research Fellowship (Seattle, WA; to K.N.). S.M. was supported in part by a fellowship from the UW Institute for Stem Cell and Regenerative Medicine.

Author contributions

Investigation for *in vitro* experiments: S. M., H. R., M. L., F. P., A. M. F., L. W., A. B.; investigation for *in vivo* experiments: K. N., L. N., S. K., S. M., X. Y., J. M. K., L. P. B., S. D., H. T.; investigation for cell prep for animal surgery: S. M., H. R., A. J., F. A. K., A. F. T.; investigation for histological analysis: S. M., H. R., X. Y., S. D., H. T. Formal analysis: E. K., P. A. F., K. M. B., G. J. W. Methodology: S. M., K. N., L. N., X. Y., E. K., G. J. W., L. P., S. K., N. J. S., W. R. M., A. B., C. E. M. Writing – Original Draft: S. M., Writing – Review & Editing: K. N., M. L., S. K.,J. M. K., E. K., A. M. F., K. M. B., R. S. T., N. J. S., W. R. M., A. B., C. E. M. Supervision: L.P., B. C. J., S. K., R. S. T., N. J. S., W. R. M., A. B., C. E. M. Conceptualization: S. M., K. N., H. R., L. N., X. Y., L. P., B. C. J., S. K., R. S. T., N. J. S., W. R. M., A. B., C. E. M. Funding acquisition: R. S. T, W. R. M., C. E. M.

Declaration of interests

K.N., B. C. K., and W. R. M. were advisors to Sana Biotechnology. M. L., A. J., F. A. K., A. F.T., S. D., H. T., L. P., S. K., R.S. T., and C. E. M. were employees while part of this study was performed and continue to hold equity in Sana Biotechnology. S. M., H. R., A. B., and C. E. M. have submitted a provisional patent application pertaining to the work in this manuscript (PCT/US2022/027382). The remaining authors have nothing to disclose.

Inclusion and Diversity statement

One or more of the authors of this paper self-identifies as an underrepresented ethnic minority in science.

Figures titles and legends

Figure 1. Gene expression analysis of hiPSC-CMs during *in vivo* transplantation compared to 2D culture. (**A**) Representative action potential traces from hESC-CMs and adult ventricular CMs (dotted line indicates 0 mV). Adult CMs adapted from Karbassi et al.[16] (**B**) Experimental layout for RNA-seq experiments. (**C**) Representative hematoxylin and eosin-stained (H&E) histological analyses of rat heart engrafted with hiPSC-CMs at day 84 after injection (a-b), and adjacent unstained sections showing the graft site before (c, fluorescence image of GCaMP3 signal) and after laser capture microdissection (LCM; d, brightfield image). Scale bar = 200 µm for a, d; 50 µm for b, c. (**D**) Principal component analysis (PCA) of RNA-seq data set described in B. The percentage of gene expression variance expressed by each PC is indicated. *Day 0 indicates hiPSC-CMs in vitro at day 18-21 as depicted in B*. (**E**) RNA-seq expression heatmap of selected maturation-related genes (data plotted as average log_2 fold-change from day 0 for three biological replicates). (**F**) Selected RNA-seq data for ion channels involved in AP. Red shading indicates the approximate window of engraftment arrhythmia. See also Supplementary Figs. 1C, D.

Figure 2. Ablation of *HCN4* and *CACNA1H* is not sufficient to prevent automaticity of hESC-CMs. (**A**) Experimental layout for the generation of gene-edited cell lines, cardiac differentiation, and *in vitro*/*in vivo* characterization. SpCas9: *Streptococcus pyogenes* Cas9, sgRNA: single-guide RNA. (**B, C**) Patch clamp analyses of funny current (I_f) from *HCN4* knockout (B) and T-type calcium current (C) from *CACNA1H* KO, compared to WT cardiomyocytes. (For I_f, WT: n = 7, *HCN4* KO cl.1: n = 6, *HCN4* KO cl. 2: n = 4; for I_{CaT} WT: n=22, KO: n=15). Representative current traces showed on the right. Differences in I_{CaT} *vs.* WT by two-way ANOVA with Sidak correction for multiple comparison (green-shaded area from -20 mV to +20 mV, $p < 0.001$). The traces for I_{CaT} were recorded from quadruply edited MEDUSA hESC-CMs and reported here with the parental line for simplicity (see also Supplementary Fig. 3A for detail of gene-editing strategy). (**D - F**) Spontaneous electrical activity of gene-edited hESC-CMs on MEA system. Data shown as mean ± SEM of 2-3 independent experiments each with 8 technical replicates, and normalized on WT frequency (D and F) or WT spike amplitude (E). Statistical differences are reported *vs.* WT hESC-CMs by one-way ANOVA with Sidak correction for multiple comparisons (* $p < 0.05$, ** $p < 0.01$ and *** $p < 0.001$). (**G**) Quantification of engraftment arrhythmia burden (% of time each day) and heart rate after transplanting *HCN4* KO hESC-CMs compared to WT hESC-CMs. Data shown as mean ± SEM for *HCN4* KO (N = 2) and WT controls up to day 14 and as individual animals thereafter (N = 7 for starting cohort, then N = 2, shown as individual trace). Red-colored symbols represent animals that reached endpoints as defined in the Method section. Representative ECG traces shown on the right.

Figure 3. *HCN4* and *KCNJ2* perturbation is not sufficient to prevent automaticity or EA. (**A**) Gene-editing approach to knock-in *KCNJ2* under the transcriptional control of the *HCN4* promoter in RUES2 hESCs. Genotyping PCR strategies for on- and off-target insertions are indicated; see also Supplementary Figure 4A. (**B**) Time course qRT-PCR analysis of *HCN4, KCNJ2* and *TNNT2* expression during cardiac differentiation of the indicated WT and gene-edited hESCs. ES: embryonic stem cell, MS: mesoderm, CP: cardiac progenitor, CM: cardiomyocyte. N = 2 differentiations per cell line. (**C**) Representative quantification of spontaneous beating during hESC-CM differentiation from *HCN4* KO/*KCNJ2* KI clones compared to WT. See Methods for details on quantification. (**D**) Spontaneous activity of *HCN4* KO/*KCNJ2* KI clones quantified by MEA, and representative traces. Given the marked irregularity of automaticity in these lines, data are reported as average beats in 5 min recording (left panel) and the corresponding % beat irregularity (right panel), calculated as standard deviation of the beat period record in 100 sec, divided by the mean of the beat period in that same period. Data are plotted as mean ± SEM of 3 independent experiments each with 8 technical replicates. (**E**) *In vivo* data showing EA burden (left panel) and heart rate of animals transplanted with *HCN4* KO/*KCNJ2* KI hESC-CMs compared to WT, with representative ECG traces on the right. Data shown for WT controls as described in Fig. 2G and individual traces (N = 2) for *HCN4* KO/*KCNJ2* KI. Red-colored symbol represents animals that reached prespecified EA endpoints leading to withdrawal from the study, as defined in the Methods section.

Figure 4. Triple gene edits decrease automaticity but do not fully prevent EA. (**A**) qRT-PCR gene expression analysis of HCNs, T-type ion channel genes, and *KCNJ2* in *HCN4*/*CACNA1H* 2KO/*KCNJ2* KI compared to WT hESC-CMs at day 14 of differentiation. Data shown as mean ± SEM of 3 independent experiments normalized on WT. Differences *vs*. WT by multiple paired t test (* $p < 0.05$, ** $p < 0.01$ and *** $p < 0.001$). (**B**) Representative onset of beating during cardiac differentiation in *HCN4*/*CACNA1H* 2KO/*KCNJ2* KI

hESC-CMs. (**C**) MEA analysis of *HCN4*/*CACNA1H* 2KO/*KCNJ2* KI clones compared to WT hESC-CMs. Data are shown as average beats/min recorded in 5 min ± SEM of 2 independent experiments with 8 replicates each. See also Supplementary Fig. 5F. (**D**) Arrhythmia burden and heart rate of one pig engrafted with *HCN4*/*CACNA1H* 2KO /*KCNJ2* KI hESC-CMs compared to WT (N = 7), and representative EKG traces during EA. Data shown as described in Fig. 3E. Red-colored symbols represent animals that reached prespecified EA endpoints and withdrawn from the study as described in the Methods section. (**E**) Western blot of NCX1 KO clones compared to WT hESC-CMs. cTnT: cardiac troponin T. (**F**) Representative time course analysis of onset of beating during cardiac differentiation of *SLC8A1* KO clones compared to WT. (**G**) Representative field potential traces and quantifications of *SLC8A1* KO clones at different points of a 2 weeks culture on MEA plates. Data shown as average beats/min recorded in 5 min ± SEM of 3 independent experiments with 4 replicates each. (**H**) EA burden and respective heart rate of pigs transplanted with *SLC8A1*/*HCN4* 2KO/*KCNJ2* KI hESC-CMs compared to WT. Data shown for WT controls as mean ± SEM up to 14 and as individual animals thereafter (N = 7 for starting cohort), and for *SLC8A1/HCN4* 2KO/*KCNJ2* KI as individual traces to demonstrate heterogeneity (N = 3); Red-colored symbols represents animals withdrawn from the study due to death and/or EA severity, as described in Methods section. (**I**) Representative histological analysis of *SLC8A1/HCN4* 2KO/*KCNJ2* KI graft 4 weeks after injection, stained with human-specific β-myosin heavy chain antibody. Scale bar = 200 μm.

Figure 5. *In vitro* characterization of MEDUSA hESC-CMs. (**A**) qRT-PCR of gene-edited ion channels in MEDUSA hESC-CMs compared to WT control. Data shown as mean ± SEM of 3 independent experiments. Statistical differences are reported *vs.* WT hESC-CMs by unpaired t-test (* $p < 0.05$, ** $p < 0.01$ and *** $p < 0.001$). Insert showing western blotting analysis for NCX1 in MEDUSA hESC-CMs, see also Supplementary Figs. 5E, F. (**B**) Onset of beating and beating rate during cardiac differentiation of MEDUSA hESC-CMs. Data shown as mean ± SEM of 2 independent batches of monolayer differentiation (12-wells/cell line per batch of differentiation). See Methods section for details on quantification. (**C**) Representative MEA analysis of MEDUSA hESC-CMs cultured for 2 weeks on MEA plates. Data shown as average ± SEM of total beats recorded for 5 min every hour. Spontaneous activity at day 35 is shown as continuous recording for 20 hours, panel below. Differences *vs.* WT hESC-CMs by two-way ANOVA with Sidak correction (*** $p < 0.001$). (**D**) Distribution of quiescent and spontaneously depolarizing cells in patch clamp preparation. (**E**) Quantification of patch clamp metrics under pacing condition (RMP: resting membrane potential; MDP: maximum diastolic potential). Data shown as violin plots of 16 WT and 11 MEDUSA hESC-CMs. Differences *vs.* WT hESC-CMs by unpaired t-test with Welch's correction (**$p<0.01$, ***$p<0.001$). (**F**) AP traces of WT and MEDUSA hESC-CMs after electrical stimulation (RMP, MDP as in 5E; APD_{90}: action potential at 90% repolarization). (**G**) Representative AP traces of MEDUSA hESC-CMs stimulated at 0.5 - 3 Hz, during patch clamp experiments. (**H**) Calcium transient analysis of WT and MEDUSA hESC-CMs during pacing at 1 Hz. Data shown as mean ± SEM of 12 individual cells/cell line. Statistical differences are shown by multiple unpaired t-test (***$p<0.001$). Representative traces shown in Supplementary Fig. 5H.

Figure 6. Characterization of MEDUSA hESC-CMs *in vivo*. (**A, B**) Arrhythmia burden and heart rate of pigs receiving 150M MEDUSA CMs and monitored with telemetry up to 7 weeks post-transplantation. Data shown for WT controls as mean ± SEM as detailed in Fig. 2G. Yellow-colored symbols represent animals that reached EA severity endpoints leading to study withdrawal as defined in Methods section. Insert from panel in A shows arrhythmia from pig N.3 subdivided in isolated premature ventricular contraction (PVC), non-sustained VT (NSVT) and VT, with relative representative ECG traces. (**C**) Aggregate analysis of combined EA daily burden (VT, NSVT, PVC) for WT and MEDUSA hESC-CMs for the first 2 weeks after transplantation. Data shown as mean ± SEM of animals receiving either WT (N=7) or MEDUSA hESC-CMs (N=3). Yellow-colored symbols represent animals analyzed until EA severity necessitated their withdrawal from the study (day 4 and day 6, respectively; see also panel A and Supplementary Fig. 6A). Differences *vs.* WT by unpaired t-test (*** $p < 0.001$). (**D**) Representative image of MEDUSA hESC-CMs graft 7 weeks after injection stained with human-specific β-myosin heavy chain. Scale bar = 1 mm. Note the large, multifocal graft throughout the host ventricle. (**E**) Low and high magnification immunofluorescence images of MLC2v/MLC2a and ssTnI/cTnI in MEDUSA-CMs grafts 4 weeks post transplantation. Single channels monochromatic images for both MLC2a/MLC2v and ssTnI/cTnI shown on the right. Dotted lines indicate host/graft interface. Scale bars = 50 μm for low magnifications; 20 μm for high magnification.

Figure 7. Electromechanical coupling of high-dose MEDUSA hESC-CMs. (**A, B**) Arrhythmia burden and heart rate of animals receiving 500M MEDUSA hESC-CMs (N = 2). Panel A shows the cumulative incidence

of sustained VT, PVC, and NSVT; See also Supplementary Figs. 6B. Right panel in A showing representative ECG traces of one animal transitioning without intervention from sustained VT to sinus rhythm. (**C**) Representative immunofluorescence images of 3 months old MEDUSA grafts stained with Connexin 43 (white arrows indicate junctions between host, Desmin/graft, ssTnI. Scale bars = 100). (**D**) Cardiac slice model of 12 weeks old MEDUSA-CMs grafts loaded with Fluo-4 and paced with field and point stimulation from host region; mid panel showing immunofluorescence image indicating graft and host in the cardiac slice studied are shown. Yellow circle indicates ROI for Fluo-4 recording, yellow star indicates point stimulation location. Scale bar = 500 μm. Right panel showing one frame from Supplementary Video 2 showing parallel bipolar electrodes placement. White lines are plastic monofilament used to keep the cardiac slice in place during recording. (**E**) MLC2a/MLC2v (left) and ssTnI/cTnI (right) staining of 3 months-old MEDUSA grafts, with relative monochromatic images on the right side. Scale bar: 200 μm.

Supplementary Figures titles and legends

Supplementary Fig. 1 – RNA-seq analysis of *in vivo* transplanted hiPSC-CMs. (**A**) Percentage of human/rat reads from *in vivo* samples after laser capture microdissection in the experiment described in Figs. 1B-D. "Unspecific" indicates reads that do not uniquely map to either genome. (**B**) GO term analysis of selected upregulated and downregulated pathways at 3 months after hiPSC-CMs transplantation. See also Supplementary Table 1. **(C)** RNA-seq expression dynamics of HCN channel isoforms and **(D)** T-type calcium channel isoforms during *in vivo* maturation of hiPSC-CMs. See also Fig. 1F.

Supplementary Fig. 2 – Pharmacological inhibition of hESC-CMs automaticity *in vitro*. (**A, B**) Dose-response curves of Ivabradine (I_f inhibitor, A) and Zacopride (I_{K1} agonist, B) on MEA system. (**C-F**) Frequencies (left y-axis) and spike amplitude (right y-axis) dose-response curves and representative traces of ML218, Mibefradil (I_{CaT} inhibitors, C, D); Verapamil (I_{CaL} inhibitor, E) and SEA0400 and KB-R7943 (I_{NCX} inhibitors, F). Data shown as mean ± SEM of 2 independent experiments each with 6 technical replicates, normalized on baseline and expressed as % *vs.* control (DMSO). Lines represents nonlinear regression of normalized response.

Supplementary Fig. 3 – Characterization of gene-edited cell lines targeting phase 4 of action potential. (**A**) Gene editing approach for the generation of the different cell lines. *pHCN4/KCNJ2 KI indicates the targeting vector described in Fig. 3A*. (**B**) Sanger sequencing validation of *HCN4* KO clones (*HCN4* KO cl.1 = 1 bp homozygous deletion; *HCN4* KO cl. 2 = 5 bp homozygous deletion), *CACNA1H* KO clones (*CACNA1H* KO cl.1= 20 bp homozygous deletion, *CACNA1H* KO cl.2= compound heterozygous indels leading to frameshift on the different alleles) and double edited cells (*HCN4*/*CACNA1H* KO cl.1= 1 bp homozygous insertion, *HCN4*/*CACNA1H* KO cl.2= 1 bp homozygous deletion). (**C**) Western blot for HCN4, TNNT2 (cardiac troponin T) and GAPDH (loading control) in different batches of MEDUSA hESC-CMs, reported here with the parental line for simplicity. (**D, E**) Gene expression analyses by qRT-PCR of HCN channel subunits in *HCN4* KO, *CACNA1H* KO and *HCN4*/*CACNA1H* 2KO clones compared to WT in 4 independent batches of CMs. In some batches, *CACNA1I* was undetectable (cycle threshold > 40). Differences quantified by one-way ANOVA with Sidak correction for multiple comparisons (** p <0.01, *** p <0.001). (**F**) Spike amplitude of *CACNA1H* KO and *HCN4/CACNA1H* 2KO clones from MEA analysis. Data shown as mean ± SEM of 2-3 independent experiments normalized on WT Spike amplitude. (**G**) Kaplan-Meier curve for freedom from EA mortality (described as death, unstable VT or heart failure necessitating either euthanasia or pharmacological intervention) in uninjured animals receiving 150M WT cells (n=7) or infarcted animals receiving 500M WT cells (n=8,). Yellow-colored marks on the treatment line indicate non-cardiac deaths due to opportunistic infection or planned euthanasia. (**H**) EA burden in uninjured and injured animals shown as mean and peak EA of animals receiving WT cells (Mann-Whitney test). Yellow-colored symbols represent animals that reached endpoint as described in the Method section. Data for 500M + MI in G and H from *Nakamura K. et al., Stem Cell Reports 2021.*

Supplementary Fig. 4 – Genotyping and characterization of triple-edited cell lines. (**A**) Genotyping of *HCN4* KO/*KCNJ2* KI clones generated with CRISPR/Cas9-mediated homology directed repair using the targeting plasmid described in Fig. 3A. (**B**) Representative flow cytometry data of *HCN4* KO/*KCNJ2* KI clones at day 14 of differentiation stained for cardiac troponin T (cTnT, pan-CM marker). (**C**) Genotyping of *HCN4*/*CACNA1H* 2KO/*KCNJ2* KI clones generated with the targeting plasmid described in Fig. 3A. Refer also to Supplementary Fig. 3A for parental lines. (**D**) Karyotype analyses of *HCN4*/*CACNA1H* 2KO/*KCNJ2* KI clones. (**E**) Representative flow cytometry analysis of *HCN4*/*CACNA1H* 2KO/*KCNJ2* KI CMs at day 14 of differentiation stained for cTnT. (**F**) Beat period irregularity quantified as standard deviation of the beat period record in 100 sec, divided by the mean of the beat period in that same period. Data shown as mean ± SEM of 2 independent experiment (for *HCN4*/*CACNA1H* 2KO/*KCNJ2* KI cl.2, n=1 due to lack of spontaneous activity in the second experiment that prevented calculation of beat irregularity). (**G**) Genotype of *SLC8A1* KO clones generated via combination of 3 gRNAs. (**H**) Genotype of *SLC8A1*/*HCN4* 2KO/*KCNJ2* KI clones generated with same approach described in Fig. 3A. Due to heterozygosity of clone 3, this clone was not used for further experiment.

Supplementary Fig. 5 – Characterization of MEDUSA cell line. (**A**) Karyotype analysis of MEDUSA hESCs. (**B**) Representative flow cytometry analysis of MEDUSA hESCs and WT hESCs stained with Oct3/4 as pluripotency marker, as compared to respective isotype control. (**C, D**) Representative flow cytometry analysis of mesoderm markers (CD56/PDGFRα) and ventricular markers (NKX2.5/cTnT) during cardiac differentiation in

WT and MEDUSA, compared to isotype controls. MS= Mesoderm state. (**E**) Western blotting for NCX1 and GAPDH (loading control) in WT and MEDUSA hESC-CMs. Dotted squares represent inserts shown in Fig. 5A. (**F**) qRT-PCR analysis of genes encoding for I_f, I_{CaT}, I_{K1} and I_{NCX} in MEDUSA hESC-CMs, compared to WT-matched controls. Note the absence of nonsense-mediated decay for *SLC8A1.* Data shown as mean ± SEM of 3 independent biological replicates. Differences *vs.* WT by multiple unpaired t test (* $p < 0.05$, ** $p < 0.01$ and *** $p < 0.001$). See also Fig. 5A. (**G**) Action potential duration at 90% of repolarization (APD_{90}) and capacitance current of WT and MEDUSA CMs. Data shown as described in Figs. 5E. (**H**) Representative calcium transient trace from WT and MEDUSA hESC-CMs. See also Fig. 5H. (**I**) Current density plot for I_{CaL} currents and qRT-PCR for *CACNA1C* in MEDUSA hESC-CMs, compared to WT controls. For I/V plot, data shown as mean ± SEM of n = 22 for WT and n = 15 for MEDUSA hESC-CMs. Green-shaded area indicates difference vs. WT hESC-CMs by two-way ANOVA with Sidak correction for multiple comparison ($p = 0.002$). For qRT-PCR. Data shown as mean ± SEM of 3 independent biological replicates.

Supplementary Figure 6. Characterization of transplanted MEDUSA hESC-CMs. (**A**) Daily arrhythmia burden focused on the first 2 weeks after transplantation for animals receiving 150 x 10^6 (150M) WT or MEDUSA hESC-CMs (See also Fig. 6A for arrhythmia burden over 7-weeks observation period). Differences vs. WT by multiple unpaired t-test (* $p < 0.05$ and ** $p < 0.01$). Yellow-colored symbols indicate animals that reached EA endpoint as detailed in Fig. 6A and Methods section. (**B**) Quantification of EA burden divided in PVCs, VT and NSVT for both 500M MEDUSA animals in the first 3 weeks after transplantation. See also Methods section for details on EA characterization. (**C**) Whole-slide scanning showing MEDUSA grafts at 500M dose at 3 months after transplantation. (**D**) Graft mass of 500M MEDUSA hESC-CMs transplanted into the uninjured pig heart compared to 500M WT hESC-CMs transplanted into infarcted animals. Data shown as average ± SEM, differences by Mann-Whitney test. For 500M WT hESC-CMs + MI, data points from *Nakamura K., et al., Stem Cell Reports 2021*. (**E**) Cardiac slice model of 12 weeks old MEDUSA-CMs grafts. Left panel showing Fluo-4 traces of cardiac slice paced with field and point stimulation from graft region with relative immunofluorescence and monochromatic images on the right side. Yellow circle indicates ROI for Fluo-4 recording, yellow star indicates point stimulation location. Scale bar = 500 µm. See also Supplementary Video 3.

STAR Methods text

RESOURCE AVAILABILITY

Lead contact

Further information and requests about reagents and other resources used in this work should be directed to and will be fulfilled by the lead contact: Charles E. Murry (murry@uw.edu).

Materials availability

Plasmids and cell lines generated in this study are available upon request to the Lead contact and with a complete Materials Transfer Agreement.

Data and code availability

- Bulk-RNA-seq data have been deposited at GEO and are publicly available as of the date of publication (accession number can be found in the key resource table). Original western blot images are included in the supplementary material as specified in the figure legends. Microscopy data reported in this paper will be shared by the lead contact upon request.
- All original codes utilized in this study is described in the Methods section and will be shared upon request to the Lead contact.
- Any further information required to reanalyzed the data reported in this paper is available from the lead contact upon request.

EXPERIMENTAL MODEL AND SUBJECT DETAILS

hPSC-CMs culture and differentiation (monolayer and suspension)

Human induced pluripotent stem cells (hiPSCs, 253G1-Camp3, Kyoto University, JP) and human embryonic stem cells (hESCs, RUES2e002-A, Rockefeller University, USA) were maintained and differentiated into cardiomyocytes as previously described[61]. Briefly, hiPSCs and hESCs were cultured in mTeSR Plus on Matrigel-coated plates (0.17 mg/mL) and passaged with 10μM Y-27632 when ~70% confluency was reached using Versene. For monolayer cardiac differentiation, ~90%-confluent hiPSCs/hESCs were primed with mTeSR Plus supplemented with 1 μM CHIR99021 for 24 hours. On day 0 of differentiation, mesoderm was induced using a cell line-optimized concentration of CHIR99021 (range: 3-5 μM) in RPMI 1640 supplemented with 213 μg/mL ascorbic acid and 500 μg/mL bovine serum albumin (RBA media). After 48 hours, on day 2 of differentiation, cells were washed with DPBS and cardiac progenitors were induced with 2 μM Wnt-C59 in RBA. After 48 hours, on day 4, cells were washed again with DPBS and incubated with plain RBA media for an additional 48 hours. From day 6 to day 10 cardiomyocytes were maintained in RPMI 1640 supplemented with Penicillin-Streptomycin and B-27 (RPMI-B27 media), performing media changes every 48 hours. Lactate selection was performed from day 10 through 14 by culturing cells in RPMI without glucose supplemented with 4 mM sodium L-lactate, with a media change after 48 hours. Media was changed with RPMI B-27 media until heat shock. The day before cryopreservation (Day 16-20), hPSC-CMs were heat-shocked for 30 min at 42°C. The following day, hPSC-CMs were dissociated using 5X TrypLE in Versene, washed in RPMI B-27, frozen in Cryostor CS10 at cell density of 3 x 10^7 cells/mL, and stored in liquid nitrogen.

As listed in Supplementary Table 2, WT controls, *HCN4* KO, *HCN4* KO/*KCNJ2* KI, *HCN4*/*CACNA1H* 2KO/*KCNJ2* KI hESC-CMs were differentiated and cryopreserved in suspension cultures, as previously described[20]. This same procedure was followed to generate MEDUSA hESC-CMs for high-dose animals described in Fig. 7. Briefly, pluripotent aggregates were expanded in suspension culture using Essential 8 media; cardiomyocytes differentiation was induced on day 0 using cell-line optimized CHIR99021 (range: 5-6 μM) for 24 hours as described in[14]. WNT pathway inhibition was performed at timing optimized empirically for each cell line. When cardiac state was reached (~ day 6 of differentiation), suspension cultures were fed using RPMI 1640, supplemented with B-27; purified between day 10 – 14 using lactate selection media (as described for monolayer differentiation) and heat-shocked the day before harvesting. *HCN4* KO/*KCNJ2* KI and *HCN4*/*CACNA1H* 2KO/*KCNJ2* KI hESC-CMs were differentiated by the same method until the fourth day of differentiation, at which point aggregates were dissociated with TrypLE, plated on rhLaminin-521 (BioLamina), and maintained as adherent cultures for the remainder of the differentiation protocol.All cells were harvested enzymatically 17-22 days after initiating differentiation and cryopreserved in CryoStor CS10.

Athymic Sprague Dawley rats (Hsd:RH-*Foxn1*^{rnu})

All protocols were approved and conducted in accordance with the University of Washington (UW) Office of Animal Welfare and the Institutional Animal Care and Use Committee. Eight-ten weeks old male athymic rats (240-300 g)

were housed and monitored by the Department of Comparative Medicine at UW, received ad libitum water and food. For all surgical procedures, rats were anesthetized by intraperitoneal injection of 68.2 mg/kg ketamine and 4.4 mg/kg xylazine (first thoracotomy) or isoflurane by inhalation (second thoracotomy), intubated and mechanically ventilated. Rats received analgesic (buprenorphine 0.05 mg/kg) twice daily for 48 hours after each surgery. Cyclosporine A (5 mg/kg/day) was given for 7 days beginning the day before transplantation to prevent graft cell death and euthanized by intravenous Euthasol.

Yucatán mini pigs

All protocols were approved and conducted in accordance with the University of Washington (UW) Office of Animal Welfare and the Institutional Animal Care and Use Committee. Castrated male, Yucatán minipigs between 30-40 kg were used in this study. Animals received ad libitum water and were fed twice a day (Lab Diet-5084 Laboratory Porcine Grower Diet). For surgical procedures, anesthesia was induced with a combination of intramuscular butorphanol, acepromazine and ketamine. Animals were intubated and mechanically ventilated using isoflurane and oxygen to maintain a surgical plane of anesthesia. Vital signs were monitored continuously throughout each procedure. All animals received subcutaneous Buprenorphine SR-Lab for post-operative analgesia and were euthanized by intravenous Euthasol. All post-mortem examinations were performed by a blinded board-certified veterinary pathologist. Immunosuppression regimen consisted of oral cyclosporine, which was titrated to a goal serum trough of 300 ng/mL for the duration of the study. Two days before transplant, oral methylprednisolone was started at 1.5 mg/kg for 2 weeks, and then was decreased to 1 mg/kg for the remained of the study. On the day of cell transplantation, Abatacept (CTLA4-Ig, Bristol-Myers Squibb), 12.5 mg/kg, was administered intravenously and dosed every 2 weeks thereafter. Prophylactic cephalexin (500 mg PO BID) was initiated at the time of central venous catheter placement and sulfamethoxazole/trimethoprim (50 mg/kg PO daily), valganciclovir (450 mg PO daily) and probiotics five days prior to transplant.

METHOD DETAILS

In vitro experiments for hPSCs editing and hPSC-CMs characterization.

Flow cytometry assessment of hPSC-CM differentiation and purity.

Flow cytometry analysis to assess pluripotency of hESCs (expressed as OCT-4 %) was performed after every round of gene-editing and at day 0 of cardiac differentiation using from BD StemflowTM Human and Mouse Pluripotent Stem Cell Analysis Kit, according to manufacturers' instruction. For mesoderm markers (CD56 and PDGFRα), an aliquot of hESCs at day 4-5 of cardiac differentiation were resuspend in DBPS supplemented with 5% bovine serum albumin (blocking buffer) and incubated with APC-/PE-conjugated antibodies or isotype controls diluted in blocking buffer for 1 hour at room temperature. Cells were then washed with DPSB and resuspend in blocking buffer before flow cytometry analysis. For cardiac markers (cardiac troponin T [cTnT] and NKX2.5), hESC-CMs were fixed in BD Cytofix (BD Life Science) and permeabilized in BD Wash/Perm Buffer (BD Life Science) supplemented with 0.1% Triton-X100 for 5 minutes at room temperature. HESC-CMs were then incubated with NXK2.5 primary antibody/isotype control diluted in BD Wash/Perm Buffer for 1 hour at room temperature. Cells were then wash twice with DPBS and resuspended in BD Wash/Perm Buffer containing APC-conjugated cTnT antibody or isotype control and Alexa Fluor anti-rabbit 488. After 1-hour incubation, hESC-CMs were resupsended in BD Wash/Perm Buffer and analyzed by flow cytometry.

Gene-editing for HCN4 and CACNA1H KO.

For HCN4 and CACNA1H KO, single gRNAs targeting key coding exons were cloned in pX459V2 plasmid (which includes the SpCas9 coding sequence driven by the CMV enhancer, see Supplementary Table 3 for gRNAs sequence) according to the Zhang lab's protocol and verified by Sanger sequencing. Plasmids for gene editing were prepared using QIGEN Midi prep kit. RUES2 hESCs were seeded at 15,000 cells/cm2 in mTeSR Plus supplemented with 10 μM Y-27632, and transfected using 6 μL of GeneJuice and 2 μg of pX459V2_gRNA plasmid in 100 μL of OPTI-MEM. After 24 hours, cells were washed with DPBS and incubated with mTeSR Plus supplemented with 5 μM Y-27632 and 0.5 μg/mL puromycin for 48 hours. Cells were subsequently washed with DPBS and maintained as described above. Single clones were isolated using a limiting dilution protocol by seeding single cells at 0.5 cell/well in 96-well cell culture plates. Genotype analysis was performed on clonal lines using Sanger sequencing of PCR amplicons obtained using the primer listed in Methods Table 1 and Q5 High-Fidelity Master Mix. When a mixed sequencing trace was observed, amplicons were TOPO-cloned and Sanger sequencing was performed on at least 48 individual bacterial clones to determine edits on individual alleles. Standard G-banding analysis was performed on undifferentiated cells to confirm absence of karyotype abnormalities. CRISPR/Cas9 off-target analysis was performed using Cas-OFFinder software (cut-off: up to 4 mismatches with 1 bulge on either DNA or RNA sequence) and potential

off-targets in an exon of a gene expressed in hESC-CMs were selected for genotyping by Sanger sequencing to exclude the presence of indels.

Gene-editing for KCNJ2 KI in HCN4 locus

Knockin of KCNJ2 in the HCN4 locus was performed through CRISPR/Cas9 homology-directed repair (HDR). The donor vector was generated using the NEBuilder Hifi DNA Assembly kit. 3' and 5' HCN4 homology arms (3'/5'-HAs) were amplified by PCR from hESCs RUES2 genomic DNA, while an SV40 polyA fragment was amplified from AAVS1_CAGGS_EGFP (all using primers listed in Supplementary Table 3). The Puro-T2A-TK cassette was isolated from on MV-PGK-Puro-TK plasmid through restriction digestion using NsiI and BsiWI. The same MV-PGK-Puro-TK plasmid was digested with NotI and AscI to isolate a backbone vector containing transposon inverted tandem repeats and ampicillin resistance genes. The donor plasmid resulting from this assembly (pbHCN4) and a synthetic fragment carrying the KCNJ2 cDNA were then digested with ClaI and NcoI restriction enzymes and ligated using Quick Ligation kit. To generate a control vector, the same procedure was performed but using EGFP amplified from AAVS1_CAGGS_EGFP. The resulting targeting plasmids (pbHCN4_KCNJ2 or pbHCN4_GFP) were amplified as described above. CRISPR/Cas9 plasmids designed to induce double strand breaks necessary to drive HDR were obtained by cloning two gRNAs targeting the HCN4 promoter (HCN4_gRNA1_KI and HCN4_gRNA2_KI, see Supplementary Table 3) in pX330-U6-Chimeric_BB-CBh-hSpCas9, all according to Zhang lab's protocol and amplified as described above. RUES2 hESCs were then transfected with 1 µg of donor plasmid (either pbHCN4_KCNJ2 or pbHCN4_GFP) and 0.5 µg for each of pX330_HCN4gRNA1_KI and pX330_HCN4gRNA2_KI using GeneJuice as described above. After puromycin selection, single clones were obtained through limiting dilution and genotyped through PCR. On site integration of the transgene cassette downstream of the HCN4 locus was confirmed using primers mapping on the cassette and on the locus but outside of the homology arm; the number of gene edited loci was determined by amplifying the wild-type allele (resulting in loss of amplification in homozygous edited cells); absence of random integrations of the targeting plasmids were confirmed using primers mapping to the insert and plasmid backbone. Karyotype analysis was performed to confirm absence of abnormalities, and CRISPR/Cas9 off-targets were excluded as described above.

Gene-editing for SLC8A1 KO series

To induce SLC8A1 KO, hESCs were electroporated with CRISPR/Cas9 ribonucleoprotein complexes targeting exon 1 of SLC8A1. Briefly, 500,000 RUES2 hESCs were resuspended in a mixture of 60 pmol of SpCas9 2xNLS nuclease (Synthego) and 60 pmol of SLC8A1 gRNAs mix (20 pmol/gRNA, Supplementary Table 3) and 300 µL of Neon Buffer R. Cells were then electroporated (1 pulse at 1,300 V for 30 milliseconds) using a Neon electroporation system, and immediately replated on Matrigel-coated 6-well plate in mTeSR1 supplemented with 10 µM Y-27632. SLC8A1 KO clones were isolated through limiting dilution and genotyped by PCR and Sanger sequencing. Karyotype analysis was performed to confirm absence of abnormalities, and CRISPR/Cas9 off-targets were excluded as described above.

Gene expression analysis via quantitative real-time PCR

Total RNA was extracted from day 14 RUES2 CMs from the different cell lines using RNAesy Mini kit according to manufacturer's instruction. Single-stranded cDNA was obtained by reverse transcription using M-MLV RT kit, and quantitative real-time reverse transcription PCR (RT-qPCR) was performed with SYBR Select Master Mix using 10 ng of cDNA and 400 nM forward and reverse primers (Supplementary Table 4). Reactions were run on a CFX384 Real-Time System (Biorad), and data was analyzed using the ΔΔCt method using HPRT1 as the housekeeping gene. Primers were designed using PrimerBlast and confirmed to amplify a single product.

Western Blotting

Day 14 hESC-CMs WT and SLC81A KO clone series and MEDUSA hESC-CMs clones were incubated with ice-cold RIPA Buffer (150 mM NaCl, 1% NP-40, 0.5% deoxycholate, 0.1% SDS, 50 mM Tris·HCl, 1X protease inhibitors) for 30 minutes at 4°C. Protein lysates were cleared by centrifugation at 21,000 rcf for 15 minutes at 4 °C and quantified by BCA assay. 30 µg of protein per sample were incubated in 1X non-reducing sample buffer for 30 minutes at 37 °C, run on a 4-20% Mini-Protean gel and transferred on a PVDF membrane. Membranes were incubated with 5% BSA in TBS buffer supplemented with 0.1% Tween-20 (blocking buffer) for 1 hour at room temperature. Primary antibodies were incubated in blocking buffer for 2 hours at room temperature; membranes were then washed three times in blocking buffer and incubated for 1 hour with fluorophore-conjugated secondary antibodies. Fluorescent signals were acquired using with a GelDoc Imager.

Spontaneous electrical activity measurements with MEA system and during differentiation

For MEA, CytoView MEA 48 well plates were coated with 0.17 mg/mL of Matrigel for 1 hour at 37 °C. 50,000 hESC-CMs were resuspended in 6 µL and plated on each MEA well, as previously described5. Media was changed with

RPMI-1640 supplemented with B-27 every other day for 1 week. For spontaneous beat recording, spontaneous electrical activity was recorded for 5 minutes using Maestro Pro system at 37 °C with 5% CO2. Considering the irregular beat rate of the cell lines bearing KCNJ2 KI, the data are shown as total number of beats recorded per experiment, divided by the total time of recording (average beats/min). For pharmacological studies, the different compounds were diluted in DMSO and incubated directly on MEA plates for 5 minutes at 37°C. Effects on spontaneous beat rate was determined by recording for 15 minutes after drug incubation. A non-linear regression curve was calculated as Y=100/(1+10^((LogIC50-X)*HillSlope))). Voltage was acquired simultaneously for all the electrodes at 12.5 kHz, with a low-pass digital filter of 2 kHz for noise reduction. Quantification of beat rate, spike amplitude and beat period irregularity was performed using Axis Navigator (beat detector threshold: 30-100 µV; minimum beat period: 200-500 milliseconds; maximum beat period: 30 seconds).

For quantification of spontaneous electrical activity/onset of beating during monolayer differentiation, 12-wells plates with hESCs were monitored from day 0 to day 18 or 35 of cardiac differentiation; spontaneous contraction was quantified as percentage of beating wells observed for 5 minutes.

Patch-clamp Electrophysiology

Single hESC-CMs (Day 14 – 21) were seeded on laminin-coated glass coverslips at a density of 13-18.5k cells/cm2. Perforated-patch action potential (AP) recordings were conducted in current-clamp mode using borosilicate glass pipettes with typical resistances of 2 - 4 MΩ. Data were acquired at 5 kHz and filtered at 2 kHz using a Multiclamp 700B amplifier, Digidata 1550 digitizer, and Clampex 11 software. Experiments were performed 35 ± 1 °C under continuous perfusion of Tyrode's solution containing (in mM): 140 NaCl, 5.4 KCl, 1.8 $CaCl_2$, 1 $MgCl_2$, 10 glucose and 10 HEPES, with the pH adjusted to 7.4 with NaOH. The pipette solution contained (in mM): 150 KCl, 5 NaCl, 5 MgATP, 10 HEPES, 5 EGTA, 2 $CaCl_2$, and 240 µg/mL of amphotericin B, with the pH adjusted to 7.2 with KOH. Evoked action potentials were recorded using 5 milliseconds current injection pulses (0.3 – 0.5 nA) at a frequency of 1Hz. Spontaneous action potential parameters were determined from 30 seconds recordings, while stimulated AP parameters were determined from 10 second recordings. APs were analyzed using Clampfit 11 software.

For I_f, currents were recorded in the modified Tyrode solution (with 0.2 mmol/L $CdCl_2$) at room temperature. From the holding potential of -40 mV, I_f currents were elicited by 2-s test pulses from -120 to -50 mV at 10-mV increments. I_f currents were defined as 0.5 mmol/L Ba^{2+}-insensitive and 5 mmol/L Cs^+-sensitive currents. Modified Tyrode solution was composed of (mM):120 NaCl, 20 KCl, 10 HEPES, 10 Glucose, 2 $CaCl_2$, and 1 $MgCl_2$, pH adjusted to 7.4 with NaOH. The pipette solution contained (mM): 100 KCl, 10 NaCl, 14 EGTA, 10 HEPES, 5 MgATP, 1 $CaCl_2$; pH adjusted to 7.2 with KOH.

To record I_{CaT}, whole-cell Ca^{2+} currents were recorded using pipettes with resistances between 1.5 and 3 MΩ. Data was acquired at 20 kHz and filtered at 1kHz using a HEKA EPC10 amplifier and Patchmaster v2x73 software. Experiments were performed at room temperature in extracellular solution containing (in mM): 130 TEA-Cl, 2 $CaCl_2$, 1 $MgCl_2$, 10 4-aminopyridine, and 25 HEPES, with the pH adjusted to 7.4 with TEA-OH. The pipette solution contained (in mM): 130 CsCl, 10 EGTA, 25 HEPES, 3 Mg-ATP, and 0.4 NaGTP, with the pH adjusted to 7.2 with CsOH. Total Ca^{2+} current (I_{Ca}) was elicited by 100 milliseconds depolarizing voltage steps between -80 and +70 mV, in +10 mV increments, following 3 seconds at a holding potential of -90 mV. L-type Ca2+ current (I_{CaL}) was elicited by 100 milliseconds depolarizing voltage steps from -80 to +70 mV following 3 seconds at a holding potential of -50 mV. I_{CaT} was calculated by subtracting I_{CaL} from I_{Ca}. Series resistance was compensated at least 60%. Voltages were corrected for a -8 mV liquid junction potential. Data analysis was performed using Fitmaster v2x91 software.

Calcium transient analysis

HESC-CMs were seeded at 5,000 cells/cm^2 in Matrigel-coated 6-well plates with RPMI-1640 supplemented with B-27 and penicillin-streptomycin. Cells were fed every other day for 1 week before incubation with 1 µM Fluo-4 AM for 30 min at 37 °C. Calcium transients were acquired while the culture was electrically paced at 1 Hz (0.025 seconds pulse duration, 40 mV) using an IonOptix pacing system and analyzed with custom MATLAB code[62].

Rodents and pig surgeries and *in vivo* experiments.

Cell injection preparation (rodent surgery)

hiPSC-CMs used in rodent surgery were cryopreserved on day 18-20 of differentiation, and thawed immediately prior to cell injection, all following our previously described protocol[28,57,63]. One day prior to cryopreservation, cells were heat shocked for 30 min at 42°C. Prior to enzymatic dispersion, the ROCK inhibitor Y-27632 (10 µM) was added to culture medium for 1 hour, and cells were dispersed by incubation with Versene followed by 0.05% Trypsin in EDTA.

hiPSC-CMs were re-suspended in CryoStor cell preservation media and frozen in cryovials in a controlled rate freezer to -80°C before being stored in liquid nitrogen. To thaw cryopreserved cells, cryovials were thawed briefly at 37°C followed by addition of RPMI+B27+insulin with Y-27632 (10 μM). Cells were washed with PBS and re-suspended in an RPMI-based pro-survival cocktail[63] containing 50% growth factor-reduced Matrigel, 100μM ZVAD (benzyloxycarbonyl-Val-Ala-Asp(O-methyl)-fluoromethyl ketone, Calbiochem), 50 nM Bcl-XL BH4 (cell-permeant TAT peptide, Calbiochem), 200 nM cyclosporine A (Novaritis), 100 ng/mL IGF-1 (Peprotech), and 50 μM pinacidil (Sigma).

Rodent surgery and laser-capture microscopy

Eight-ten weeks old male athymic rats (240-300 g) were anesthetized as described in "Experimental model and subject details" section. A thoracotomy exposed the heart and LAD was occluded for 60 minutes, reperfused, and the chest was closed. Four days after ischemia/reperfusion injury, rats were anesthetized by isoflurane inhalation, and mechanically ventilated. The heart was exposed via a second thoracotomy and 10×10^6 hiPSC-CMs were injected to the center of infarcted left ventricle wall (3-4 injections, 30 μl each).

RNA-seq preparation and sequencing

For *in vitro* samples, total RNA was isolated using the RNeasy Mini Kit according to the manufacturer's protocol, including DNase treatment. For *in vivo* samples, rat hearts were harvested, sliced, immediately embedded in Tissue-Tek® O.C.T. Compound (VWR), and stored at −80 °C. Tissues were sectioned at 10 μm thickness using a cryostat (Leica), and serial sections were mounted with 4', 6-diamidino-2-phenylindole (DAPI) to visualize the graft area through green fluorescent protein autofluorescence. The graft areas were captured from unstained unfixed specimens attached to membrane-coated using a laser capture microdissection system. Total RNA was extracted from the graft areas in rat heart tissues using the Arcturus PicoPure RNA isolation kit. RNA integrity (RNA integrity number equivalent ≥ 7) and quantity were determined using an Agilent 4200 Tapestation (Agilent Technologies). cDNA was synthesized using the SMART-Seq v4 ultra low input RNA kit for sequencing (Takara Bio). Library preparations were conducted using Nextera XT DNA Library Preparation Kit (Illumina) according to manufacturer's instructions. RNA-seq libraries were sequenced on an Illumina Next-Seq 500 with single end configuration (72 bp). Reads were mapped to a custom library, a hybrid of human (hg38) and rat (Rnor_6.0) genomes using STAR aligner[64]. Reads that mapped specifically and uniquely to the human genome were used for downstream analysis using Cufflinks[65]. Reads that mapped uniquely to the rat or to both rat and human genomes were not used. Gene ontology analysis was performed using topGO R package[66].

Histology (rodent heart)

Rat hearts of each time point were collected, sliced as described above, and immediately embedded in an OCT-embedding compound and stored at −80 °C. Tissues were sectioned at a thickness of 10 μm using a Cryostat (Leica), fixed in 4% paraformaldehyde for 5 minutes and stained with hematoxylin and eosin.

Cell injection preparation (pig surgery)

The day of cell transplant, hESC-CMs were thawed in RPMI 1640 without phenol red supplemented with 500 μg/mL bovine serum albumin and 100 KU/mL of DNAse I. Thawed hESC-CMs were collected by centrifugation at 400 g for 5 min at 4°C. hESC-CMs were washed twice with RPMI 1640 without phenol red and resuspended at 0.2×10^6 hESC-CMs/μL for percutaneous trans-endocardial transplant or 5 syringes for direct epicardial injection[20]. Syringes were individually packed in sterile containers and kept on ice until the moment of injection.

Pig surgery

As listed in Supplementary Table 2, WT controls, *HCN4* KO, *HCN4* KO/*KCNJ2* KI and *HCN4*/*CACNA1H* 2KO/*KCNJ2* KI hESC-CMs recipients underwent cell transplantation *via* percutaneous trans-endocardial injection using the NOGA-MyoStar platform, as previously described without myocardial infarction[20]. Briefly, percutaneous transplantation was performed by first mapping the left ventricle and then deliver five discrete endocardial injections of 150 μL each for total dose of 150×10^6 hESC-CMs to the anterior wall. Injections were only performed with excellent location and loop stability, ST-segment elevation and presence of premature ventricular contraction (PVC) with needle insertion in an appropriate location by electroanatomical map.

Cell transplantation for the remaining edits, namely *SLC8A1*/*HCN4* 2KO/*KCNJ2* KI and MEDUSA hESC-CMs, were performed by direct transepicardial surgical injection as previously described without myocardial infarction[20] due to discontinuation of the NOGA-MyoStar device by the manufacturer or availability of a suitable alternative platform for percutaneous delivery. Briefly, transepicardial injection via partial median sternotomy was performed to expose the anterior left ventricle. Purse-string sutures were preplaced at five discrete locations subtended by the LAD. After cinching the purse-string tightly around the needle, three injections of 150 μL each were performed by partial

withdrawal and lateral repositioning, for a total of 15 injections to deliver total dose of 150 x 10^6 hESC-CMs (most experiments) or 500 x 10^6 hESC-CMs for high-dose experiments with MEDUSA hESC-CMs. The pericardium was closed by primary repair and the sternum and chest reapproximated using standard surgical technique.

Telemetry characterization for EA and endpoint description

Telemetric ECG was continuously monitored in real-time from the time of transplant to detect arrythmia as previously described[20]. Briefly, semi-automated quantification of heart rate and arrhythmia was performed by a board-certified cardiologist using the ecgAUTO 3.5.5.28 software package (EMKA Technologies). EA was defined as sustained ventricular tachycardia lasting ≥ 30 seconds. Premature ventricular contractions (PVCs) were defined as 1 or 2 ectopic ventricular contractions and non-sustained ventricular tachycardia (NSVT) as ≥ 3 consecutive PVCs but < 30 seconds in duration. The original endpoint screening was set at day 14 after injection; to ensure absence of EA recrudescence, we extended the period of observation to 4-7 weeks (for 150 x 10^6 hESC-CMs dose) and 3 months (for 500 x 10^6 hESC-CMs dose). For control animals, the endpoints at 35- and 49-days post injection were chosen to support ex vivo electrophysiology studies of EA. Animals were removed from further study when they met prespecified endpoints defined as either spontaneous death (from arrhythmia or heart failure), clinically directed rescue antiarrhythmic therapy with amiodarone/lidocaine or euthanasia necessitated by sustained tachycardia > 350 bpm or signs of heart failure.

Histology (pig heart)

Whole heart was harvested and processed as previously described[20]. Briefly, the left ventricle was isolated from the whole heart, weighed, and embedded in 2% agar for slicing. Sections of 2.5 mm were obtained and fixed over-night in 4% paraformaldehyde at 4°C. Sections were then dehydrated in 70% ethanol before embedding in paraffin. Sections were then cut at 4 µm and placed on positively charged microscopy slides. Before staining, slides were progressively deparaffinized and re-hydrated by subsequent washes in xylene and ethanol at different concentration. After quenching in a mixture of hydrogen peroxide and methanol (1:20), heat-induced antigen retrieval treatment was performed using citrate buffer (or proteinase K digestion for MLC2a and MLC2v staining). Slides then were incubated in 1.5% normal horse serum diluted in DPBS (blocking buffer) for 1 hour at room temperature. Primary antibodies were diluted in blocking buffer and incubated over-night at 4°C. Secondary antibodies were diluted in blocking buffer and incubated for 1 hour at room temperature. For avidin-biotin complex (ABC) detection, slides were incubated with ABC Peroxidase for 30 min at room temperature before visualization with 3,3' diaminobenzidine. Graft was quantified using a custom code on whole-slide images and normalized on both area of block and LV weight (see Supplementary Table 2)[20]. For immunofluorescence, after secondary antibody incubation, slides were imaged with a 20X and 60X oil objective on a Nikon Eclipse microscope with Yokogawa W1 spinning disk head and Nikon A1R confocal microscope. Fiji software was used to process the images.

Cardiac slice model for electrical coupling

For cardiac slices, the animal was maintained under mechanical ventilation and isoflurane anesthesia while a sternotomy was performed to access the heart. The whole heart was perfused by cannulating the aorta to allow retrograde perfusion using St. Thomas cardioplegic solution until cardiac arrest (St. Thomas solution: 110mM NaCl, 16mM KCl, 16mM $MgCl_2$, 1.2mM $CaCl_2$, 10mM $NaHCO_3$). The whole heart was then harvested and kept at 4°C in perfusion buffer until slicing (4 mm sections as described above). The 4 mm slices were stored in Custodial solution (15 mM NaCl, 0.015 mM $CaCl_2$*$2H_2O$, 9 mM KCl, 4 mM $MgCl_2$, 18 mM Histidine HCl, 180 mM Histidine, 2 mM Tryptophan, 0.03 mM Mannitol, 0.001 mM Ketoglutarate, pH 7.4) at 4°C. A vibratome was used to generate ultra-thin (300 µm) living cardiac slices (LCS), which performed well when stored at 4°C for up to 24 h from the heart isolation. The LCS were generated with an adaptation of the previously described protocols[67,68]. Briefly, the 2.5 mm slice was trimmed to select the portion with the grafted cells, which was glued to the specimen holder and sliced into 300 µm LCS with a high-precision vibratome (7000smz-2, Camden Instrument) in slicing Tyrode's solution (10 mM BDM, 140 mM NaCl, 9mM KCl, 1 mM Glucose, 10 mM HEPES, 1mM MgCl2, 0.9 mM CaCl2, pH 7.4). The LCS were then loaded for 20 minutes (in Medium199) at 37°C with calcium (Fluo-4 AM 5 µg/ml) or voltage (FluoVolt - 1:1000 dilution as per manufacturer's instruction) indicators and used for optical mapping. An upright Nikon ECLIPSE FN1 microscope with a Kinetix sCMOS camera was used to record videos at 200 frames per second. The experiments were performed at 37°C in Recording Tyrode's solution (10 mM BDM, 140 mM NaCl, 5 mM KCl, 1 mM Glucose, 10 mM HEPES, 1 mM MgCl2, 1.8 mM CaCl2, pH 7.4) and monofilament anchors were positioned on top to keep the LCS flat and facilitate the live imaging. The LCS were electrically paced by field stimulation with two custom-made platinum electrodes connected to an IonOptix MyoPacer at 20V (5 milliseconds duration). A parallel bipolar microelectrode was used to electrically pace (1-2V and 5 milliseconds duration) a small portion of the LCS, and therefore apply a point stimulation either to the host tissue or to the graft. Calcium and voltage traces and kinetics were analyzed with Labchart8. After analysis, LCS were then fixed in 4% paraformaldehyde and processed for staining as described above.

QUANTIFICATION AND STATISTICAL ANALYSIS

For *in vitro* studies, the number of biological replicates (intended as independent batches of hESC-CMs differentiated and harvested at different days) is detailed in the corresponding figure legends. For each experiment, a minimum of three technical replicates were used. Statistical testing was performed using an unpaired t-test for two-group comparisons. For multiple-group comparison, one-way or two-way ANOVA with a post-hoc Sidak correction was used. Differences between groups were considered statistically significant when p value was < 0.05. All analyses were performed using GraphPad Prism software (Version 9.3.1). All results are expressed as mean ± SEM, unless otherwise stated.

Supplementary items titles.

Supplementary Table 1. Extended top 40 GO terms from Supplementary Fig. 1B.

Supplementary Table 2. Graft size quantification.

Supplementary Table 3. Oligonucleotides sequences for cloning gRNAs and genotyping.

Supplementary Table 4. Oligonucleotides sequences for RTqPCR.

Supplementary Video 1. Injection of hPSC-CMs into uninjured pig heart through direct thoracotomy.

Supplementary Video 2. Point stimulation of host myocardium and calcium transient elicited in graft (related to Figure 7D).

Supplementary Video 3. Point stimulation of graft and calcium transient elicited in host myocardium (related to Supplementary Fig. 6E).

References

1. Bergmann, O., Bhardwaj, R.D., Bernard, S., Zdunek, S., Barnabe-Heider, F., Walsh, S., Zupicich, J., Alkass, K., Buchholz, B.A., Druid, H., et al. (2009). Evidence for cardiomyocyte renewal in humans. Science *324*, 98-102. 10.1126/science.1164680.

2. Marchiano, S., Bertero, A., and Murry, C.E. (2019). Learn from Your Elders: Developmental Biology Lessons to Guide Maturation of Stem Cell-Derived Cardiomyocytes. Pediatr Cardiol *40*, 1367-1387. 10.1007/s00246-019-02165-5.

3. Velagaleti, R.S., Pencina, M.J., Murabito, J.M., Wang, T.J., Parikh, N.I., D'Agostino, R.B., Levy, D., Kannel, W.B., and Vasan, R.S. (2008). Long-term trends in the incidence of heart failure after myocardial infarction. Circulation *118*, 2057-2062. 10.1161/CIRCULATIONAHA.108.784215.

4. Prabhu, S.D., and Frangogiannis, N.G. (2016). The Biological Basis for Cardiac Repair After Myocardial Infarction: From Inflammation to Fibrosis. Circ Res *119*, 91-112. 10.1161/CIRCRESAHA.116.303577.

5. Diseases, G.B.D., and Injuries, C. (2020). Global burden of 369 diseases and injuries in 204 countries and territories, 1990-2019: a systematic analysis for the Global Burden of Disease Study 2019. Lancet *396*, 1204-1222. 10.1016/S0140-6736(20)30925-9.

6. Roth, G.A., Mensah, G.A., Johnson, C.O., Addolorato, G., Ammirati, E., Baddour, L.M., Barengo, N.C., Beaton, A.Z., Benjamin, E.J., Benziger, C.P., et al. (2020). Global Burden of Cardiovascular Diseases and Risk Factors, 1990-2019: Update From the GBD 2019 Study. J Am Coll Cardiol *76*, 2982-3021. 10.1016/j.jacc.2020.11.010.

7. Eschenhagen, T., Bolli, R., Braun, T., Field, L.J., Fleischmann, B.K., Frisen, J., Giacca, M., Hare, J.M., Houser, S., Lee, R.T., et al. (2017). Cardiomyocyte Regeneration: A Consensus Statement. Circulation *136*, 680-686. 10.1161/CIRCULATIONAHA.117.029343.

8. Nakamura, K., and Murry, C.E. (2019). Function Follows Form- A Review of Cardiac Cell Therapy. Circ J *83*, 2399-2412. 10.1253/circj.CJ-19-0567.

9. Bertero, A., and Murry, C.E. (2018). Hallmarks of cardiac regeneration. Nat Rev Cardiol *15*, 579-580. 10.1038/s41569-018-0079-8.

10. van Laake, L.W., Passier, R., Monshouwer-Kloots, J., Verkleij, A.J., Lips, D.J., Freund, C., den Ouden, K., Ward-van Oostwaard, D., Korving, J., Tertoolen, L.G., et al. (2007). Human embryonic stem cell-derived cardiomyocytes survive and mature in the mouse heart and transiently improve function after myocardial infarction. Stem Cell Res *1*, 9-24. 10.1016/j.scr.2007.06.001.

11. Caspi, O., Huber, I., Kehat, I., Habib, M., Arbel, G., Gepstein, A., Yankelson, L., Aronson, D., Beyar, R., and Gepstein, L. (2007). Transplantation of human embryonic stem cell-derived cardiomyocytes improves myocardial performance in infarcted rat hearts. J Am Coll Cardiol *50*, 1884-1893. 10.1016/j.jacc.2007.07.054.

12. Shiba, Y., Fernandes, S., Zhu, W.Z., Filice, D., Muskheli, V., Kim, J., Palpant, N.J., Gantz, J., Moyes, K.W., Reinecke, H., et al. (2012). Human ES-cell-derived cardiomyocytes electrically couple and suppress arrhythmias in injured hearts. Nature *489*, 322-325. 10.1038/nature11317.

13. Shiba, Y., Gomibuchi, T., Seto, T., Wada, Y., Ichimura, H., Tanaka, Y., Ogasawara, T., Okada, K., Shiba, N., Sakamoto, K., et al. (2016). Allogeneic transplantation of iPS cell-derived cardiomyocytes regenerates primate hearts. Nature *538*, 388-391. 10.1038/nature19815.

14. Liu, Y.W., Chen, B., Yang, X., Fugate, J.A., Kalucki, F.A., Futakuchi-Tsuchida, A., Couture, L., Vogel, K.W., Astley, C.A., Baldessari, A., et al. (2018). Human embryonic stem cell-derived cardiomyocytes restore function in infarcted hearts of non-human primates. Nat Biotechnol *36*, 597-605. 10.1038/nbt.4162.

15. Selvakumar, D., Clayton, Z.E., and Chong, J.J.H. (2020). Robust Cardiac Regeneration: Fulfilling the Promise of Cardiac Cell Therapy. Clin Ther *42*, 1857-1879. 10.1016/j.clinthera.2020.08.008.

16. Karbassi, E., Fenix, A., Marchiano, S., Muraoka, N., Nakamura, K., Yang, X., and Murry, C.E. (2020). Cardiomyocyte maturation: advances in knowledge and implications for regenerative medicine. Nat Rev Cardiol *17*, 341-359. 10.1038/s41569-019-0331-x.

17. Guo, Y., and Pu, W.T. (2020). Cardiomyocyte Maturation: New Phase in Development. Circ Res *126*, 1086-1106. 10.1161/CIRCRESAHA.119.315862.

18. Peinkofer, G., Burkert, K., Urban, K., Krausgrill, B., Hescheler, J., Saric, T., and Halbach, M. (2016). From Early Embryonic to Adult Stage: Comparative Study of Action Potentials of Native and Pluripotent Stem Cell-Derived Cardiomyocytes. Stem Cells Dev *25*, 1397-1406. 10.1089/scd.2016.0073.

19. Romagnuolo, R., Masoudpour, H., Porta-Sanchez, A., Qiang, B., Barry, J., Laskary, A., Qi, X., Masse, S., Magtibay, K., Kawajiri, H., et al. (2019). Human Embryonic Stem Cell-Derived Cardiomyocytes Regenerate the Infarcted Pig Heart but Induce Ventricular Tachyarrhythmias. Stem Cell Reports *12*, 967-981. 10.1016/j.stemcr.2019.04.005.

20. Nakamura, K., Neidig, L.E., Yang, X., Weber, G.J., El-Nachef, D., Tsuchida, H., Dupras, S., Kalucki, F.A., Jayabalu, A., Futakuchi-Tsuchida, A., et al. (2021). Pharmacologic therapy for engraftment arrhythmia induced by transplantation of human cardiomyocytes. Stem Cell Reports *16*, 2473-2487. 10.1016/j.stemcr.2021.08.005.

21. Yu, J.K., Franceschi, W., Huang, Q., Pashakhanloo, F., Boyle, P.M., and Trayanova, N.A. (2019). A comprehensive, multiscale framework for evaluation of arrhythmias arising from cell therapy in the whole post-myocardial infarcted heart. Sci Rep *9*, 9238. 10.1038/s41598-019-45684-0.

22. Selvakumar, D., Clayton, Z.E., Prowse, A., Dingwall, S., George, J., Shah, H., Chen, S., Hume, R.D., Tjahjadi, L., Igoor, S., et al. (2022). Cellular Heterogeneity of Pluripotent Stem Cell Derived Cardiomyocyte Grafts is Mechanistically Linked to Treatable Arrhythmias. bioRxiv, 2022.2009.2015.500719. 10.1101/2022.09.15.500719.

23. Filice, D., Dhahri, W., Solan, J.L., Lampe, P.D., Steele, E., Milani, N., Van Biber, B., Zhu, W.Z., Valdman, T.S., Romagnuolo, R., et al. (2020). Optical mapping of human embryonic stem cell-derived cardiomyocyte graft electrical activity in injured hearts. Stem Cell Res Ther *11*, 417. 10.1186/s13287-020-01919-w.

24. Ma, J., Guo, L., Fiene, S.J., Anson, B.D., Thomson, J.A., Kamp, T.J., Kolaja, K.L., Swanson, B.J., and January, C.T. (2011). High purity human-induced pluripotent stem cell-derived

cardiomyocytes: electrophysiological properties of action potentials and ionic currents. Am J Physiol Heart Circ Physiol *301*, H2006-2017. 10.1152/ajpheart.00694.2011.

25. Wang, L., Wada, Y., Ballan, N., Schmeckpeper, J., Huang, J., Rau, C.D., Wang, Y., Gepstein, L., and Knollmann, B.C. (2021). Triiodothyronine and dexamethasone alter potassium channel expression and promote electrophysiological maturation of human-induced pluripotent stem cell-derived cardiomyocytes. J Mol Cell Cardiol *161*, 130-138. 10.1016/j.yjmcc.2021.08.005.

26. Zhao, Z., Lan, H., El-Battrawy, I., Li, X., Buljubasic, F., Sattler, K., Yucel, G., Lang, S., Tiburcy, M., Zimmermann, W.H., et al. (2018). Ion Channel Expression and Characterization in Human Induced Pluripotent Stem Cell-Derived Cardiomyocytes. Stem Cells Int *2018*, 6067096. 10.1155/2018/6067096.

27. Ivashchenko, C.Y., Pipes, G.C., Lozinskaya, I.M., Lin, Z., Xiaoping, X., Needle, S., Grygielko, E.T., Hu, E., Toomey, J.R., Lepore, J.J., and Willette, R.N. (2013). Human-induced pluripotent stem cell-derived cardiomyocytes exhibit temporal changes in phenotype. Am J Physiol Heart Circ Physiol *305*, H913-922. 10.1152/ajpheart.00819.2012.

28. Kadota, S., Pabon, L., Reinecke, H., and Murry, C.E. (2017). In Vivo Maturation of Human Induced Pluripotent Stem Cell-Derived Cardiomyocytes in Neonatal and Adult Rat Hearts. Stem Cell Reports *8*, 278-289. 10.1016/j.stemcr.2016.10.009.

29. Kim, J.J., Yang, L., Lin, B., Zhu, X., Sun, B., Kaplan, A.D., Bett, G.C., Rasmusson, R.L., London, B., and Salama, G. (2015). Mechanism of automaticity in cardiomyocytes derived from human induced pluripotent stem cells. J Mol Cell Cardiol *81*, 81-93. 10.1016/j.yjmcc.2015.01.013.

30. Zhang, X.H., and Morad, M. (2020). Ca(2+) signaling of human pluripotent stem cells-derived cardiomyocytes as compared to adult mammalian cardiomyocytes. Cell Calcium *90*, 102244. 10.1016/j.ceca.2020.102244.

31. Tsutsui, K., Monfredi, O.J., Sirenko-Tagirova, S.G., Maltseva, L.A., Bychkov, R., Kim, M.S., Ziman, B.D., Tarasov, K.V., Tarasova, Y.S., Zhang, J., et al. (2018). A coupled-clock system drives the automaticity of human sinoatrial nodal pacemaker cells. Sci Signal *11*. 10.1126/scisignal.aap7608.

32. Lakatta, E.G., Maltsev, V.A., and Vinogradova, T.M. (2010). A coupled SYSTEM of intracellular Ca2+ clocks and surface membrane voltage clocks controls the timekeeping mechanism of the heart's pacemaker. Circ Res *106*, 659-673. 10.1161/CIRCRESAHA.109.206078.

33. Lyashkov, A.E., Behar, J., Lakatta, E.G., Yaniv, Y., and Maltsev, V.A. (2018). Positive Feedback Mechanisms among Local Ca Releases, NCX, and ICaL Ignite Pacemaker Action Potentials. Biophys J *114*, 1176-1189. 10.1016/j.bpj.2017.12.043.

34. Maltsev, V.A., and Lakatta, E.G. (2012). The funny current in the context of the coupled-clock pacemaker cell system. Heart Rhythm *9*, 302-307. 10.1016/j.hrthm.2011.09.022.

35. Mesirca, P., Torrente, A.G., and Mangoni, M.E. (2015). Functional role of voltage gated Ca(2+) channels in heart automaticity. Front Physiol *6*, 19. 10.3389/fphys.2015.00019.

36. Verkerk, A.O., van Ginneken, A.C., and Wilders, R. (2009). Pacemaker activity of the human sinoatrial node: role of the hyperpolarization-activated current, I(f). Int J Cardiol *132*, 318-336. 10.1016/j.ijcard.2008.12.196.

37. Kernik, D.C., Morotti, S., Wu, H., Garg, P., Duff, H.J., Kurokawa, J., Jalife, J., Wu, J.C., Grandi, E., and Clancy, C.E. (2019). A computational model of induced pluripotent stem-cell derived cardiomyocytes incorporating experimental variability from multiple data sources. J Physiol *597*, 4533-4564. 10.1113/JP277724.

38. DiFrancesco, D. (2010). The role of the funny current in pacemaker activity. Circ Res *106*, 434-446. 10.1161/CIRCRESAHA.109.208041.

39. Niehoff, J., Matzkies, M., Nguemo, F., Hescheler, J., and Reppel, M. (2019). The Effect of Antiarrhythmic Drugs on the Beat Rate Variability of Human Embryonic and Human Induced Pluripotent Stem Cell Derived Cardiomyocytes. Sci Rep *9*, 14106. 10.1038/s41598-019-50557-7.

40. Chen, K., Zuo, D., Wang, S.Y., and Chen, H. (2018). Kir2 inward rectification-controlled precise and dynamic balances between Kir2 and HCN currents initiate pacemaking activity. FASEB J *32*, 3047-3057. 10.1096/fj.201701260R.

41. Liu, Q.H., Li, X.L., Xu, Y.W., Lin, Y.Y., Cao, J.M., and Wu, B.W. (2012). A novel discovery of IK1 channel agonist: zacopride selectively enhances IK1 current and suppresses triggered arrhythmias in the rat. J Cardiovasc Pharmacol *59*, 37-48. 10.1097/FJC.0b013e3182350bcc.

42. Xiang, Z., Thompson, A.D., Brogan, J.T., Schulte, M.L., Melancon, B.J., Mi, D., Lewis, L.M., Zou, B., Yang, L., Morrison, R., et al. (2011). The Discovery and Characterization of ML218: A Novel, Centrally Active T-Type Calcium Channel Inhibitor with Robust Effects in STN Neurons and in a Rodent Model of Parkinson's Disease. ACS Chem Neurosci *2*, 730-742. 10.1021/cn200090z.

43. Leuranguer, V., Mangoni, M.E., Nargeot, J., and Richard, S. (2001). Inhibition of T-type and L-type calcium channels by mibefradil: physiologic and pharmacologic bases of cardiovascular effects. J Cardiovasc Pharmacol *37*, 649-661. 10.1097/00005344-200106000-00002.

44. Godfraind, T. (2017). Discovery and Development of Calcium Channel Blockers. Front Pharmacol *8*, 286. 10.3389/fphar.2017.00286.

45. Vohra, J. (1982). Verapamil in cardiac arrhythmias: an overview. Clin Exp Pharmacol Physiol Suppl *6*, 129-134.

46. Watanabe, Y., Koide, Y., and Kimura, J. (2006). Topics on the Na+/Ca2+ exchanger: pharmacological characterization of Na+/Ca2+ exchanger inhibitors. J Pharmacol Sci *102*, 7-16. 10.1254/jphs.fmj06002x2.

47. Tanaka, H., Nishimaru, K., Aikawa, T., Hirayama, W., Tanaka, Y., and Shigenobu, K. (2002). Effect of SEA0400, a novel inhibitor of sodium-calcium exchanger, on myocardial ionic currents. Br J Pharmacol *135*, 1096-1100. 10.1038/sj.bjp.0704574.

48. Li, S., Chen, G., and Li, R.A. (2013). Calcium signalling of human pluripotent stem cell-derived cardiomyocytes. J Physiol *591*, 5279-5290. 10.1113/jphysiol.2013.256495.

49. Lieu, D.K., Fu, J.D., Chiamvimonvat, N., Tung, K.C., McNerney, G.P., Huser, T., Keller, G., Kong, C.W., and Li, R.A. (2013). Mechanism-based facilitated maturation of human pluripotent stem cell-derived cardiomyocytes. Circ Arrhythm Electrophysiol *6*, 191-201. 10.1161/CIRCEP.111.973420.

50. Sun, Y., Timofeyev, V., Dennis, A., Bektik, E., Wan, X., Laurita, K.R., Deschenes, I., Li, R.A., and Fu, J.D. (2017). A Singular Role of IK1 Promoting the Development of Cardiac Automaticity during Cardiomyocyte Differentiation by IK1 -Induced Activation of Pacemaker Current. Stem Cell Rev Rep *13*, 631-643. 10.1007/s12015-017-9745-1.

51. Hibino, H., Inanobe, A., Furutani, K., Murakami, S., Findlay, I., and Kurachi, Y. (2010). Inwardly rectifying potassium channels: their structure, function, and physiological roles. Physiol Rev *90*, 291-366. 10.1152/physrev.00021.2009.

52. Costa, A.D.S., Mortensen, P., Hortigon-Vinagre, M.P., van der Heyden, M.A.G., Burton, F.L., Gao, H., Simitev, R.D., and Smith, G.L. (2021). Electrophysiology of hiPSC-Cardiomyocytes Co-Cultured with HEK Cells Expressing the Inward Rectifier Channel. Int J Mol Sci *22*. 10.3390/ijms22126621.

53. Bertero, A., Pawlowski, M., Ortmann, D., Snijders, K., Yiangou, L., Cardoso de Brito, M., Brown, S., Bernard, W.G., Cooper, J.D., Giacomelli, E., et al. (2016). Optimized inducible shRNA and CRISPR/Cas9 platforms for in vitro studies of human development using hPSCs. Development *143*, 4405-4418. 10.1242/dev.138081.

54. El-Brolosy, M.A., Kontarakis, Z., Rossi, A., Kuenne, C., Gunther, S., Fukuda, N., Kikhi, K., Boezio, G.L.M., Takacs, C.M., Lai, S.L., et al. (2019). Genetic compensation triggered by mutant mRNA degradation. Nature *568*, 193-197. 10.1038/s41586-019-1064-z.

55. Bers, D.M. (2008). Calcium cycling and signaling in cardiac myocytes. Annu Rev Physiol *70*, 23-49. 10.1146/annurev.physiol.70.113006.100455.

56. Henderson, S.A., Goldhaber, J.I., So, J.M., Han, T., Motter, C., Ngo, A., Chantawansri, C., Ritter, M.R., Friedlander, M., Nicoll, D.A., et al. (2004). Functional adult myocardium in the absence of Na+-Ca2+ exchange: cardiac-specific knockout of NCX1. Circ Res *95*, 604-611. 10.1161/01.RES.0000142316.08250.68.

57. Gerbin, K.A., Yang, X., Murry, C.E., and Coulombe, K.L. (2015). Enhanced Electrical Integration of Engineered Human Myocardium via Intramyocardial versus Epicardial Delivery in Infarcted Rat Hearts. PLoS One *10*, e0131446. 10.1371/journal.pone.0131446.

58. Clauss, S., Bleyer, C., Schuttler, D., Tomsits, P., Renner, S., Klymiuk, N., Wakili, R., Massberg, S., Wolf, E., and Kaab, S. (2019). Animal models of arrhythmia: classic electrophysiology to genetically modified large animals. Nat Rev Cardiol *16*, 457-475. 10.1038/s41569-019-0179-0.

59. Antzelevitch, C., and Burashnikov, A. (2011). Overview of Basic Mechanisms of Cardiac Arrhythmia. Card Electrophysiol Clin *3*, 23-45. 10.1016/j.ccep.2010.10.012.

60. Reuter, H., Henderson, S.A., Han, T., Mottino, G.A., Frank, J.S., Ross, R.S., Goldhaber, J.I., and Philipson, K.D. (2003). Cardiac excitation-contraction coupling in the absence of Na(+) - Ca2+ exchange. Cell Calcium *34*, 19-26. 10.1016/s0143-4160(03)00018-6.

61. Palpant, N.J., Pabon, L., Friedman, C.E., Roberts, M., Hadland, B., Zaunbrecher, R.J., Bernstein, I., Zheng, Y., and Murry, C.E. (2017). Generating high-purity cardiac and endothelial derivatives from patterned mesoderm using human pluripotent stem cells. Nat Protoc *12*, 15-31. 10.1038/nprot.2016.153.

62. Bertero, A., Fields, P.A., Smith, A.S.T., Leonard, A., Beussman, K., Sniadecki, N.J., Kim, D.H., Tse, H.F., Pabon, L., Shendure, J., et al. (2019). Chromatin compartment dynamics in a

haploinsufficient model of cardiac laminopathy. J Cell Biol *218*, 2919-2944. 10.1083/jcb.201902117.

63. Laflamme, M.A., Chen, K.Y., Naumova, A.V., Muskheli, V., Fugate, J.A., Dupras, S.K., Reinecke, H., Xu, C., Hassanipour, M., Police, S., et al. (2007). Cardiomyocytes derived from human embryonic stem cells in pro-survival factors enhance function of infarcted rat hearts. Nat Biotechnol *25*, 1015-1024. 10.1038/nbt1327.

64. Dobin, A., Davis, C.A., Schlesinger, F., Drenkow, J., Zaleski, C., Jha, S., Batut, P., Chaisson, M., and Gingeras, T.R. (2013). STAR: ultrafast universal RNA-seq aligner. Bioinformatics *29*, 15-21. 10.1093/bioinformatics/bts635.

65. Trapnell, C., Roberts, A., Goff, L., Pertea, G., Kim, D., Kelley, D.R., Pimentel, H., Salzberg, S.L., Rinn, J.L., and Pachter, L. (2012). Differential gene and transcript expression analysis of RNA-seq experiments with TopHat and Cufflinks. Nat Protoc *7*, 562-578. 10.1038/nprot.2012.016.

66. Alexa, A., Rahnenfuhrer, J., and Lengauer, T. (2006). Improved scoring of functional groups from gene expression data by decorrelating GO graph structure. Bioinformatics *22*, 1600-1607. 10.1093/bioinformatics/btl140.

67. Wen, Q., Gandhi, K., Capel, R.A., Hao, G., O'Shea, C., Neagu, G., Pearcey, S., Pavlovic, D., Terrar, D.A., Wu, J., et al. (2018). Transverse cardiac slicing and optical imaging for analysis of transmural gradients in membrane potential and Ca(2+) transients in murine heart. J Physiol *596*, 3951-3965. 10.1113/JP276239.

68. Watson, S.A., Scigliano, M., Bardi, I., Ascione, R., Terracciano, C.M., and Perbellini, F. (2017). Preparation of viable adult ventricular myocardial slices from large and small mammals. Nat Protoc *12*, 2623-2639. 10.1038/nprot.2017.139.

69. Lacoste, A., Berenshteyn, F., and Brivanlou, A.H. (2009). An efficient and reversible transposable system for gene delivery and lineage-specific differentiation in human embryonic stem cells. Cell Stem Cell *5*, 332-342. 10.1016/j.stem.2009.07.011.

70. Ran, F.A., Hsu, P.D., Wright, J., Agarwala, V., Scott, D.A., and Zhang, F. (2013). Genome engineering using the CRISPR-Cas9 system. Nat Protoc *8*, 2281-2308. 10.1038/nprot.2013.143.

71. Hockemeyer, D., Soldner, F., Beard, C., Gao, Q., Mitalipova, M., DeKelver, R.C., Katibah, G.E., Amora, R., Boydston, E.A., Zeitler, B., et al. (2009). Efficient targeting of expressed and silent genes in human ESCs and iPSCs using zinc-finger nucleases. Nat Biotechnol *27*, 851-857. 10.1038/nbt.1562.

72. Perez, A.R., Pritykin, Y., Vidigal, J.A., Chhangawala, S., Zamparo, L., Leslie, C.S., and Ventura, A. (2017). GuideScan software for improved single and paired CRISPR guide RNA design. Nat Biotechnol *35*, 347-349. 10.1038/nbt.3804.

73. Bae, S., Park, J., and Kim, J.S. (2014). Cas-OFFinder: a fast and versatile algorithm that searches for potential off-target sites of Cas9 RNA-guided endonucleases. Bioinformatics *30*, 1473-1475. 10.1093/bioinformatics/btu048.

KEY RESOURCE TABLE

REAGENT or RESOURCE	SOURCE	IDENTIFIER
Antibodies (working concentration, application*)		
NCX1 Mouse monoclonal (dil. 1:200, WB)	Swant	RRID: AB_2716744
Cardiac Troponin T Antibody Rabbit polyclonal (dil. 1:1000, WB)	Abcam	RRID: AB_956386
HCN4 Mouse monoclonal (S114/10) (dil. 1:200, WB)	NovusBio	RRID: AB_2935644
GAPDH Mouse monoclonal (dil. 1:3000, WB)	Abcam	RRID: AB_2107448
Cardiac Troponin T-APC REA400 (dil. 1:100, FC)	Miltenyi Biotec	RRID: AB_2783887
REA293-APC (dil. 1:100, FC)	Miltenyi Biotec	RRID: AB_2733446
Mouse monoclonal anti-CD56-PE (dil. 1:5, FC)	BD Bioscience	RRID: AB_395906
Mouse monoclonal anti-PDGFRα-APC (dil. 1:10, FC)	R&D System	RRID: AB_883910
Mouse monoclonal IgG1-PE (dil. 1:5, FC)	BD Biosceince	RRID: AB_396091
Mouse monoclonal IgG1-APC (dil. 1:10, FC)	R&D System	RRID: AB_398576
Rabbit monoclonal anti NKX2.5 (dil. 1:200, FC)	Cell Signaling	RRID: AB_2935645
Rabbit IgG1 (dil. 1:500, FC)	Cell Signaling	RRID: AB_1031062
Slow Skeletal Troponin I Mouse monoclonal (dil. 1:200, IHC/IF)	Novus Biological	RRID: AB_2935646
β-Myosin Heavy chain Mouse A4.951 (dil. 1:1, IHC/IF)	Developmental Studies Hybridoma Bank	RRID: AB_528385
Biotin-SP-conjugated AffiniPure Goat anti-Mouse IgG (dil. 1:500, IHC)	Jackson Immunoresearch	RRID: AB_2338557
Cardiac Troponin I Rabbit Monoclonal (dil. 1:100, IF)	Abcam	RRID: AB_869983
MLC2a Mouse monoclonal (dil. 1:500, IF)	BD Life Science	RRID: AB_2739265
MLC2v Rabbit polyclonal (dil. 1:100, IF)	Proteintech	RRID: AB_2147453
Connexin43 Rabbit polyclonal (dil 1:200, IF)	Merck	RRID: AB_476857
Desmin goat polyclonal (dil. 1:100)	Origene	RRID: AB_2935647
Goat anti-Mouse IgG (H+L) Cross-Adsorbed Secondary Antibody, Alexa Fluor 680 (dil. 1:1000, IF)	Life Technologies	RRID: AB_141436
Goat anti-Rabbit IgG (H+L) Cross-Adsorbed Secondary Antibody, Alexa Fluor 488 (dil. 1:1000, IF/FC)	Life Technologies	RRID: AB_143165
Donkey anti-Goat IgG (H+L) Cross-Adsorbed Secondary Antibody, Alexa Fluor 647 (dil. 1:1000, IF)	Life Technologies	RRID: AB_141844
**WB: Western blotting, FC: flow cytometry; IF: Immunofluorescence, IHC: Immunohistochemistry*		
Bacterial and virus strains		
α-Select Gold Efficiency Chemically competent cells	BIOLINE	Cat # BIO-85027
Chemicals, peptides, and recombinant proteins		
Fast Digest BpiI	Thermo Scientific	Cat # FD1014
Fast Digest Mph1103I (NsiI)	Thermo Scientific	Cat # FD0734
Fast Digest Pfi23II (BsiWI)	Thermo Scientific	Cat # FD0854
Fast Digest SgsI (AscI)	Thermo Scientific	Cat # FD1894
Fast Digest NotI	Thermo Scientific	Cat # FD0593
Fast Digest ScaI	Thermo Scientific	Cat # FD0434
Fast Digest BamHI	Thermo Scientific	Cat # FD0054
Fast Digest Bsu15I (ClaI)	Thermo Scientific	Cat # FD0143
Fast Digest NcoI	Thermo Scientific	Cat # FD0575
T4 DNA Ligase Reaction Buffer	New England Bio-Labs	Cat # B0202S
Quick Ligation Kit	New England Bio-Labs	Cat # M2200S
T4 Polynucleotide Kinase	New England Bio-Labs	Cat # M0201S
Ampicillin sodium salt	Sigma-Aldrich	Cat # A0166
LB Agar, Miller (Luria-Bertani)	BD Life Sciences	Cat # 244520

LB Broth, Miller (Luria-Bertani)	BD Life Sciences	Cat # 244620
Granulated Agar	BD Life Sciences	Cat # 214530
OPTI-MEM Reduced Serum Medium	Gibco	Cat # 31985062
GeneJuice Transfection Reagent	Sigma-Aldrich	Cat # 70967-3
DPBS, no calcium, no magnesium	Gibco	Cat # 14190-250
mTeSR Plus	Stem Cell Technologies	Cat # 100-0276
Essential 8™ Medium	Thermo Scientific	Cat # A1517001
Matrigel Growth Factor Reduced (GFR), Phenol Red-free, LDEV-free	Corning	Cat # 356231
rLaminin-521 (human)	Corning	Cat # 354221
Y-27632 dihydrochloride	Tocris	Cat # 1254-50
Versene Solution	Gibco	Cat # 15040066
TrypLE Select	Gibco	Cat # A12177-02
RPMI 1640 medium	Gibco	Cat # 11875119
RPMI 1640 medium, no glucose	Life Technologies	Cat # 11879020
RPMI 1640 medium, no phenol red	Life Technologies	Cat # 11835055
Bovine Serum Albumin, suitable for cell culture	Sigma-Aldrich	Cat # A9418-50G
L-Ascorbic Acid 2-phosphate sesquimagnesium salt hydrate	Sigma-Aldrich	Cat # A8960-5G
CHIR99021	Cayman	Cat # 13122
Wnt-C59	Selleck Chemicals	Cat # S7037
Sodium L-lactate	Sigma-Aldrich	Cat # L7022-10G
B-27 Supplement (50X), serum free	Gibco	Cat # 17504044
CryoStor cell cryopreservation media - CS10	Sigma-Aldrich	Cat # C2874
Q5 High-Fidelity 2X Master Mix	New England Bio-Labs	Cat # M0492S
M-MLV Reverse Transcriptase	Invitrogen	Cat # 28025013
RNaseOUT Recombinant Ribonuclease Inhibitor	Invitrogen	Cat # 10777019
SYBR Select Master Mix	Applied Biosystems	Cat # 4472913
SpCas9 2NLS Nuclease	Synthego	NA
4-15% Mini-PROTEAN TGX Precast Protein Gel	Biorad	Cat # 4561084
Immobilon-P membrane (0.45 µm)	Millipore	Cat # IPVH00010
Hematoxylin Solution (Mayer's, Modified)	Abcam	Cat # ab220365
Hoechst 33342 Solution	Thermo Scientific	Cat # 62249
DNase I	Millipore	Cat # 260913
Fluo-4 AM	Invitrogen	Cat # 14201
Ivabradine hydrochloride	Tocris	Cat # 6542
ML-218 hydrochloride	Tocris	Cat # 4507
Mibefradil dihydrochloride	Tocris	Cat # 2198
Zacopride hydrochloride	Tocris	Cat # 1795
SEA0400	Tocris	Cat # 6164
KB-R7943 mesylate	Tocris	Cat # 1244
Verapamil hydrochloride	Tocris	Cat # 0654
Cyclosporine A	Cayman	Cat # 12088
Buprenorphine SR-Lab	ZooPharm	NA
Euthasol	Virbac	NA
Abatacept (CTLA4-Ig)	Bristol-Myers Squibb	NA
4% Paraformaldehyde	Santa Cruz Biotechnology	Cat # sc-281692
Membrane-coated slides	Leica Microsystem	Cat #11600289
VECTASTAIN Elite ABC HRP kit	Vector Laboratories	Cat # PK-6100
SIGMAFAST™ 3,3′-Diaminobenzidine tablets	Sigma-Aldrich	Cat # D4168
HEPES	Fisher	Cat # BP310-500

D-(+)-Glucose	Sigma-Aldrich	Cat # G5767
EGTA	Sigma-Aldrich	Cat # E3889
ATP Magnesium Salt	Sigma-Aldrich	Cat # A9187
Amphotericin B	Sigma-Aldrich	Cat # A9528
Tetraethylammonium Chloride	Sigma-Aldrich	Cat # T2265
4-Aminopyridine	Sigma-Aldrich	Cat # 275875
Tetraethylammonium Hydroxide	Sigma-Aldrich	Cat # 177806
Cesium Chloride	Sigma-Aldrich	Cat # 289329
GTP Sodium Salt Hydrate	Sigma-Aldrich	Cat # G8877
Cesium Hydroxide Monohydrate	Sigma-Aldrich	Cat # 516988
Critical commercial assays		
QIAEX II Gel Extraction Kit	Qiagen	Cat # 20021
QIAprep Miniprep Kit	Qiagen	Cat # 27104
QIAfilter Plasmid Midiprep Kit	Qiagen	Cat # 12243
BD StemflowTM Human and Mouse Pluripotent Stem Cell Analysis Kit	BD Life Sciences	Cat # 560477
RNAesy Mini kit	Qiagen	Cat # 74106
PicoPure® RNA Isolation Kit	Applied Biosystems	Cat # KIT0204
Leica Laser Microdissection (LMD) System	Leica Microsystem	Cat # 8118616
Pierce BCA Protein assay kit	Thermo Scientific	Cat # 23225
NEBuilder HiFi DNA Assembly Cloning kit	New England Bio-Labs	Cat # E5520S
Maestro Pro multiwell microelectrode array (MEA)	Axion Biosystems	Cat #CP-MCV48W-UPF
Deposited data		
RNA-seq data set	This paper	GSE190758
Experimental models: Cell lines		
Human induced-pluripotent Stem Cells – 253G1 -Camp3	Kyoto University	CVCL_B518[28]
Human Embryonic Stem Cells – RUESe002-A	Rockefeller University	CVCL_C1W3[69]
Experimental models: Organisms/strains		
Athymic male Sprague Dawley rats (Hsd:RH-*Foxn1*^{rnu})	Envigo	RGD_5508395
Yucatan minipigs	Premier BioSource	NA
Oligonucleotides (see also Methods Tables 1, 2)		
HCN4_gRNA1 TCGTGAAGCGGACAATGCGC	This paper	NA
CACNA1H_gRNA1 GGATTTCTTCATCGTCGTGG	This paper	NA
CACNA1H_gRNA2 GACCATCTCCACCGCAAAAA	This paper	NA
HCN4_gRNA1_KI CAGCTTGTCCATGGCGCCAG	This paper	NA
HCN4_gRNA2_KI GGCAGCTTGTCCATGGCGCC	This paper	NA
SLC8A1_gRNA1 GGATCATATTACTGTAAGAA	Synthego	NA
SLC8A1_gRNA2 CAGCAATTACATGGTCCACA	Synthego	NA
SLC8A1_gRNA3 TGAAATCCCATTGAAAAGGT	Synthego	NA
Recombinant DNA		
pSpCas9(BB)-2A-Puro (pX459) V2.0	Addgene	Addgene_62988[70]
AAV_CAGGS_EGFP	Addgene	Addgene_22212[71]
MV-PGK-Puro-TK	Hera BioLabs	Cat # SGK-00[62]
KCNJ2 cDNA cloning fragment (RefSeq: NM_000891.3)	IDT	NA
pX330-U6-Chimeric_BB-CBh-hSpCas9	Addgene	Addgene_42230
Software and algorithms and equipment		
Guidescan (https://guidescan.com/)	Ventura lab	[72]
Cas-OFFinder (http://www.rgenome.net/cas-offinder/)	Kim lab	[73]
Axis Navigator 2.0.3	Axion Biosystem	NA
Prism 8.4.2	GraphPad	NA
FlowJo V9	BD Life Sciences	NA

SnapGene 5.0.8	SnapGene	NA
ImageJ	Fiji	NA
ecgAUTO 3.3.5.10	EMKA Technologies	NA
Graft quantification analysis	This paper	[20]
Calcium analysis Fluo4 MatLab	Sniadecki Lab	[62]
pClamp 11.1	Molecular Devices	NA
Multiclamp 700B	Molecular Devices	NA
Digidata 1550B	Molecular Devices	NA
Patchmaster v2x73	HEKA Elektronik	NA
Fitmaster v2x91	HEKA Elektronik	NA
Other		
Karyotype analysis	Diagnostic Cytogenetics, Seattle WA	NA
ChemiDoc Imaging system	Biorad	NA
Vibratome 7000smz-2	Camden Instrument	NA
NOGA-MyoStar platform	BioSense Webster	NA
PBS-0.5 MAG Single-Use Vessel	PBS Biotech	Cat #IA-0.5-D-001
PBS-Mini Mag Drive Bioreactor Base Unit	PBS Biotech	Cat #FA-UNI-B-501
Neon Transfection System	Life Technologies	Cat # MPK5000

Figure 1

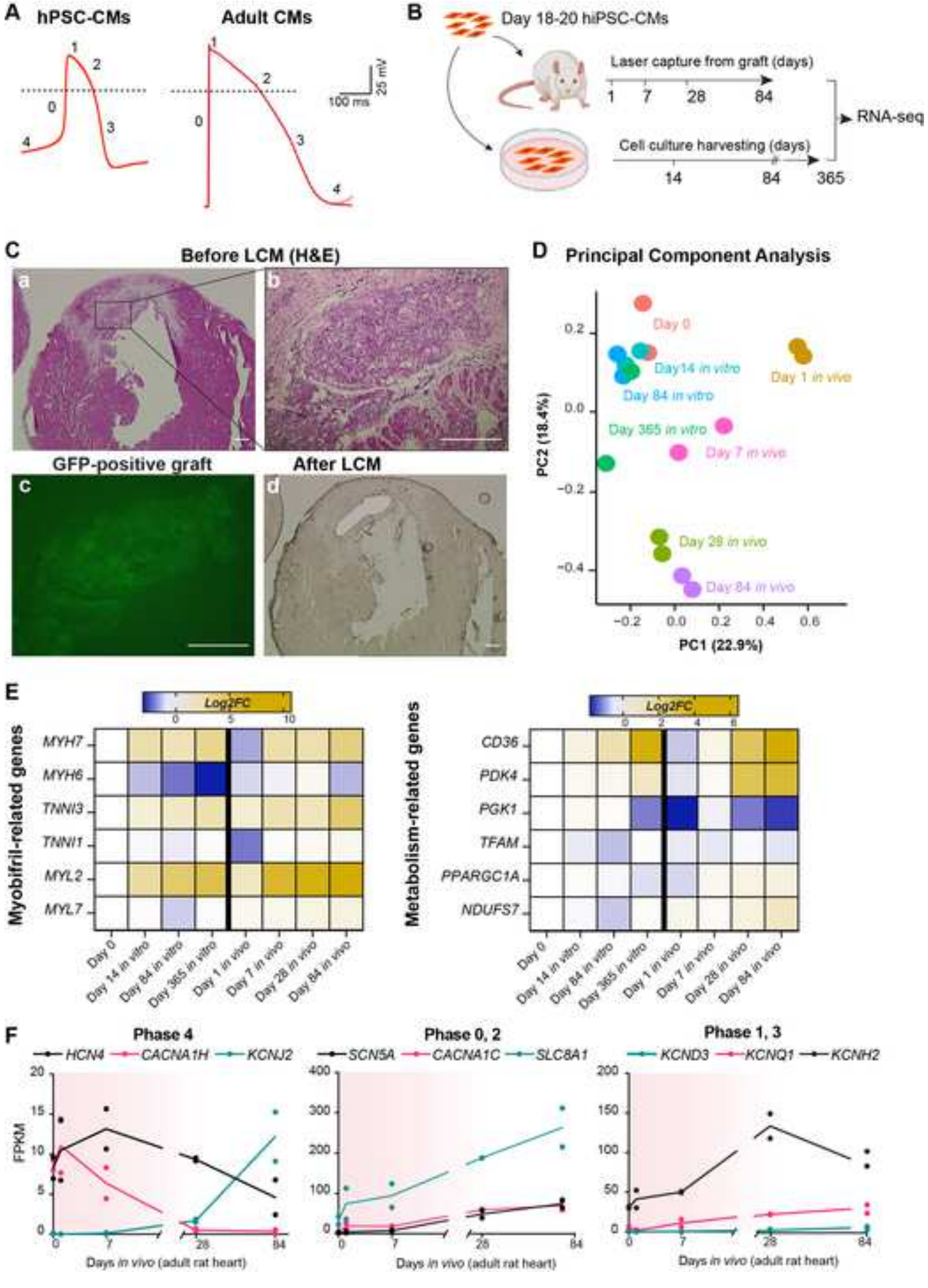

Figure 2

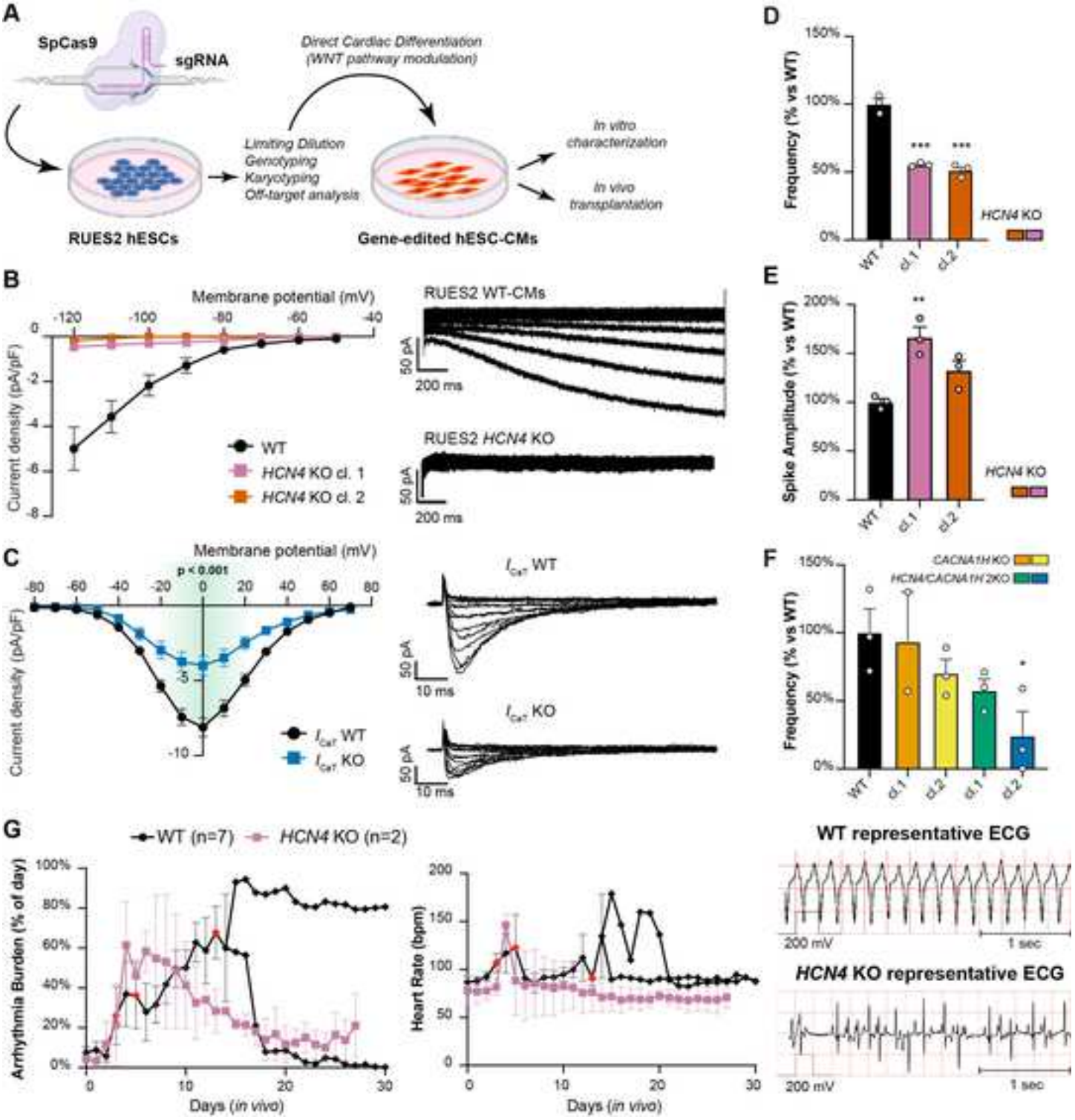

Figure 3

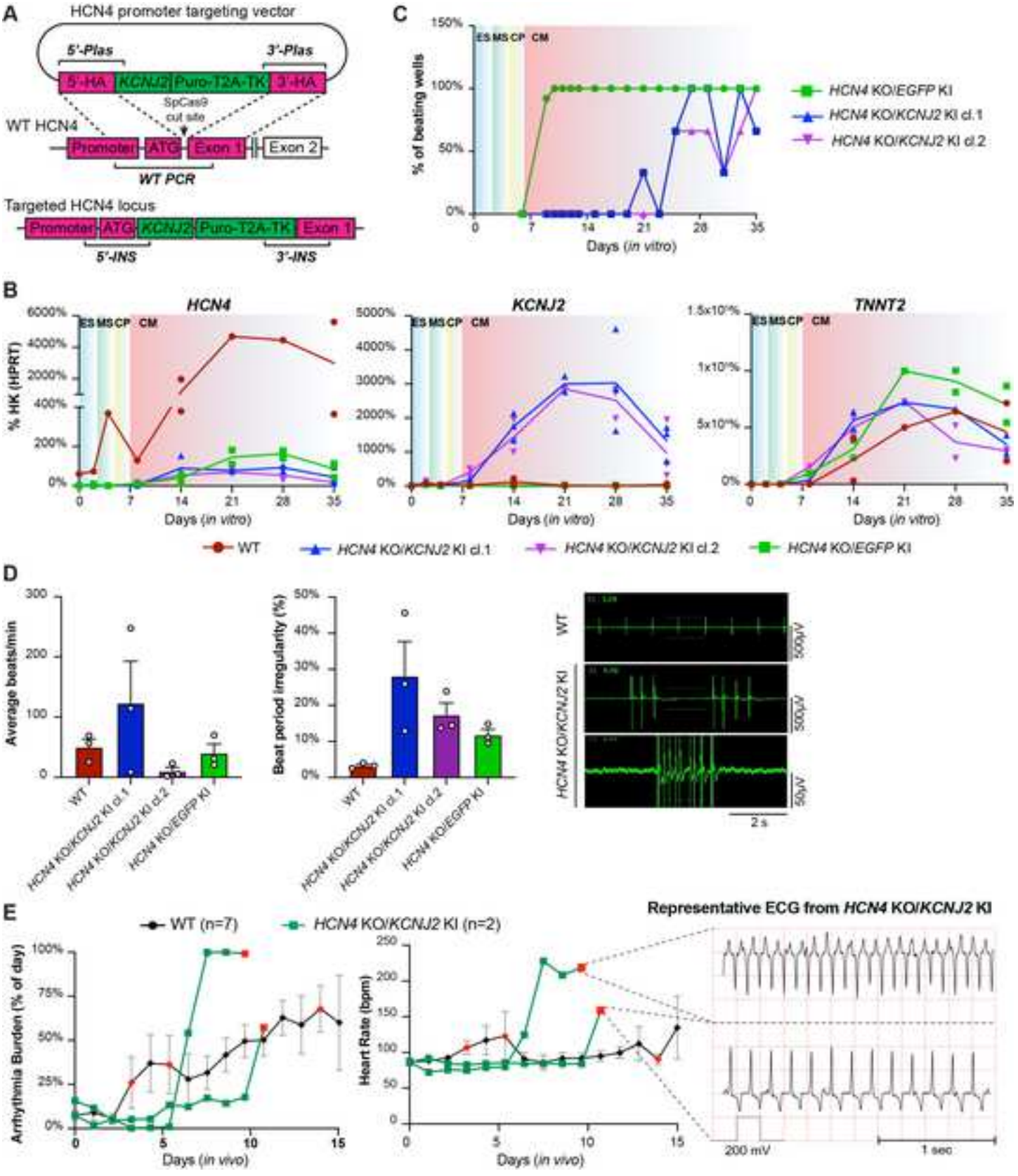

Figure 4

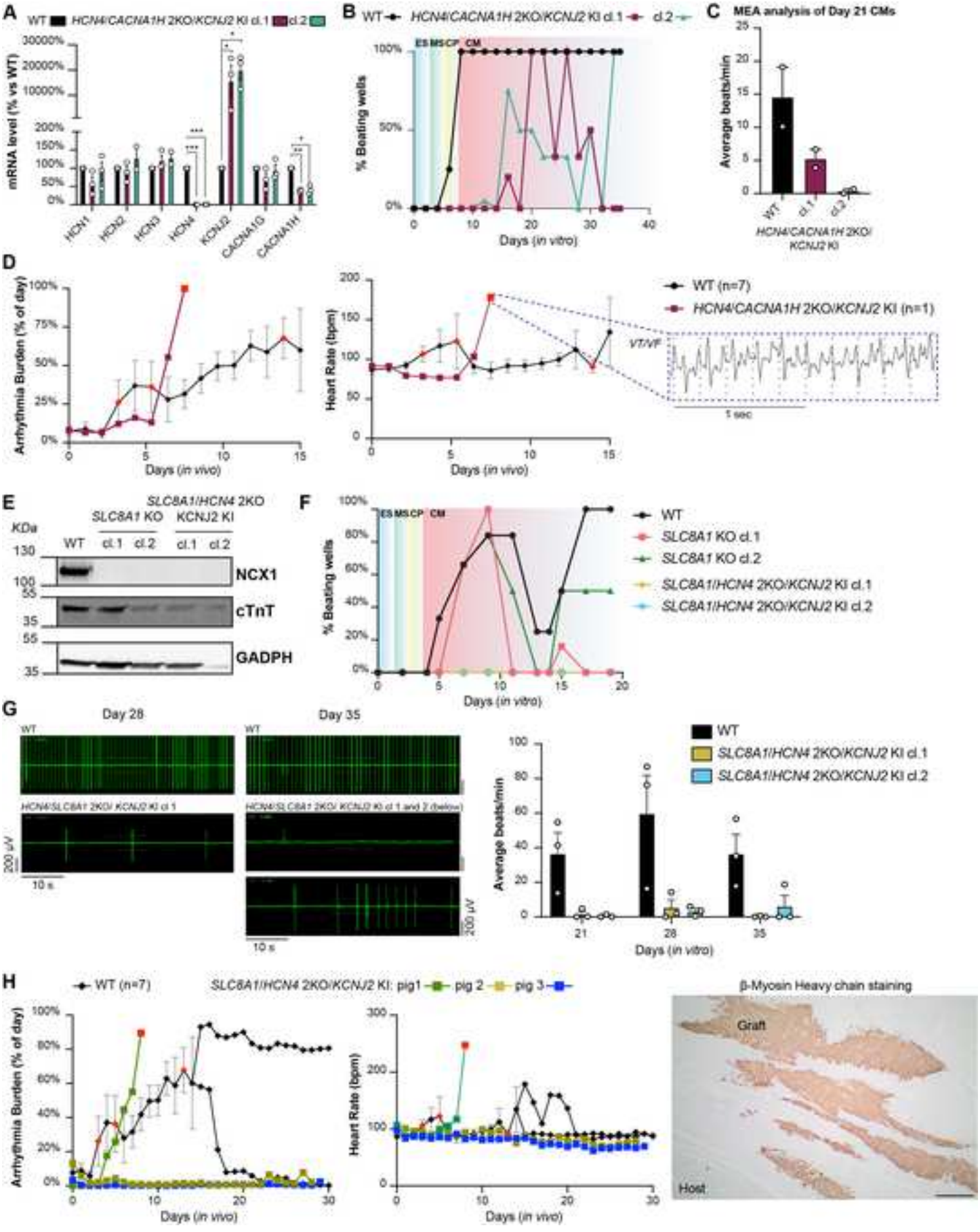

Figure 5

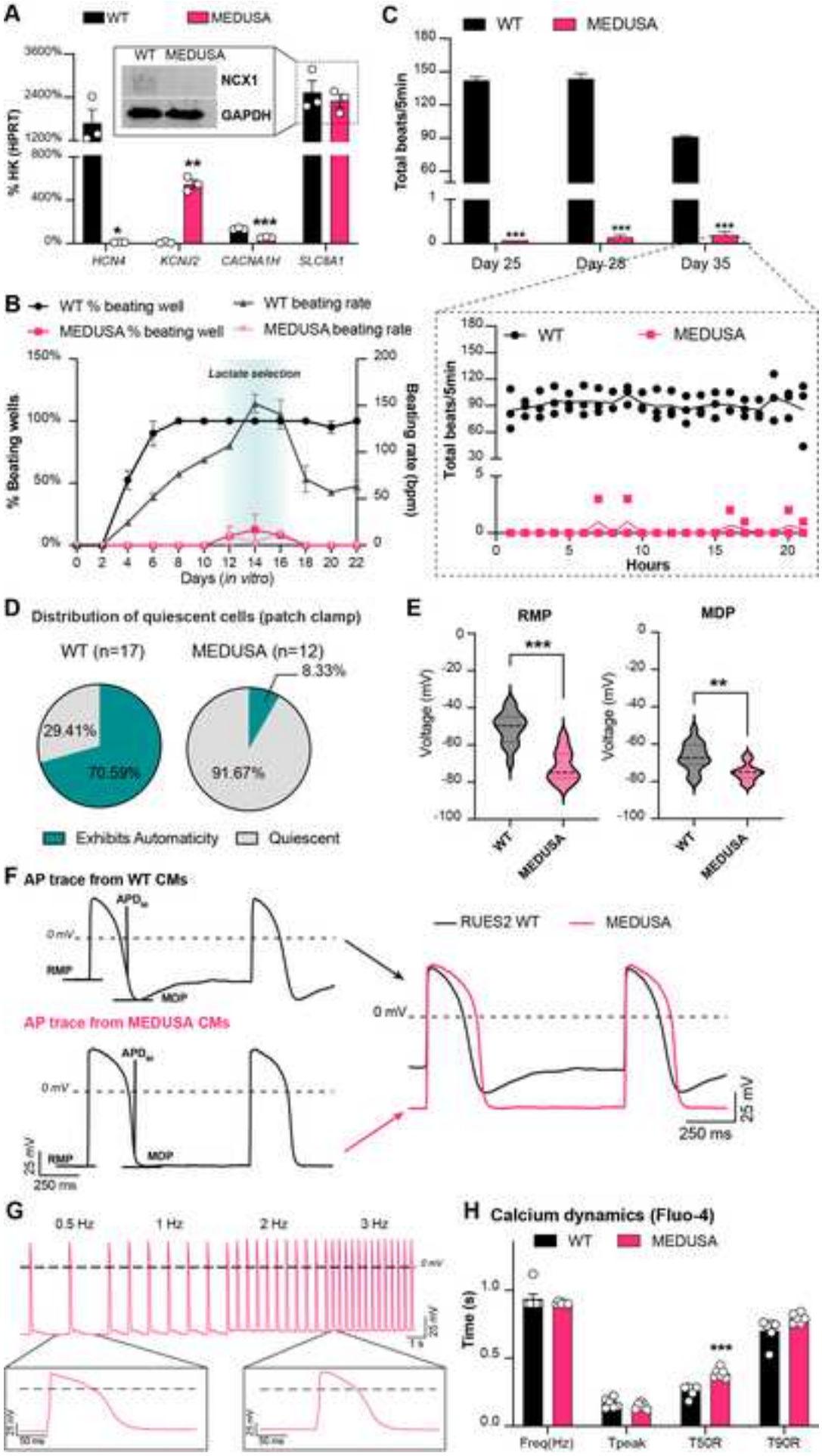

Figure 6

Click here to access/download;Figure;2023023 Figure 6 highres.jpg

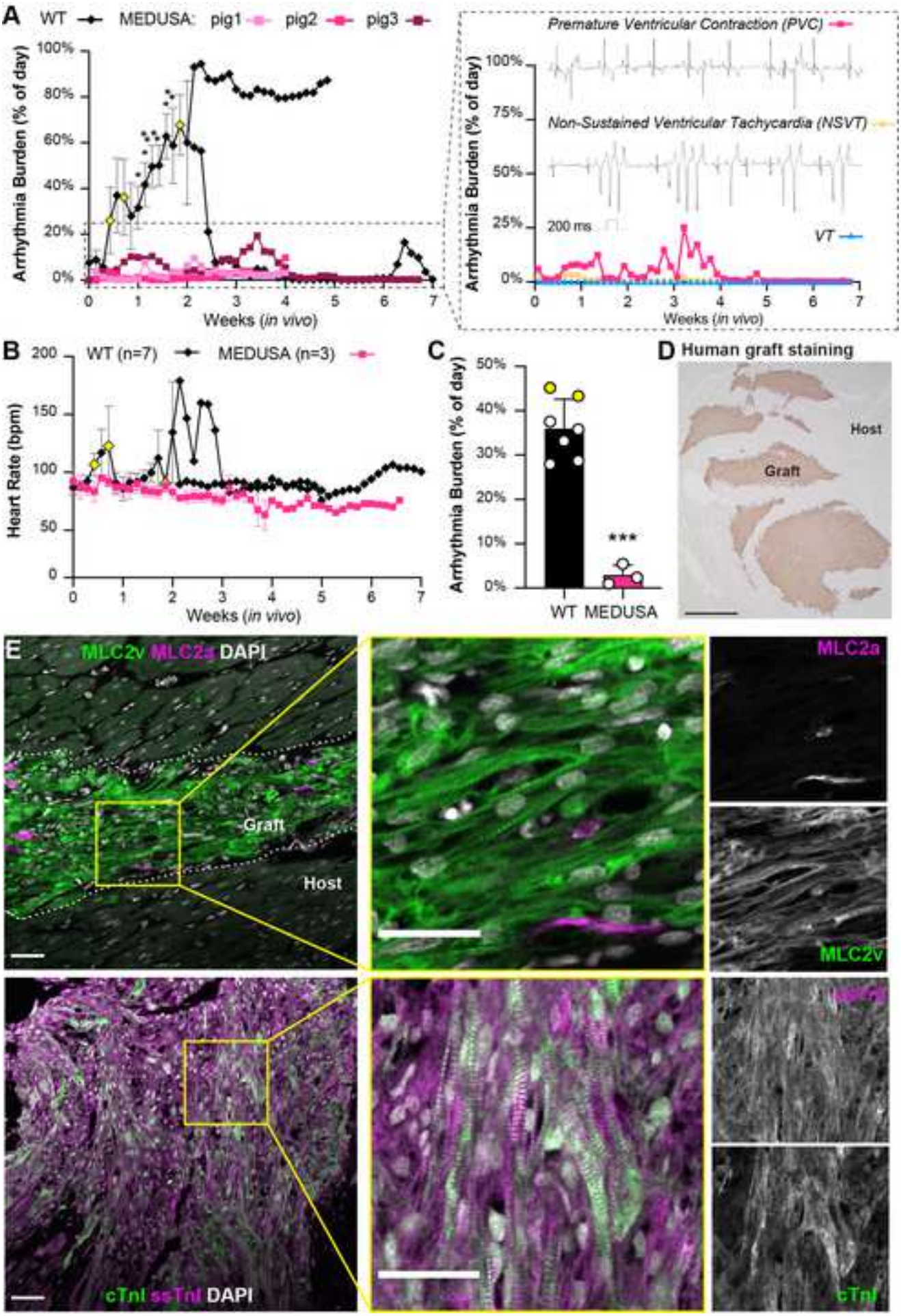

Figure 7

Click here to access/download;Figure;20221231 Figure 7 version 2.jpg

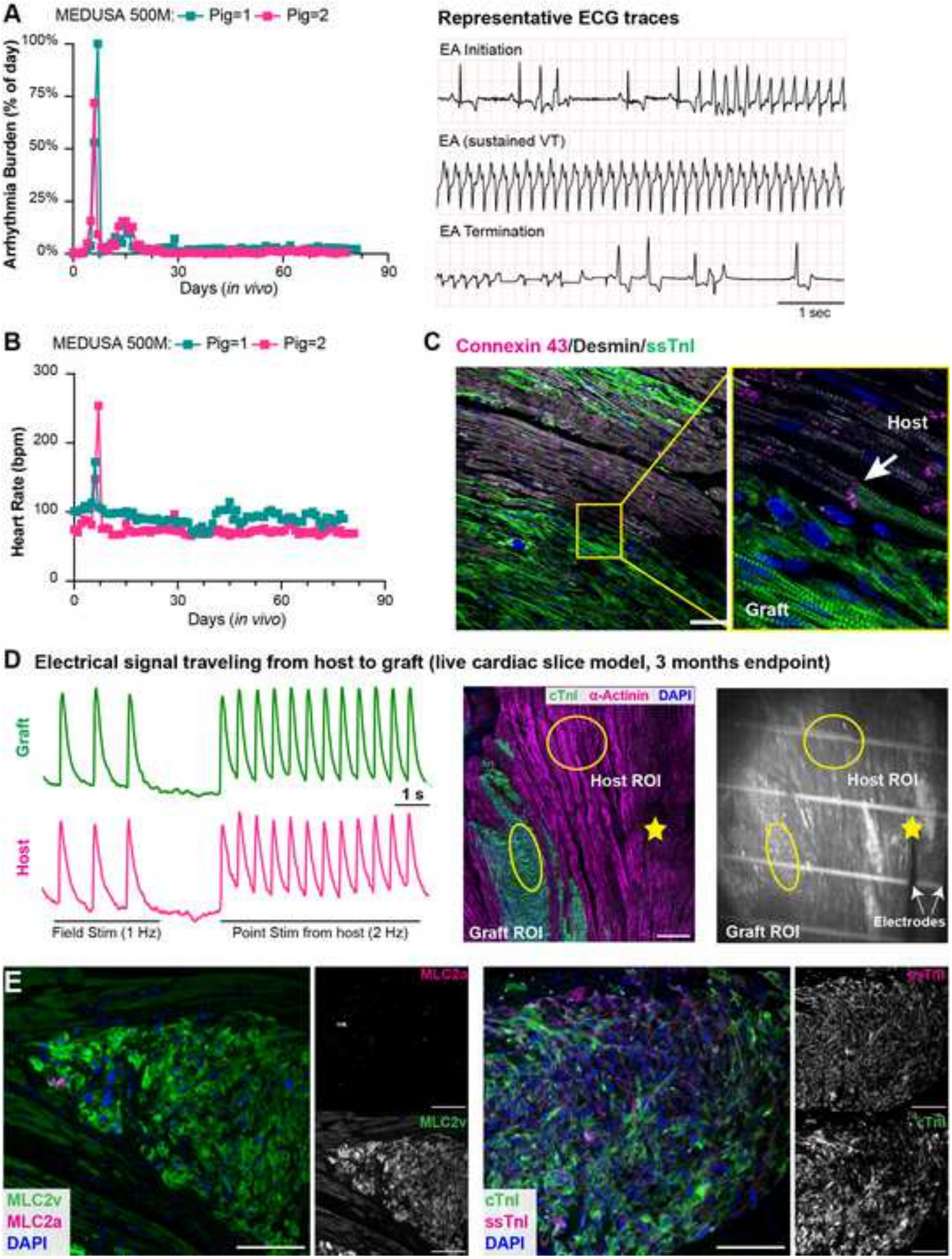

Supplementary Material

Gene editing to prevent ventricular arrhythmias associated with cardiomyocyte cell therapy

Marchiano S., Nakamura K., Reinecke H., Neidig L., Lai M., Kadota S., Perbellini F., Yang X., Klaiman J. M., Blakley L. P., Karbassi E., Fields P. A., Fenix A. M., Beussman K. M., Jayabalu A., Kalucki F. A., Futakuchi-Tsuchida A., Weber G. J., Dupras S., Tsuchida H., Pabon L., Wang L., Knollmann B. C., Kattman S., Thies R. S., Sniadecki N., MacLellan W. R., Bertero A., and Murry C. E.

Table of Contents:

Supplementary Figures

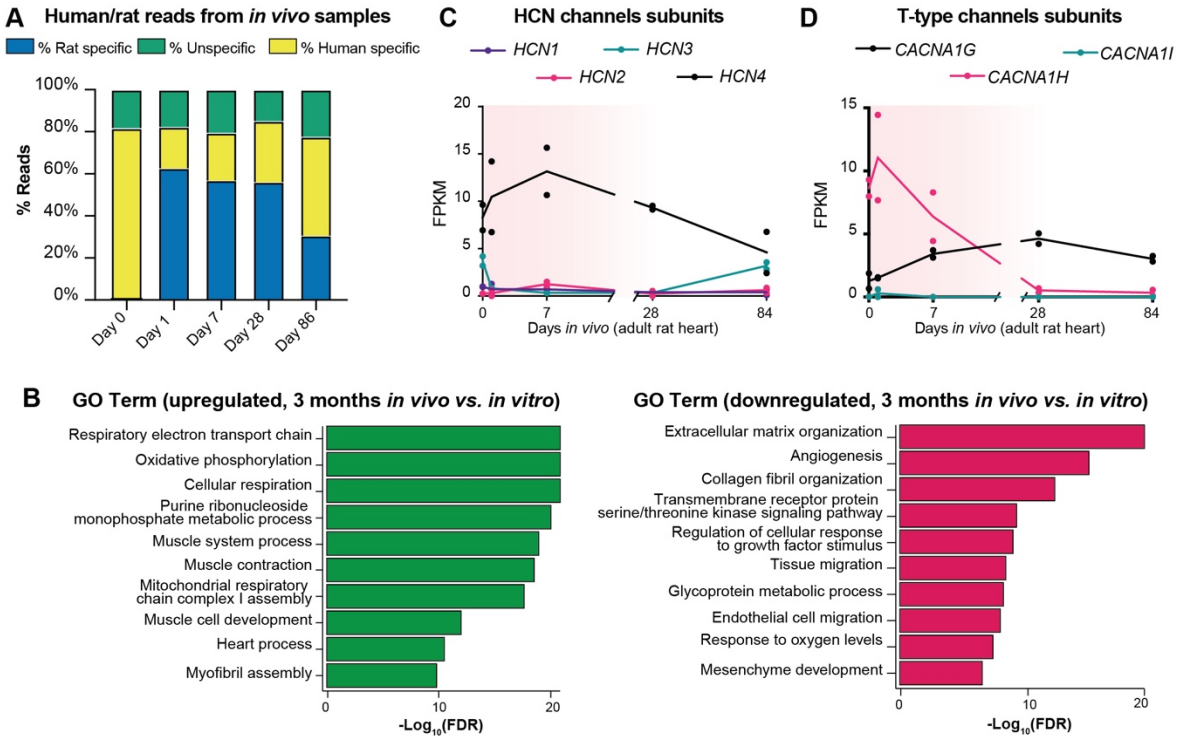

Supplementary Fig. 1 – RNA-seq analysis of *in vivo* transplanted hiPSC-CMs. (**A**) Percentage of human/rat reads from *in vivo* samples after laser capture microdissection in the experiment described in Figs. 1B-D. "Unspecific" indicates reads that do not uniquely map to either genome. (**B**) GO term analysis of selected upregulated and downregulated pathways at 3 months after hiPSC-CMs transplantation. See also Supplementary Table 1. **(C)** RNA-seq expression dynamics of HCN channel isoforms and **(D)** T-type calcium channel isoforms during *in vivo* maturation of hiPSC-CMs. See also Fig. 1F.

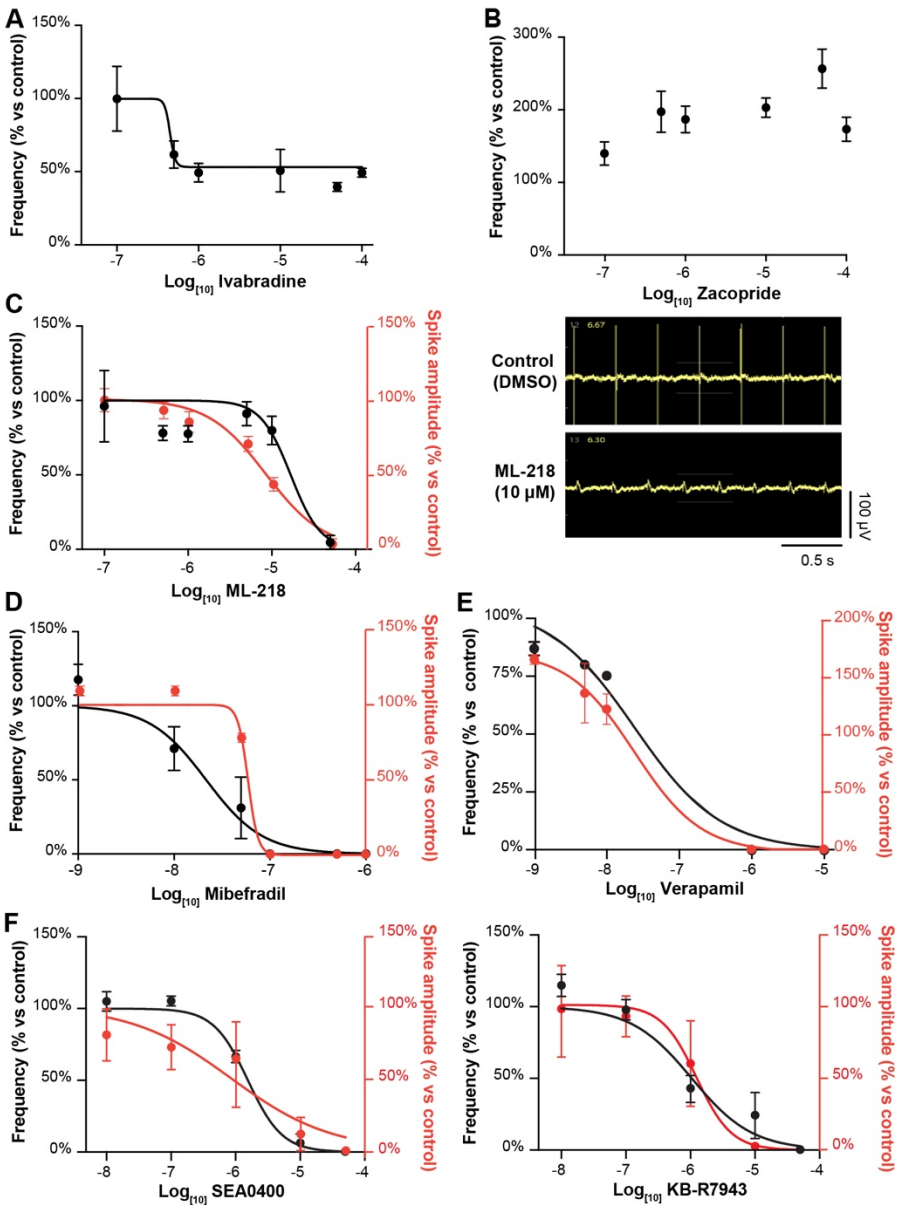

Supplementary Fig. 2 – Pharmacological inhibition of hESC-CMs automaticity *in vitro*. (**A, B**) Dose-response curves of Ivabradine (I_f inhibitor, A) and Zacopride (I_{K1} agonist, B) on MEA system. (**C-F**) Frequencies (left y-axis) and spike amplitude (right y-axis) dose-response curves and representative traces of ML218, Mibefradil (I_{CaT} inhibitors, C, D); Verapamil (I_{CaL} inhibitor, E) and SEA0400 and KB-R7943 (I_{NCX} inhibitors, F). Data shown as mean ± SEM of 2 independent experiments each with 6 technical replicates, normalized on baseline and expressed as % *vs.* control (DMSO). Lines represents nonlinear regression of normalized response.

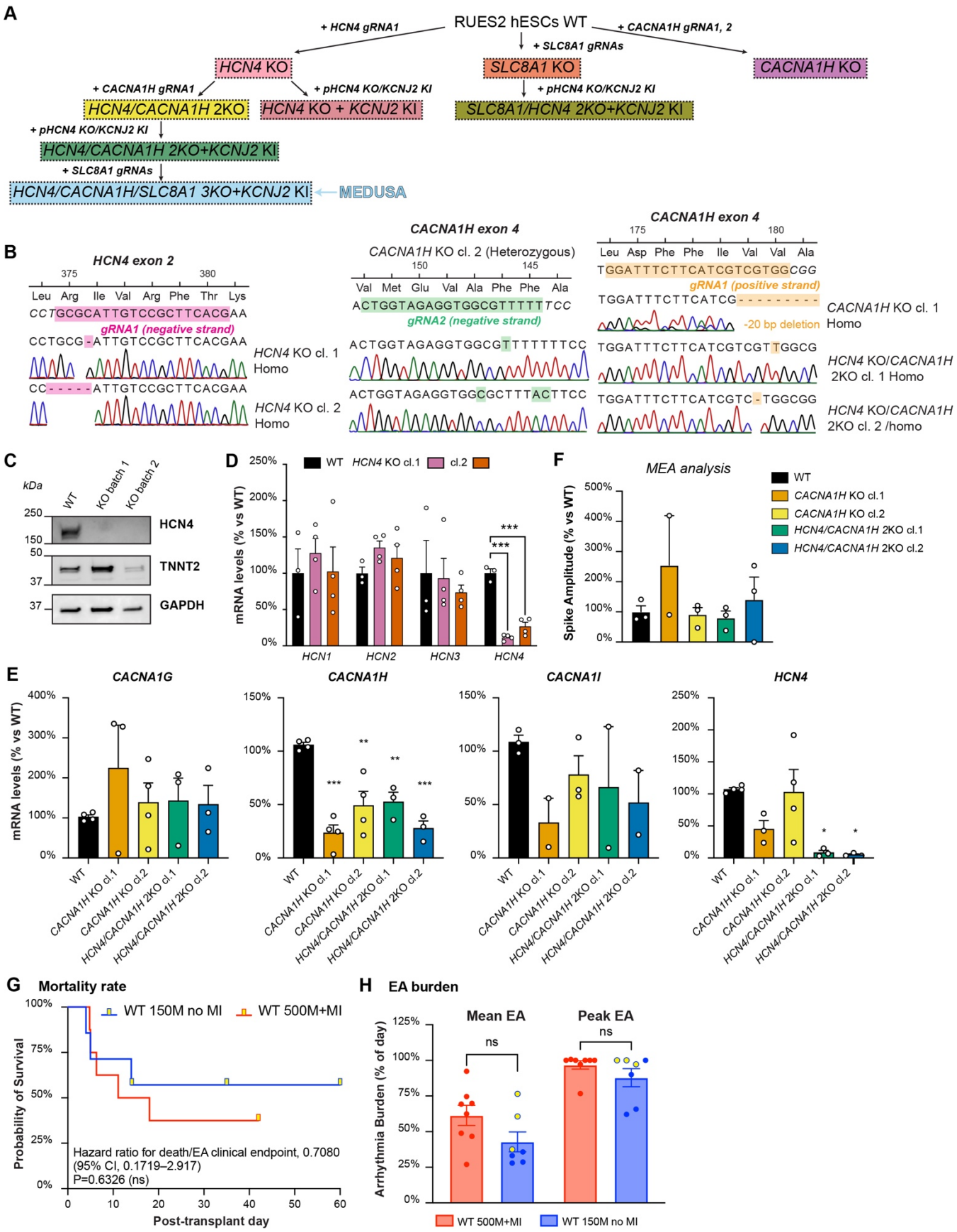

Supplementary Fig. 3 – Characterization of gene-edited cell lines targeting phase 4 of action potential. (**A**) Gene editing approach for the generation of the different cell lines. *pHCN4/KCNJ2 KI*

indicates the targeting vector described in Fig. 3A. (**B**) Sanger sequencing validation of *HCN4* KO clones (*HCN4* KO cl.1 = 1 bp homozygous deletion; *HCN4* KO cl. 2 = 5 bp homozygous deletion), *CACNA1H* KO clones (*CACNA1H* KO cl.1= 20 bp homozygous deletion, *CACNA1H* KO cl.2= compound heterozygous indels leading to frameshift on the different alleles) and double edited cells (*HCN4*/*CACNA1H* KO cl.1= 1 bp homozygous insertion, *HCN4*/*CACNA1H* KO cl.2= 1 bp homozygous deletion). (**C**) Western blot for HCN4, TNNT2 (cardiac troponin T) and GAPDH (loading control) in different batches of MEDUSA hESC-CMs, reported here with the parental line for simplicity. (**D, E**) Gene expression analyses by qRT-PCR of HCN channel subunits in *HCN4* KO, *CACNA1H* KO and *HCN4*/*CACNA1H* 2KO clones compared to WT in 4 independent batches of CMs. In some batches, *CACNA1I* was undetectable (cycle threshold > 40). Differences quantified by one-way ANOVA with Sidak correction for multiple comparisons (** $p < 0.01$, *** $p < 0.001$). (**F**) Spike amplitude of *CACNA1H* KO and *HCN4/CACNA1H* 2KO clones from MEA analysis. Data shown as mean ± SEM of 2-3 independent experiments normalized on WT Spike amplitude. (**G**) Kaplan-Meier curve for freedom from EA mortality (described as death, unstable VT or heart failure necessitating either euthanasia or pharmacological intervention) in uninjured animals receiving 150M WT cells (n=7) or infarcted animals receiving 500M WT cells (n=8,). Yellow-colored marks on the treatment line indicate non-cardiac deaths due to opportunistic infection or planned euthanasia. (**H**) EA burden in uninjured and injured animals shown as mean and peak EA of animals receiving WT cells (Mann-Whitney test). Yellow-colored symbols represent animals that reached endpoint as described in the Method section. Data for 500M + MI in G and H from *Nakamura K. et al., Stem Cell Reports 2021.*

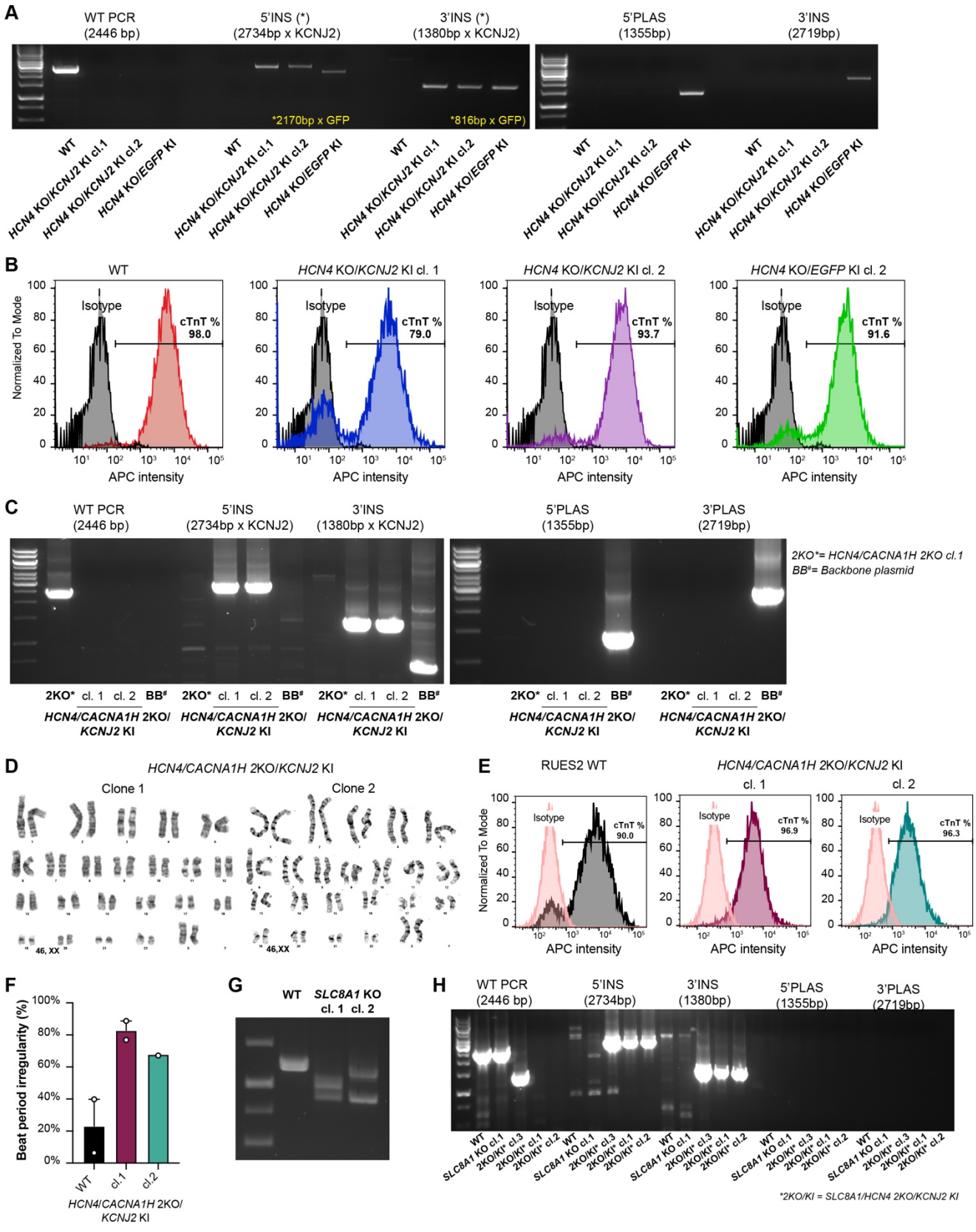

Supplementary Fig. 4 – Genotyping and characterization of triple-edited cell lines. (**A**) Genotyping of *HCN4* KO/*KCNJ2* KI clones generated with CRISPR/Cas9-mediated homology directed repair using

the targeting plasmid described in Fig. 3A. (**B**) Representative flow cytometry data of *HCN4* KO/*KCNJ2* KI clones at day 14 of differentiation stained for cardiac troponin T (cTnT, pan-CM marker). (**C**) Genotyping of *HCN4*/*CACNA1H* 2KO/*KCNJ2* KI clones generated with the targeting plasmid described in Fig. 3A. Refer also to Supplementary Fig. 3A for parental lines. (**D**) Karyotype analyses of *HCN4*/*CACNA1H* 2KO/*KCNJ2* KI clones. (**E**) Representative flow cytometry analysis of *HCN4*/*CACNA1H* 2KO/*KCNJ2* KI CMs at day 14 of differentiation stained for cTnT. (**F**) Beat period irregularity quantified as standard deviation of the beat period record in 100 sec, divided by the mean of the beat period in that same period. Data shown as mean ± SEM of 2 independent experiment (for *HCN4*/*CACNA1H* 2KO/*KCNJ2* KI cl.2, n=1 due to lack of spontaneous activity in the second experiment that prevented calculation of beat irregularity). (**G**) Genotype of *SLC8A1* KO clones generated via combination of 3 gRNAs. (**H**) Genotype of *SLC8A1*/*HCN4* 2KO/*KCNJ2* KI clones generated with same approach described in Fig. 3A. Due to heterozygosity of clone 3, this clone was not used for further experiment.

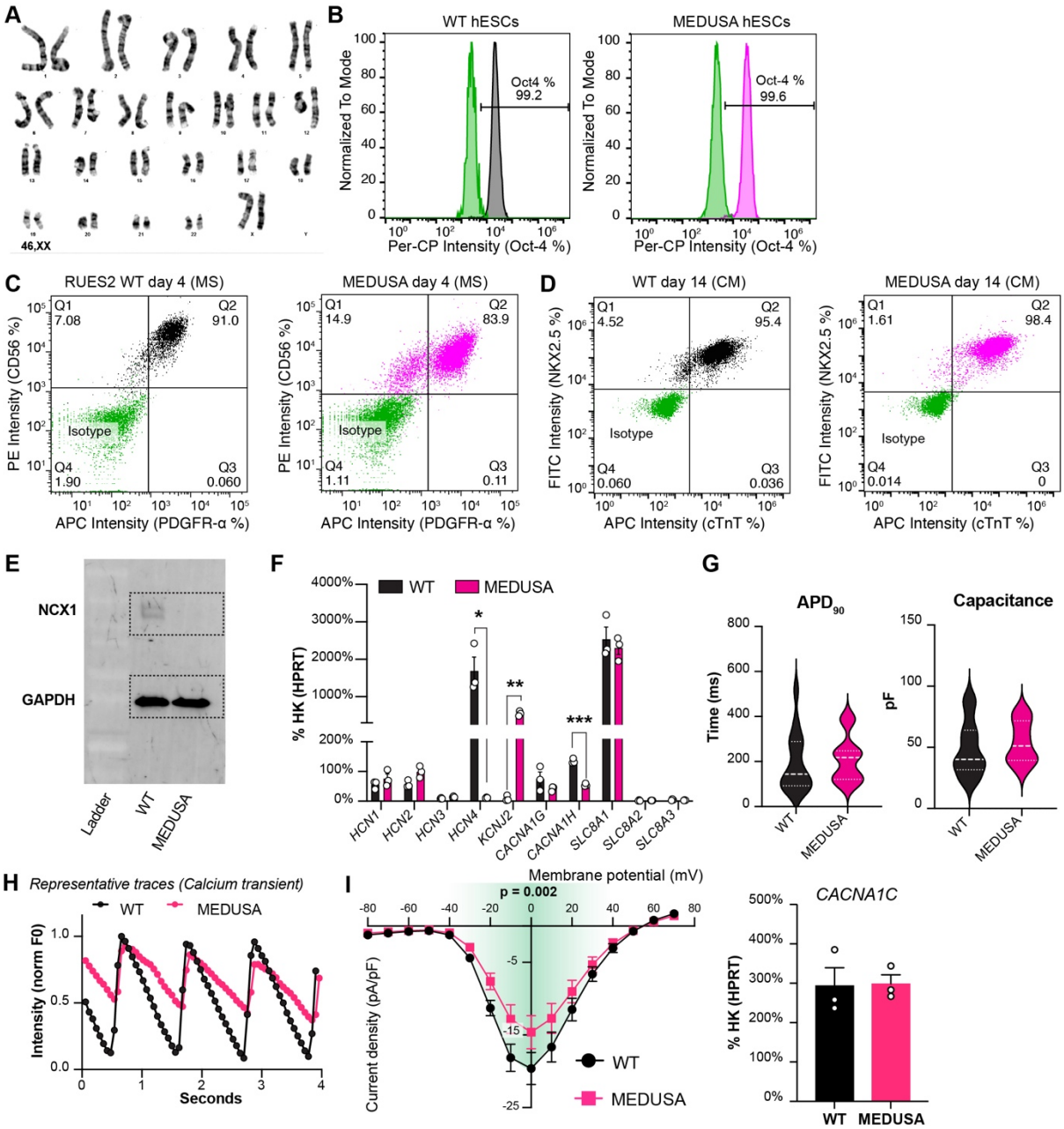

Supplementary Fig. 5 – Characterization of MEDUSA cell line. (**A**) Karyotype analysis of MEDUSA hESCs. (**B**) Representative flow cytometry analysis of MEDUSA hESCs and WT hESCs stained with Oct3/4 as pluripotency marker, as compared to respective isotype control. (**C, D**) Representative flow cytometry analysis of mesoderm markers (CD56/PDGFRα) and ventricular markers (NKX2.5/cTnT) during cardiac differentiation in WT and MEDUSA, compared to isotype controls. MS= Mesoderm state. (**E**) Western blotting for NCX1 and GAPDH (loading control) in WT and MEDUSA hESC-CMs. Dotted squares represent inserts shown in Fig. 5A. (**F**) qRT-PCR analysis of genes encoding for I_f, I_{CaT}, I_{K1} and I_{NCX} in MEDUSA hESC-CMs, compared to WT-matched controls. Note the absence of nonsense-mediated decay for *SLC8A1.* Data shown as mean ± SEM of 3 independent biological replicates. Differences *vs.* WT by multiple unpaired t test (* p <0.05, ** p <0.01 and *** p <0.001). See also Fig. 5A. (**G**) Action potential duration at 90% of repolarization (APD_{90}) and capacitance current of WT and MEDUSA CMs. Data shown as described in Figs. 5E. (**H**) Representative calcium transient trace from WT and MEDUSA hESC-CMs. See also Fig. 5H. (**I**) Current density plot for I_{CaL} currents and qRT-PCR for *CACNA1C* in MEDUSA hESC-CMs, compared to WT controls. For I/V plot, data shown as mean ± SEM of n = 22 for WT and n = 15 for MEDUSA hESC-CMs. Green-shaded area indicates difference vs.

WT hESC-CMs by two-way ANOVA with Sidak correction for multiple comparison ($p = 0.002$). For qRT-PCR. Data shown as mean ± SEM of 3 independent biological replicates.

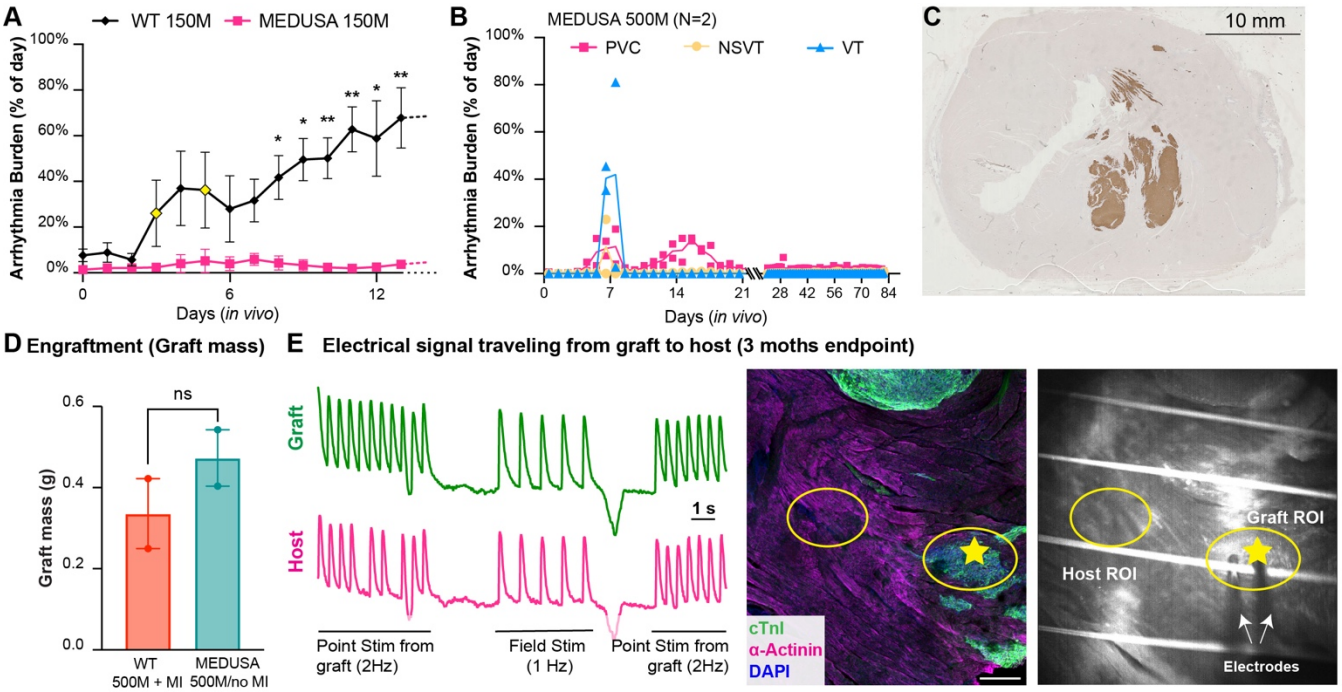

Supplementary Figure 6. Characterization of transplanted MEDUSA hESC-CMs. (**A**) Daily arrhythmia burden focused on the first 2 weeks after transplantation for animals receiving 150 x 10^6 (150M) WT or MEDUSA hESC-CMs (See also Fig. 6A for arrhythmia burden over 7-weeks observation period). Differences vs. WT by multiple unpaired t-test (* $p < 0.05$ and ** $p< 0.01$). Yellow-colored symbols indicate animals that reached EA endpoint as detailed in Fig. 6A and Methods section. (**B**) Quantification of EA burden divided in PVCs, VT and NSVT for both 500M MEDUSA animals in the first 3 weeks after transplantation. See also Methods section for details on EA characterization. (**C**) Whole-slide scanning showing MEDUSA grafts at 500M dose at 3 months after transplantation. (**D**) Graft mass of 500M MEDUSA hESC-CMs transplanted into the uninjured pig heart compared to 500M WT hESC-CMs transplanted into infarcted animals. Data shown as average ± SEM, differences by Mann-Whitney test. For 500M WT hESC-CMs + MI, data points from *Nakamura K., et al., Stem Cell Reports 2021*.
(**E**) Cardiac slice model of 12 weeks old MEDUSA-CMs grafts. Left panel showing Fluo-4 traces of cardiac slice paced with field and point stimulation from graft region with relative immunofluorescence and monochromatic images on the right side. Yellow circle indicates ROI for Fluo-4 recording, yellow star indicates point stimulation location. Scale bar = 500 µm. See also Supplementary Video 3.

Supplementary Table 1. Extended top 40 GO terms from Supplementary Fig. 1B.

Top 40 upregulated GO terms 3 months in vivo vs in vitro

GO term	***-LogFDR***
mitochondrial ATP synthesis coupled electron transport	26.7593509
ATP synthesis coupled electron transport	26.7593509
respiratory electron transport chain	26.7593509
oxidative phosphorylation	26.7593509
cellular respiration	26.7593509
muscle system process	24.905479
electron transport chain	24.905479
muscle contraction	24.3724063
energy derivation by oxidation of organic compounds	23.8385322
ATP metabolic process	23.7816273
mitochondrial electron transport, NADH to ubiquinone	23.4889897
purine ribonucleotide metabolic process	22.4583209
purine ribonucleoside monophosphate metabolic process	22.4583209
purine nucleoside monophosphate metabolic process	22.400329
purine ribonucleoside triphosphate metabolic process	22.1572909
mitochondrial respiratory chain complex assembly	21.8021029
ribonucleoside triphosphate metabolic process	21.6997652
purine nucleoside triphosphate metabolic process	21.6435556
nucleoside triphosphate metabolic process	21.6148587
ribonucleoside monophosphate metabolic process	21.4475971
NADH dehydrogenase complex assembly	21.0603809
mitochondrial respiratory chain complex I assembly	21.0603809
nucleoside monophosphate metabolic process	20.6662339
generation of precursor metabolites and energy	19.0256188
muscle cell development	16.1158982
striated muscle contraction	15.5888635
mitochondrion organization	15.1695254
striated muscle cell development	14.9634709
heart process	13.3913741
heart contraction	13.3913741
myofibril assembly	12.7808906
striated muscle tissue development	11.6790402
muscle tissue development	10.8758565
cardiac muscle contraction	10.8758565
cellular component assembly involved in morphogenesis	10.5252677
mitochondrial translational elongation	10.5027401
mitochondrial translational termination	10.3981337
striated muscle cell differentiation	10.3179452
muscle cell differentiation	9.92716966
sarcomere organization	9.89901292

Top 40 downregulated GO terms 3 months in vivo vs in vitro

GO term	***-LogFDR***
extracellular matrix organization	17.7593509
extracellular structure organization	17.1853197
angiogenesis	12.9354422
collagen fibril organization	11.8842897
response to transforming growth factor beta	8.36141092
cellular response to transforming growth factor beta stimulus	8.31441435
regulation of cellular response to growth factor stimulus	8.31441435
transmembrane receptor protein serine/threonine kinase signaling pathway	8.20004291
glycoprotein metabolic process	7.97323075
negative regulation of cellular component movement	7.77955431
tissue migration	7.77955431
ameboidal-type cell migration	7.54849756
epithelial cell migration	7.25524618
negative regulation of locomotion	7.19507949
endothelial cell migration	7.19507949
epithelium migration	7.18531966
epithelial cell proliferation	7.14470181
regulation of transmembrane receptor protein serine/threonine kinase signaling pathway	7.11153344
ossification	7.1086856
urogenital system development	6.99968308
transforming growth factor beta receptor signaling pathway	6.93544218
glycoprotein biosynthetic process	6.8465011
kidney development	6.82004877
response to oxygen levels	6.79713949
skeletal system development	6.28222967
aminoglycan biosynthetic process	6.24490535
mesenchyme development	6.21299108
renal system development	6.12732771
response to endoplasmic reticulum stress	6.09141515
negative regulation of cell motility	6.0323522
glycosaminoglycan biosynthetic process	5.99544011
mesenchymal cell differentiation	5.99166511
cholesterol biosynthetic process	5.99166511
secondary alcohol biosynthetic process	5.99166511
negative regulation of cellular response to growth factor stimulus	5.99166511
regulation of vasculature development	5.92648734
response to decreased oxygen levels	5.80131543
response to hypoxia	5.80131543
cell-substrate adhesion	5.7220266
chondrocyte differentiation	5.66680572

Supplementary Table 2. Graft size quantification.

Animal	*Procedure*	*Cell Prep*[a]	*%Area graft*[b]	*%Graft size*[c]	*Endpoint*	*EA observed*[d]
WT #1	Catheter	SC	0.245%	0.00310%	Endpoint 2 weeks	Yes
WT #2	Catheter	SC	0.742%	0.00932%	Euthanized day 6	Yes, rapid
WT #3	Catheter	SC	1.676%	0.01275%	Endpoint 2 weeks	Yes
WT #4	Direct thoracotomy	SC	NA	NA	Amiodarone at day 4	Yes, rapid
WT #5	Direct thoracotomy	SC	NA	NA	Endpoint 5 weeks	Yes
WT #6	Direct thoracotomy	SC	NA	NA	Amiodarone at 2 weeks	Yes, rapid
WT #7	Direct thoracotomy	SC	NA	NA	Endpoint 3 months	Yes
HCN4 *KO #1*	Catheter	SC	0.913%	0.00953%	Endpoint 4 weeks	Yes
HCN4 *KO #2*	Catheter	SC	2.351%	0.02200%	Endpoint 4 weeks	Yes
HCN4 *KO*/KCNJ2 *KI #1*	Catheter	SC	0.986%	0.01574%	Euthanized day 7	Yes, rapid
HCN4 *KO*/KCNJ2 *KI #2*	Catheter	SC	0.120%	0.00128%	Euthanized day 9	Yes, rapid
HCN4 *KO*/CACNA1H *2KO*/KCNJ2 *KI #1*	Catheter	SC	4.116%	0.04128%	Euthanized day 8	Yes, rapid
HCN4 *KO*/SLC8A1 *2KO*/KCNJ2 *KI #1*	Direct thoracotomy	Mono	2.444%	0.03165%	Euthanized day 7	Yes, rapid
HCN4 *KO*/SLC8A1 *2KO*/KCNJ2 *KI #2*	Direct thoracotomy	Mono	0.294%	0.00367%	Endpoint 4 weeks	No
HCN4 *KO*/SLC8A1 *2KO*/KCNJ2 *KI #3*	Direct thoracotomy	Mono	6.281%	0.05714%	Endpoint 4 weeks	No
MEDUSA #1	Direct thoracotomy	Mono	0.747%	0.00837%	Endpoint 4 weeks	No
MEDUSA #2	Direct thoracotomy	Mono	2.701%	0.02459%	Endpoint 4 weeks	No
MEDUSA #3	Direct thoracotomy	SC	9.284%	0.07453%	Endpoint 7 weeks	No
MEDUSA 500M #1	Direct thoracotomy	SC	36.94%	0.29081%	Endpoint 3 months	Yes, self-terminating
MEDUSA 500M #2	Direct thoracotomy	SC	28.70%	0.24330%	Endpoint 3 months	Yes, self-terminating

[a] SC: suspension culture differentiation; Mono: monolayer differentiation
[b] %Area graft expressed as percentage of the relative myocardial section.
[c] %Graft size: (% area graft x block weight) / left ventricle mass.
[d] Rapid indicates extreme tachycardia over 300 beats per minute necessitating euthanasia

Supplementary Table 3. Oligonucleotides sequences for cloning gRNAs and genotyping.

Primer Name	Sequence	Target
HCN4_gRNA1_FWD	CACCGTCGTGAAGCGGACAATGCGC	HCN4 gRNA1
HCN4_gRNA1_RVS	AAACGCGCATTGTCCGCTTCACGAC	
CACNA1H_gRNA1_FWD	CACCGGATTTCTTCATCGTCGTGG	CACNA1H gRNA1
CACNA1H_gRNA1_RVS	AAACCCACGACGATGAAGAAATCC	
HCN4_gRNA1_KI_FWD	CACCGCAGCTTGTCCATGGCGCCAG	HCN4 KO_KCNJ2 gRNA1
HCN4_gRNA1_KI_RVS	AAACCTGGCGCCATGGACAAGCTGC	
HCN4_gRNA2_KI_FWD	CACCGGCAGCTTGTCCATGGCGCC	HCN4 KO_KCNJ2 gRNA2
HCN4_gRNA2_KI_RVS	AAACGGCGCCATGGACAAGCTGCC	
SLC8A1_gRNA1	GGAUCAUAUUACUGUAAGAA	SLC8A1 gRNA1
SLC8A1_gRNA2	CAGCAAUUACAUGGUCCACA	SLC8A1 gRNA2
SLC8A1_gRNA3	UGAAAUCCCAUUGAAAAGGU	SLC8A1 gRNA3
HCN4-KI_5HA_FW	gaatgcgtcgagatATTGGGTCgcggccgcACGAACC CGGTCGCCTCCCA	Cloning HCN4 5' HA
HCN4-KI_5HA_REV	TGGCTGATCATTAATTAAGCGGGTTTAAACG GGCCCATGGCGCCAGGGGCCGG	
HCN4-KI_3HA_FW	AAAGAGAGAGCAATATTTCAAGAATGCAtgcgt caattttacgcagactatctttctagggTTAAGACAAGCTG CCGCCGTCC	Cloning HCN4 3' HA
HCN4-KI_3HA_REV	ggtcccggcatccgatACCCAATggcgcgccGGCTGAA TGACCCGGAGCTG	
pA_FW	AAACCCGCTTAATTAATGATCAGCCATCGATT CGActgtgccttctagttgccag	Cloning polyA
pA_REV	AATTTTACGCATGATTATCTTTAACgtacgtcaca atatgattatctttctagggTTAAacccatagagcccaccgc	
EGFP_Amp_FW	GACCTTAACCatggtgagcaaggg	Cloning EGFP
EGFP_Amp_REV	GGTTCCATCGATttacttgtacagctcgtccatg	
eSpCas9_seq	GGCCTATTTCCCATGATTCCT	Sequencing pX459 and pX330 cloned plasmids
HCN4_gen_FWD	GAGAACACCACACCCTGGATT	Genotype HCN4 KO clones
HCN4_gen_RVS	TGCCACAATCTGACAGCCTAT	
CACNA1H_gen_FWD	TTTCCTGATGAGCCAACGCC	Genotype CACNA1H KO clones
CACNA1H_gen_RVS	CCGGTCACTTACTAGGCACG	
SLC8A1_gen_FWD	TCATGTACAACATGCGGCGA	Genotype SLC8A1 KO clones
SLC8A1_gen_RVS	CTCCGTCAGGCACCACATAA	
WT_PCR_FWD	CACCCTGCCCATGTCACAGG	Genotype HCN4 KO_KCNJ2 KI clones
WT_PCR_RVS	GTGACTTCGGTCCTCCAGGG	
5'INS_FWD	CACCCTGCCCATGTCACAGG	
5'INS_RVS	CGTCAATTTTACGCATGATTATCTTTAAC	
3'INS_FWD	GCGACGGATTCGCGCTATTTAGAAAG	
3'INS_RVS	GTGACTTCGGTCCTCCAGGG	
5'PLAS_FWD	GAGCGGATAACAATTTCACACAGG	
5'PLAS_RVS	GCGACGGATTCGCGCTATTTAGAAAG	

3'PLAS_FWD	CGTCAATTTTACGCATGATTATCTTTAAC	
3'PLAS_RVS	AGGGTTTTCCCAGTCACGACGTT	

Supplementary Table 4. Oligonucleotides sequences for RTqPCR

Gene target	Sequence
HCN4_FWD	GATCCTCAGCCTCTTACGCC
HCN4_RVS	CCCCAGGAGTTGTTCACCAT
HCN1_FWD	ATGGTAATCCAGAGGTCAGACA
HCN1_RVS	TTCTTCGAGGCGGCAGTATC
HCN2_FWD	GGCATGGTGAACCACTCGT
HCN2_RVS	TGTACTGCTCCACCTGCTTG
HCN3_FWD	GGTTCCTGGTTGACCTCATCT
HCN3_RVS	GTGAAAGATCTCCTCCCACTGGT
CACNA1H_FWD	ATGCTGGTAATCATGCTCAACTG
CACNA1H_RVS	AAAAGGCGAAAATGAAGGCGT
CACNA1G_FWD	CGCCATCTTCCAGGTCATCA
CACNA1G_RVS	TCTGAGAACTGCGTGGCAAT
CACNA1I_FWD	GGATGGAGCTGATCCTCATGT
CACNA1I_RVS	AAGATGAAGTCATCAAAGACCTGC
KCNJ2_FWD	GTGCGAACCAACCGCTACA
KCNJ2_RVS	CCAGCGAATGTCCACACAC
SLC8A1_FWD	AGACCTGGCTTCCCACTTTG
SLC8A1_RVS	TGGCAAATGTGTCTGGCACT
SLC81A2_FWD	GTCACTGCCTCTTGGAGCAT
SLC81A2_RVS	CACACCGGGAAGAAGACCAG
SLC81A3_FWD	CCGAAATGGATGGAACGTGG
SLC81A3_RVS	GAATGGGTCCCCACAACCAA
TNNT2_FWD	TTCACCAAAGATCTGCTCCTCGCT
TNNT2_RVS	TTATTACTGGTGTGGAGTGGGTGTGG
HPRT_FWD	TGACACTGGCAAAACAATGCA
HPRT_RVS	GGTCCTTTTCACCAGCAAGCT